The Dissertation Committee for Ryan Scott Stowers Certifies that this is the approved version of the following dissertation:

Dynamic Photo-tunable Hydrogels for Temporal Modulation of Matrix Mechanical Properties

Committee:

Laura J. Suggs, Supervisor

Roger T. Bonnecaze

Amy L. Brock

Jeanne C. Stachowiak

Carla Van Den Berg

Dynamic Photo-tunable Hydrogels for Temporal Modulation of Matrix Mechanical Properties

by

Ryan Scott Stowers, B.S. Bioengineering

Dissertation

Presented to the Faculty of the Graduate School of

The University of Texas at Austin

in Partial Fulfillment

of the Requirements

for the Degree of

Doctor of Philosophy

The University of Texas at Austin

December 2014

Dedication

To Jamie, for your patience, support and love.

Acknowledgements

Many people deserve acknowledgement for their support, guidance, and encouragement throughout my graduate career. First, I am sincerely appreciative of my advisor, Dr. Laura Suggs. Her mentorship has greatly helped me mature as a scientist. I am grateful for the freedom to pursue a new and risky research area, and for support during times of discouraging results. I would like to thank Dr. Jeanne Stachowiak for guidance during the early development of my project, invaluable career advice, insightful manuscript review, and for her willingness to find time to help however possible. I would like to thank my committee members, Dr. Amy Brock, Dr. Carla Van Den Berg, and Dr. Roger Bonnecaze for their help in directing my dissertation research. I would also like to acknowledge Dr. Stanislav Emelianov and Dr. James Tunnell, who allowed me to access equipment from their laboratories, without which this work would not be possible. Finally, I would like to thank Dr. Dan Simionescu and Dr. Agneta Simionescu for introducing me to research and encouraging me to pursue it.

I have had the opportunity to work with many wonderful and intelligent people while at UT. I would like to thank all present and former members of the Suggs lab for making an enjoyable and exciting work environment. Specifically, I would like to thank Charlie Drinnan, for training me during my first year and providing advice ever since. I would also like to thank Eunna Chung, I learned a great deal from her and appreciated her positive, high-energy attitude in lab every day. To Kevin Eckes, I always enjoyed coffee breaks and interesting conversations. I am tremendously appreciative of the contributions from the undergraduate researchers who have worked with me at UT,

Kelsey Weaver, Laura Puckett, Bill Han, Courtney Davis, Stewart Holloway, and Karla Sanchez.

I would like to thank several other graduate students and postdocs for their assistance in my research. Varun Pattani provided excellent technical guidance on lasers and optics, I am appreciative of his patience with my ignorance on these matters. Geoff Luke provided a sounding board for new ideas and a mentor for career advice. I would like to recognize Derek Hernandez for assistance with AFM studies, Sam Lim for access to motorized stages, and Danielle Ebelt for assistance and guidance with MCF10A 3D assays.

Finally, I would like to thank my family for their unconditional love and support. My parents have always encouraged me to pursue my dreams and sacrificed a great deal to ensure that I have those opportunities. They have instilled in me the value of hard work and pursuit of lofty goals. I am truly grateful to call you Mom and Dad. To my siblings Lauren, Seth, and Aubrey, thank you for your support, understanding, and encouragement. Finally, without the love, support, patience, and friendship of my wife, Jamie, this would not be possible. I am incredibly grateful that you have sacrificed so much so that I can pursue a dream. I consider it a blessing and privilege to undertake this journey alongside you.

Dynamic Photo-tunable Hydrogels for Temporal Modulation of Matrix Mechanical Properties

Ryan Scott Stowers, Ph.D.

The University of Texas at Austin, 2014

Supervisor: Laura J. Suggs

The extracellular matrix is highly influential in regulating cell fate and function in vivo. Biophysical cues from the microenvironment are involved in nearly every cellular phenomenon, from initial embryogenesis to diseases such as atherosclerosis and cancer. This dissertation seeks to develop 3D hydrogel models to more accurately recapitulate the in vivo microenvironment by allowing for temporal modulation of stiffness. A strategy is presented to spatially and temporally tune the mechanical properties of 3D alginate-based hydrogels using a light-triggered mechanism. This approach is demonstrated to be cytocompatible and highly tunable. The system is employed to elucidate the morphological response of fibroblasts to stiffening 3D environments. Additionally, the platform is translated to an in vivo application of transdermal gel modulation. Finally, the phototunable hydrogels are used to evaluate the effect of matrix stiffening on breast epithelial cells in a mechanical environment that mimics tumor stiffening. Changes in the mechanical properties of the gel induce phenotypic changes to MCF10A epithelial cells, including collective cell migration from the mammary acini. This system is broadly applicable to the biomaterials community and could shed light on a number of outstanding biological questions.

Table of Contents

List of Figures

Chapter 1: Introduction

"A model is a lie that helps you see the truth"

– Howard Skipper

1.1 In vivo cellular microenvironment

Biomaterial models of the extracellular matrix (ECM) are necessary to gain a more in depth understanding of basic biology. In vitro models can be used to elucidate mechanisms that are difficult to determine in vivo, either because of the complexity involved in controlling and isolating variables in living animals or because of technological limitations. Further, biomaterials that mimic the native ECM can be used to direct cells for therapeutic purposes. The fields of tissue engineering and regenerative medicine rely on biomaterials systems to maintain cell viability, promote stem cell differentiation, or stimulate therapeutic paracrine secretion. Ultimately, our understanding of cell biology and the advancement of biomaterials are intricately coupled. Knowledge gained from cell biology can inform design of biomaterials platforms, while advancement of more sophisticated systems allows for new investigations of biological hypotheses. For these reasons, biomaterials platforms that more accurately resemble the native ECM must be developed.

In vivo, cells reside in a complex and dynamic microenvironment. Each individual cell is in contact with neighboring cells through cell-cell junctions and with the ECM through a number of adhesion molecules. The cell is coupled physically through receptors and biochemically through signaling molecules in the microenvironment and downstream signaling of the bound adhesion sites (1). The cell and its neighbors are continuously signaling to one another and dynamically remodeling their microenvironment (2). This complex scenario represents the most simplistic situation

found physiologically and does not account for major events that alter the homeostasis such as wound healing, tumor development, or myocardial infarction. Yet, it remains exceedingly challenging to develop accurate and predictive recapitulations of even the most simplistic in vivo scenarios, much less complex disease models. However, major advances are being made in the biomaterials field to generate more realistic and predictive model systems (3).

The composition and organization of the ECM must be well understood before attempts to create engineered ECM-equivalents are undertaken. The ECM is primarily composed of two classes of macromolecules, fibrous proteins and polysaccharides (4). The most abundant protein in the ECM is collagen, of which 28 distinct types have been discovered. The majority of collagen in the body is type I collagen, which forms a linear, triple helical fibril (5). These fibrils can aggregate into large fiber bundles to provide tensile strength to the ECM. Elastin, fibronectin, and laminin are also primary components of the ECM and function to provide elasticity, cell adhesion, and basal support to epithelial cells respectively. Glycosaminoglycans (GAGs) constitute the main polysaccharide component of the ECM. GAGs are unbranched chains of disaccharides units. GAGs are very negatively charged as they are highly decorated with sulfate and carboxylate groups. The negative charges attract cations like Na^+ and thus water through osmosis. This effect, combined with an inherent hydrophilicity, causes a GAG network to be highly hydrated. GAGs form gels even at low concentrations, and the large amount of incompressible water provides good compressive resistance. As a composite of protein fibers and the GAG network, the ECM is structured to be robust to physical deformations. Protein fibers act as cables to resist tensile deformations, while the GAG network provides resistance to compressive forces. The proportion of specific proteins and polysaccharides largely dictates the mechanical properties of the tissue. For example,

the high tensile strength of tendon is produced by highly organized collagen fiber bundles, while cartilage's great compressive strength is imparted by the high proportion of hydrated GAGs. Cells are responsible for maintaining and remodeling the ECM, and therefore play an active role in regulating tissue mechanical properties. Interestingly, cells are also highly influenced by the mechanical properties of the ECM; establishing a dynamic reciprocity between cells and the ECM.

1.2 BIOPHYSICAL CUES INFLUENCE CELLS

1.2.1 Cell phenotype is regulated by matrix stiffness through mechanotransduction

Biochemical signaling has been thoroughly investigating since the advent of in vitro biology. Relatively recently, biophysical cues have been recognized to be as important in dictating cellular phenotype. Much of the seminal work has been borne out of novel biomaterials systems to investigate how cells interpret biophysical signals, such as shear stress or matrix stiffness. Early work established that cells are capable of mechanosensing, or feeling the stiffness of the substrate on which they are plated (6). These studies showed that many phenotypic traits of the cells such as morphology, migration, and proliferation were regulated, at least in part, by the stiffness of the underlying substrate (6-9). The cells adhere to the substrates through membrane bound receptors that recognize peptide sequences in ECM proteins, which are attached to the substrate of interest. These membrane-bound receptors belong to four families, integrins, cadherins, selectins, and immunoglobulin-like cell adhesion molecules (10). Of these receptors, integrin binding and signaling has been extensively studied and is best understood (11). Upon binding to an adhesion peptide, intracellular mechanotransduction proteins aggregate at the cytoplasmic integrin domain and are activated (12). Integrins are linked to the actin cytoskeletal network through talin, vinculin, and other adapter proteins

and thus, the cell is able to generate tension against the adhesive ligand by actomyosin contraction (13). The cell is able to sense the stiffness of the substrate by the amount of traction force it generates during this process. Cells can alter the number of integrin binding sites and can cluster integrins at specific sites to form focal adhesions or focal complexes (14). These sites mature through a complex but well-established signaling cascade and are involved in a number of potent signaling pathways (14). Cellular mechanotransduction will be discussed in more detail in Chapter 3, but it is important to note the strong influence that sensation of substrate stiffness has on cellular phenotype. Fibroblasts (and later other cells) have been shown to spread more on stiff substrates, as they are able to generate more tension throughout the cell body (6, 15). Cells migrate faster on stiff substrates, and migrate toward stiffer regions of a gradient; a phenomenon known as durotaxis (16).

1.2.2 Matrix stiffness directs stem cell fate

In addition to dictating cell shape and locomotion, substrate stiffness has been shown to dictate stem cell lineage commitment. Engler et al. demonstrated that mesenchymal stem cells (MSC) differentiate toward cell types that mimic that stiffness of the substrate on which they are seeded (17). Soft substrates, similar in stiffness to brain tissue (0.1-1 kPa) drove differentiation toward neural cell types, while intermediate (8-17 kPa) and stiff (25-40 kPa) substrates promoted myogenic and osteogenic differentiation respectively. This result is particularly intriguing because of the potential use in designing tissue engineering scaffolds to direct stem cell differentiation based on material properties. Later, similar investigations with different progenitors cell sources revealed similar, and in some cases very specific, differentiation programs based on substrate stiffness (18, 19). Soft substrates also appear to be essential for maintaining multipotency

in a population of progenitors cells (20). When cultured on stiff substrates, these cells typically establish a lineage commitment. In the physiological context, this result is intriguing as stem cells are generally found in soft microenvironments, such as bone marrow, adipose tissue, and dental pulp (21-23). Due to this foundational work, substrate or matrix stiffness is generally considered in the context of every new biomaterial report.

1.3 NECESSITY OF THREE-DIMENSIONAL MODELS

It is important to note that most of the seminal reports on cellular mechanotransduction were performed in two-dimensional experimental contexts (6, 15). In these experiments, a substrate with variable stiffness, usually polyacrylamide, is polymerized to the desired stiffness. Adhesion proteins or peptides are conjugated to the surface of these substrates for the cells to bind. While much has been gained from this reductionist approach, it does a poor job of recapitulating the *in vivo* cellular microenvironment for several reasons (24). First, the cells are adherent to only one plane, a geometry almost never seen in vivo (the exceptions include a subset of epithelial cells, and even in these cases a simplified system does not replicate the true biophysical environment). The cells are forced to adopt a polarized morphology in which one side of the cell is adherent while the other is free and exposed to culture media. Cell-cell contacts, if they exist, are maintained only in a thin perimeter shared by neighboring cells. Secondly, these 2D gel systems generally have a uniform distribution of a singular adhesion peptide or protein. In vivo microenvironments, on the contrary, have varied protein composition and differential spacing of ligands. Ligand density and distribution are known to play a major role in mechanosensing (25, 26). For instance, the morphological response of a cell to substrate stiffness is a function of the concentration of ligands on the surface (25). The relationship between cell spreading and ligand density

generally increases to a maximum and then decreases moderately (25). The relationship is non-linear, dependent on stiffness, and varies for different cell types. These complex relationships can be determined in simplified 2D geometries with one adhesive ligand species relatively easily, but scaling up to 3D environments with dozens of proteins that are being dynamically remodeled is not realistic given our current understanding and technology. Nonetheless, advances in cell biology and biomaterials are enabling an increase in knowledge of how cells interact with their microenvironment in realistic in vivo-like situations.

In order to more accurately recapitulate the in vivo microenvironment, three-dimensional platforms are necessary. Hydrogels, which are crosslinked networks of polymer chains swollen in water, are well-suited for use as ECM mimicking systems as they can be made with similar mechanical properties, such as stiffness and viscoelasticity to native tissues, have network pore size and crosslinking densities close to protein networks, and are well hydrated (27, 28). Most hydrogel properties are dictated primarily by the network crosslink density (ϱ), including the gel modulus (eq. 1), swelling ratio (eq. 2), diffusion of solutes (eq. 3) (29, 30). Thus, the ability to tune or control crosslink density is sought after by biomaterials scientists in all material systems.

$$G = RT\rho_x Q^{-1/3} \quad (1)$$

$$Q = \rho_x^{-3/5}\left(\frac{\frac{1}{2}-2X_1}{V_1}\right)^{3/5} \quad (2)$$

$$D = D_o\left(1-\frac{r_s}{\xi}\right)e^{\left(-Y\left(\frac{v_2}{1-v_2}\right)\right)} \quad (3)$$

1.4 HYDROGEL DESIGN STRATEGIES

Hydrogels were initially designed to simply maintain cellular viability. Biomaterials researchers worked to establish polymer systems and crosslinking

chemistries that would be compatible with cell culture. Many of these early systems relied upon natural polymers, especially proteins, that could be reconstituted and gelled either through enzymatic crosslinking (fibrinogen to fibrin), or temperature and/or pH switching (Matrigel, collagen) (31). These protein-based gels are excellent for replicating the native ECM as they form a network of protein fibers very similar to the in vivo environment. Additionally, they present recognizable adhesion ligands and degradable peptide sequences for cell interactions. However, there are a few drawbacks, most notably the lack of control, tunability, and consistency of various properties such as stiffness, degradation, and pore size (31). Further, there are issues associated with purification and immunogenicity of proteins derived from animal or human tissue. Recombinant proteins are being developed in many cases to resolve some of these issues (32). However, in light of challenges associated with natural protein gels, bioengineers began to develop synthetic, engineered hydrogels as alternatives. In many cases, control of the systems can be increased while still accurately replicating essential features of the in vivo microenvironment (33).

The first engineered networks incorporated proteins or biologically relevant peptide sequences into synthetic polymer networks. One common platform used for this is polyethylene glycol diacrylate (PEGDA), which can be gelled via photopolymerization (34). Briefly, a photoinitiator is exposed to ultraviolet light to produce a free radical and induce radical polymerization of the PEGDA chains. Multiarm PEG chains are used to generate a crosslinked network of polymer chains (35). The PEG chains can be modified with peptide sequences to promote cell adhesion or degradation to incorporate biological functionality (36, 37). Much of this early work was pioneered in the Hubbell laboratory, and has since been expanded to incorporate adhesion sequences derived from fibronectin (RGD, KQAGDV, REDV, PHSRN), laminin (YIGSR, LGRIPG, IKVAV, PDGSR, LRE,

LRGDN, IKLLI), collagen (DGEA, GFOGER), and elastin (VAPG) (38). Enzymatically degradable sequences for collagenase (GPQG_IAGQ, GPQB_IWGQ, APG_L, L_GPA), plasmin (YK_NRD, VR_N) and elastase (AAPV_RGGG, AAAAAAA) have been incorporated into PEG hydrogel backbones to allow for cell-mediated degradation and migration (38). Hydrogels such as these that were engineered to allow for cellular interactions provided avenues for novel inquiries into how cells sense and respond to their microenvironments. However, in these systems, the cells, and not the researcher govern interaction with and degradation of the matrix. Later, more advance hydrogels were developed to allow for directed environmental manipulations or modulations, which will be discussed in the next section.

1.5 DYNAMIC HYDROGELS

1.5.1 Dynamic biochemical hydrogels

In an effort to more closely mimic the dynamic microenvironment in which cells reside in vivo, researchers have sought to engineer temporal tunability into hydrogel systems. Primarily, these efforts have been dedicated toward developing either dynamic biochemical or biophysical cues. The West lab demonstrated both spatial and temporal control of RGD peptide conjugation using a PEGDA gel platform (39). The gel chemistry was engineered to leave a small fraction of reactive groups available after gelation. RGD sequences linked to an acryl-PEG chain could be swelled into the gels at a particular timepoint and selectively exposed to light to couple the peptide to the gel network. This light-based approach is advantageous because of the spatial resolution that can be achieved by optical or photomasking techniques. Using similar concepts, others have coupled full proteins within agarose gels using caged thiols and maleimide chemistry (40), and click chemistry to couple peptides, proteins, or small molecules with excellent

spatial resolution via multiphoton excitation (41-43). Notably, the click chemistry techniques are biocompatible and can be performed in the presence of cells, which is the ultimate goal for dynamic hydrogel systems. One concern with these dynamic biochemical techniques is that the protein or peptide of interest most be swollen into the gel at very high concentrations temporarily to couple them to the network. The proteins can be sufficiently washed out, but even brief exposures to high concentrations of growth factors can have significant impacts of cell fate and phenotype. New strategies to achieve spatial and temporal control of biochemical cues without universal saturation are needed, perhaps by delivering molecules that are inaccessible to cells before desired in vesicles.

1.5.2 Dynamic biophysical hydrogels

1.5.2.1 Hydrogel softening through passive degradation

Strategies to temporally modulate hydrogel biophysical properties must ultimately introduce or remove crosslinks from the hydrogel network. Degradation, either hydrolytic or enzymatic, was the first manifestation of dynamic modulation of gel mechanical properties (29). As the gels are degraded, they are inherently more compliant, due to the decreased crosslinking density. Initially, hydrogel degradation was simply a byproduct of using protein-based gels, but was later exploited by engineering hydrolytic sequences in the backbone of a PEG-based network. For instance, polylactic acid (PLA)-PEG-PLA monomers could be crosslinked together. Over time, the PLA units would hydrolyze, resulting in a controlled degradation of the gels (44). This approach was applied to other polymers and has been extensively studied to develop kinetic models of degradation (45, 46). However, the degradation rate must be determined *a priori* and is not tunable after the initial gelation event. For this reason, researchers sought a greater degree of control of hydrogel degradation.

Enzyme cleavable peptide sequences are one alternative to hydrolytically degradable units. These peptide sequences can be designed with relatively good specificity for enzymes of interest (collagenase, plasmin, matrix metalloproteinases, etc.) and allow for dynamic cellular interaction with the hydrogel network (37, 38). These networks more closely resemble the protein networks seen by cells in vivo, as the hydrogel chains must be either degraded or deformed for cell growth or migration. Additionally, the rate of degradation is dictated by cells, unlike hydrolytically degradable systems that must be tuned *a priori* for a particular rate.

1.5.2.2 Dynamic softening through photocleavage

A more recent strategy that allows for a greater degree of control for the experimenter is to employ light to soften hydrogels. The Anseth group introduced this novel concept with an engineered PEG-based hydrogel platform that incorporated photolabile groups within the hydrogel network (47). Upon irradiation with UV or visible light, the groups cleave, resulting in a decrease in crosslinking density and thus a more compliant gel. Supreme temporal control was demonstrated with both continuous and intermittent exposure. Additionally, this technique is amenable to multiphoton excitation, making possible the modulation of gel stiffness with fine resolution in three dimensions. Finally, the ability to tune the gel mechanics in the presence of cells allowed the group to demonstrate the dynamic nature of cellular mechanosensing in myofibroblast differentiation (48, 49) and stem cell mechanical memory (50).

1.5.2.3 Dynamic stiffening through kinetically slow crosslinking

Physiologically, matrix stiffening occurs in a number of important processes and diseases including wound healing, fibrosis, tumor progression, and atherosclerosis. Until very recently, there were no hydrogel platforms that could be dynamically stiffened over

time to mimic these physiological events. Dynamic stiffening requires a system that will introduce additional crosslinks within an existing network, which is a challenging design parameter. In order to introduce new crosslinks, new polymer chains, monomers or crosslinkers must be introduced to the gel in situ. Given the small pore size of many systems and the cytotoxicity associated with many monomers and initiators, especially photoinitiators, these strategies are not tractable in the presence of cells. However, a few promising platforms have emerged recently and much work is devoted toward this goal by the hydrogel biomaterials community currently.

During development, tissue stiffness changes greatly as cell remodel that ECM toward developing tissues. For example, the developing myocardium undergoes a 9-fold increase in stiffness. The Engler group has developed a hydrogel platform to mimic both the timing and magnitude of change in the developing myocardium and used this system to evaluate the effects on differentiation toward mature cardiomyocytes compared to a static gel control (51). The system is based on thiolated hyaluronic acid and PEGDA, which results in a kinetically slow Michael-type addition. The reaction kinetics could be tuned to accelerate or slow down the stiffening rate, and the initial and final moduli could be tuned based on the component ratios. For the formulation that most closely mimics myocardial development, the group saw an increase in mature cardiac markers and aligned myofibrils. This finding demonstrates the importance of mimicking temporal stiffness with hydrogel platforms, and other groups are developing strategies to increase control and stiffness range of stiffening hydrogels.

1.5.2.4 Dynamic stiffening through light-triggered secondary crosslinking

One promising strategy is to use light to trigger additional hydrogel crosslinking, which would allow for precise spatial and temporal tuning. The Burdick lab has

developed such a system that allows for secondary, light-triggered crosslinking in the presence of cells (52). Hyaluronic acid (HA) was modified with methacrylate (Me) groups, which can react with either thiols or free radicals to crosslink the network. The primary hydrogel network was formed by mixing the MeHA solution with dithiothreitol (DTT), resulting in a uniformly crosslinked hydrogel. At a later time, a photoinitiator could be swollen into the network and exposed to UV light to crosslink any remaining, unreacted methacrylate groups. Using this strategy, gels could be stiffened from an initial storage modulus of ~80 Pa to a final G' of ~1000 Pa. MSCs were shown to differentially differentiate based on the timing of stiffening. Stiffening that occurred within the first 3 days of culture promoted osteogenic differentiation, while stiffening at day 7 produced nearly equal number of adipogenic and osteogenic cells; suggesting that substrate stiffness and timing are essential to directing cell fate. Future work must be aimed at developing hydrogel platforms, either with existing platform or novel strategies, to incorporate temporal stiffness modulation, especially the ability to stiffen.

1.6 OVERVIEW

In this work, we will present a novel strategy to modulate the stiffness of 3D alginate hydrogels with light, and explore the utility of this platform in several applications. Chapter 2 will present the platform technology, which consists of alginate as the hydrogel base polymer, temperature-sensitive liposomes encapsulating calcium ions, and gold nanorods to convert light to heat. All together, the gold nanorods are excited by a near-infrared laser which cause a phase transition in the lipid bilayer, releasing calcium into the alginate network to increase the crosslinking density and thus stiffness. The chapter will present optimization and characterization of the system components and proof-of-concept experiments of light triggered release. Temporal stiffening and

softening of 3D hydrogels will be demonstrated, and spatial localization of the technique will be presented. In chapter 3, the cytocompatibility of this system will be presented. This platform will be employed to investigate the change in fibroblast morphology in 3D stiffening microenvironments. Additionally, the system will be translated to a transdermal application to show the potential for stiffness modulation *in vivo*. Chapter 4 will present a disease-specific application by employing the in vitro stiffening system to investigate the effects of matrix stiffening on breast epithelial cells. The hypothesis that matrix stiffening that occurs during tumor development can itself contribute to disease progression will be explored by stiffening the microenvironment around MCF10A cells and evaluating any phenotypic changes toward malignancy. Chapter 5 will summarize the presented research as a whole and recommended future work or other avenues of application for this technology.

1.7 REFERENCES

1. Hynes RO (2009) The extracellular matrix: not just pretty fibrils. *Science* 326(5957):1216-1219.

2. Lu P, Takai K, Weaver VM, & Werb Z (2011) Extracellular matrix degradation and remodeling in development and disease. *Cold Spring Harbor perspectives in biology* 3(12).

3. Huebsch N & Mooney DJ (2009) Inspiration and application in the evolution of biomaterials. *Nature* 462(7272):426-432.

4. Frantz C, Stewart KM, & Weaver VM (2010) The extracellular matrix at a glance. *Journal of cell science* 123(Pt 24):4195-4200.

5. Alberts BJ, A. Lewis, J. Raff, M. Roberts, K. Walter, P. (2007) *Molecular Biology of the Cell* (Garland Science) 5th Ed.

6. Pelham RJ & Wang Y-L (1997) Cell locomotion and focal adhesions are regulated by substrate flexibility. *Proceedings of the National Academy of Sciences of the United States of America* 94:13661-13665.

7. Lo C-M, Wang H-B, Dembo M, & Wang Y-L (2000) Cell Movement is Guided by the Rigidity of the Substrate. *Biophysical journal* 79:144-152.

8. Saez A, Ghibaudo M, Buguin A, Silberzan P, & Ladoux B (2007) Rigidity-driven growth and migration of epithelial cells on microstructured anisotropic substrates. *Proceedings of the National Academy of Sciences of the United States of America* 104(20):8281-8286.

9. Ulrich TA, de Juan Pardo EM, & Kumar S (2009) The mechanical rigidity of the extracellular matrix regulates the structure, motility, and proliferation of glioma cells. *Cancer research* 69(10):4167-4174.

10. Pardi R (2010) Signal Transduction by Adhesion Receptors. *Nature Education* 3(9):38-44.

11. Barczyk M, Carracedo S, & Gullberg D (2010) Integrins. *Cell and tissue research* 339(1):269-280.

12. Ingber DE (2006) Cellular mechanotransduction: putting all the pieces together again. *FASEB journal : official publication of the Federation of American Societies for Experimental Biology* 20(7):811-827.

13. Critchley DR (2000) Focal adhesions- the cytoskeletal connection. *Current opinion in cell biology* 12:133-139.

14. Geiger B, Bershadsky AD, Pankov R, & Yamada KM (2001) Transmembrane Extracellular Matrix-Cytoskeleton Crosstalk. *Nature reviews. Molecular cell biology* 2:793-805.

15. Yeung T, *et al*. (2005) Effects of substrate stiffness on cell morphology, cytoskeletal structure, and adhesion. *Cell motility and the cytoskeleton* 60(1):24-34.

16. Discher DE, Janmey P, & Wang YL (2005) Tissue cells feel and respond to the stiffness of their substrate. *Science* 310(5751):1139-1143.

17. Engler AJ, Sen S, Sweeney HL, & Discher DE (2006) Matrix elasticity directs stem cell lineage specification. *Cell* 126(4):677-689.

18. Saha K, *et al*. (2008) Substrate modulus directs neural stem cell behavior. *Biophysical journal* 95(9):4426-4438.

19. Gilbert PM, *et al*. (2010) Substrate elasticity regulates skeletal muscle stem cell self-renewal in culture. *Science* 329(5995):1078-1081.

20. Skardal A, Mack D, Atala A, & Soker S (2013) Substrate elasticity controls cell proliferation, surface marker expression and motile phenotype in amniotic fluid-derived stem cells. *Journal of the mechanical behavior of biomedical materials* 17:307-316.

21. Grove JE, Bruscia E, & Krause DS (2004) Plasticity of Bone Marrow-Derived Stem Cells. *Stem cells* 22:487-500.

22. Bunnell BA, Flaat M, Gagliardi C, Patel B, & Ripoll C (2008) Adipose-derived stem cells: isolation, expansion and differentiation. *Methods* 45(2):115-120.

23. Gronthos S, Mankani M, Brahim J, Robey PG, & Shi S (2000) Postnatal human dental pulp stem cells (DPSCs) in vitro and in vivo. *Proceedings of the National Academy of Sciences of the United States of America* 97(25):13625-13630.

24. Schwartz MA & Chen CS (2013) Deconstructing dimensionality. *Science* 339(6118):402-404.

25. Engler AJ, *et al*. (2004) Substrate compliance versus Ligand Density in Cell on Gel Responses. *Biophysical journal* 86:617-628.

26. Maheshwari G, Brown G, Lauffenburger DA, Wells A, & Griffith LG (2000) Cell adhesion and motility depend on nanoscale RGD clustering. *Journal of cell science* 113:1677-1686.

27. Tibbitt MW & Anseth KS (2009) Hydrogels as extracellular matrix mimics for 3D cell culture. *Biotechnology and bioengineering* 103(4):655-663.

28. Peppas NA, Hilt JZ, Khademhosseini A, & Langer R (2006) Hydrogels in Biology and Medicine: From Molecular Principles to Bionanotechnology. *Advanced materials* 18:1345-1360.

29. DeForest CA & Anseth KS (2012) Advances in bioactive hydrogels to probe and direct cell fate. *Annual review of chemical and biomolecular engineering* 3:421-444.

30. Vats K & Benoit DS (2013) Dynamic manipulation of hydrogels to control cell behavior: a review. *Tissue engineering. Part B, Reviews* 19(6):455-469.

31. Trappmann B & Chen CS (2013) How cells sense extracellular matrix stiffness: a material's perspective. *Current opinion in biotechnology* 24(5):948-953.

32. Lutolf MP & Hubbell JA (2005) Synthetic biomaterials as instructive extracellular microenvironments for morphogenesis in tissue engineering. *Nature biotechnology* 23(1):47-55.

33. Hubbell J (1999) Bioactive biomaterials. *Current opinion in biotechnology* 10:123-129.

34. Sawhney AS, Pathak CP, & Hubbell JA (1993) Bioerodible Hydrogels Based on Photopolymerized Poly(ethylene glycol)-co-poly(a-hydroxyacid) Diacrylate Macromers. *Macromolecules* 26:581-587.

35. Kloxin AM, Kloxin CJ, Bowman CN, & Anseth KS (2010) Mechanical properties of cellularly responsive hydrogels and their experimental determination. *Advanced materials* 22(31):3484-3494.

36. Hern DL & Hubbell JA (1998) Incorporation of adhesion peptides into nonadhesive hydrogels for tissue resurfacing. *J Biomed Mater Res* 39:266-276.

37. West JL & Hubbell J (1999) Polymeric Biomaterials with Degradation Sites for Proteases Involved in Cell Migration. *Macromolecules* 32:241-244.

38. Zhu J (2010) Bioactive modification of poly(ethylene glycol) hydrogels for tissue engineering. *Biomaterials* 31(17):4639-4656.

39. Hahn MS, Miller JS, & West JL (2006) Three-Dimensional Biochemical and Biomechanical Patterning of Hydrogels for Guiding Cell Behavior. *Advanced materials* 18:2679-2684.

40. Luo Y & Shoichet MS (2004) A photolabile hydrogel for guided three-dimensional cell growth and migration. *Nature materials* 3(4):249-253.

41. DeForest CA, Polizzotti BD, & Anseth KS (2009) Sequential click reactions for synthesizing and patterning three-dimensional cell microenvironments. *Nature materials* 8(8):659-664.

42. DeForest CA & Anseth KS (2011) Cytocompatible click-based hydrogels with dynamically tunable properties through orthogonal photoconjugation and photocleavage reactions. *Nature chemistry* 3(12):925-931.

43. DeForest CA & Anseth KS (2012) Photoreversible patterning of biomolecules within click-based hydrogels. *Angewandte Chemie* 51(8):1816-1819.

44. Metters A, Bowman CN, & Anseth KS (2000) A Statistical Kinetic Model for the Bulk Degradation of PLA-b-PEG-b-PLA Hydrogel Networks. *J Phys Chem B* 104:7043-7049.

45. Martens P, Metters A, Anseth KS, & Bowman CN (2001) A Generalized Bulk-Degradation Model for Hydrogel Networks Formed from Multivinyl Cross-linking Molecules. *J Phys Chem B* 105:5131-5138.

46. Metters A & Hubbell J (2005) Network formation and degradation behavior of hydrogels formed by Michael-type addition reactions. *Biomacromolecules* 6(1):290-301.

47. Kloxin AM, Kasko AM, Salinas CN, & Anseth KS (2009) Photodegradable hydrogels for dynamic tuning of physical and chemical properties. *Science* 324(5923):59-63.

48. Wang H, Haeger SM, Kloxin AM, Leinwand LA, & Anseth KS (2012) Redirecting valvular myofibroblasts into dormant fibroblasts through light-mediated reduction in substrate modulus. *PloS one* 7(7):e39969.

49. Wang H, Tibbitt MW, Langer SJ, Leinwand LA, & Anseth KS (2013) Hydrogels preserve native phenotypes of valvular fibroblasts through an elasticity-regulated PI3K/AKT pathway. *Proceedings of the National Academy of Sciences of the United States of America* 110:19336-19341.

50. Yang C, Tibbitt MW, Basta L, & Anseth KS (2014) Mechanical memory and dosing influence stem cell fate. *Nature materials* 13(6):645-652.

51. Young JL & Engler AJ (2011) Hydrogels with time-dependent material properties enhance cardiomyocyte differentiation in vitro. *Biomaterials* 32(4):1002-1009.

52. Guvendiren M & Burdick JA (2012) Stiffening hydrogels to probe short- and long-term cellular responses to dynamic mechanics. *Nature communications* 3:792.

Chapter 2: Hydrogel Photo-Tuning via Near Infrared Light

2.1 INTRODUCTION

2.1.1 Engineering goals for dynamic hydrogels

The ideal hydrogel platform for dynamically modulating hydrogel stiffness would allow for changes in stiffness over a wide range of time periods, magnitudes, and with excellent spatial control. This system would also alter stiffness independently of other factors that influence cells, such as ligand density or protein concentration. The ability to remotely induce a stiffness change in a cytocompatible manner is also necessary. Finally, it would be beneficial to design a dynamic system with physically crosslinked polymer networks, as these are more representative of the native ECM than covalently crosslinked gels. While much progress has been made in developing dynamic hydrogel over the last several years, the current platforms all fail to meet these criteria at one or more points. In particular, the current systems all rely on covalent crosslinking to form the initial gel and to induce secondary crosslinking, in the case of stiffening systems. Cells interact differently in physically, rather than covalently crosslinked gels, especially with regard to mechanotransduction. For example, matrix stiffness regulates stem cell fate in 3D physically crosslinked gels (1), while cell fate has been shown to be completely independent of matrix stiffness in covalently crosslinked systems (2). Since the native ECM is better represented by physically crosslinked networks, we aim to develop a dynamic platform using physically crosslinked alginate hydrogels.

2.1.2 Alginate hydrogels

Alginate is a naturally derived anionic polymer that has been used in numerous biomedical applications because of its biocompatibility, low cost, and simple gelation (3). It is a linear copolymer of (1,4)-linked β-D-mannuronate (M) and α-L-guluronate (G)

residues. Consecutive G-blocks are able to form crosslinks with divalent cations, causing the alginate solution to gel (Fig. 2.1B) (4). The ratio of mannuronate to guluronate residues (M/G) significantly affects the properties of a crosslinked alginate gel. Additionally, the polymer molecular weight and related viscosity influence the mechanical properties of these gels. Alginate has been used as a biomaterial for cell encapsulation since at least 1981 (5) and in humans for over 20 years (6, 7). In vivo studies have demonstrated that alginate has outstanding cytocompatibility and low immunogenicity. Alginate disks have been implanted in vivo and maintained their geometry and mechanical properties for up to 3 months (8). Alginate gels can dissolve through ion exchange, though this effect is diminished greatly with high-G content alginates and in the presence of solutions containing physiological concentrations of calcium ions (8). When purified, alginate has been shown to induce no foreign body reaction when implanted into mammals (9). Further, alginate is currently used in FDA approved products or in clinical trials for islet encapsulation, stem cell delivery, bone void fillers, urinary stent coatings, lung sealants, and adhesion barriers (10).

Alginate is crosslinked by physical interactions of negatively charged groups on the alginate chain with positively charged divalent ions. This interaction causes two neighboring alginate chains to become ionically bound to one another. With increasing concentration of divalent cations, more of these crosslinks are formed and the stiffness of the resulting hydrogel is increased (3). The physical crosslinks are also readily reversible by chelation of divalent ions from the alginate crosslinks (4). These two properties, concentration dependent stiffness and crosslink reversibility, make alginate an ideal candidate for developing a temporally dynamic hydrogel platform. Essentially, if the presentation of divalent ions or chelators can be temporally controlled, the gel stiffness will also fall under this control mechanism.

Another feature of alginate that makes it well suited for dynamic stiffness modulation is that it is inert to cellular interactions. Alginate does not possess any cell binding domains, and mammalian cells do not express alginase, the enzyme that degrades alginate (3, 11). This provides bioengineers a blank slate that can be readily modified to fit the experimental parameters desired. Adhesion peptides, such as RGD or YIGSR, have been conjugated to alginates chains to provide sites for cell anchorage, allowing for investigations of specific binding domains (11, 12). Alginate has also been blended with adhesion proteins, like fibronectin (13), or matrix fiber forming proteins, like collagen I (14, 15) or Matrigel (16). In both cases, ligand density can be varied by altering the concentration of peptides or proteins, while matrix stiffness is independently held constant with the divalent cation concentration. Likewise, matrix stiffness can be varied with calcium concentration while adhesion ligand density is held constant. The ability to independently tuned these variables in well controlled experiments is not possible with other natural hydrogel systems, where ligand density and stiffness are both functions of protein concentration. Systems have been designed to independently study the effect of matrix stiffness and ligand density on stem cell differentiation and epithelial cell phenotypic conversion and invasion in alginate-based gels (1, 16). Both properties independently contribute to cell fate decisions in stem cells and emergence of a malignant phenotype in normal breast epithelial cells, and are likely influential in many cellular processes. The use of alginate-based gels to independently isolate these effects will provide a greater understanding of cellular mechanotransduction. Additionally, calcium release systems could be developed to explore the influence of matrix stiffness and ligand density under dynamic control. We intend to demonstrate the utility such as strategy here.

2.1.3 Liposomes for dynamic systems

The approach we have chosen relies on light-triggered calcium release from temperature-sensitive liposomes. Liposomes are self-assembled vesicles composed of phospholipid bilayers. The observation that phospholipids undergo bilayer formation in aqueous solutions was first reported by Bangham in 1964 (17, 18). Since this discovery, liposomes have been widely employed as drug delivery vehicles due to their biocompatibility, amphiphilic nature (to carry hydrophobic and/or hydrophilic molecules), and improved circulation time compared to free drugs (19, 20). Liposomes can be formed as small as tens of nanometers, or as large as tens of micrometers (21, 22). They can have a single lipid bilayer, termed unilamellar, or have dozens of concentric bilayers; or multilamellar (23). Conjugation chemistry allows for modification of the bilayer properties; for instance, attaching a PEG group to deter macrophage uptake or increase circulation time *in vivo* (24). Most importantly for this work, liposomes can be developed to release their cargo upon exposure to light, which provides supreme spatial and temporal control of biomolecules.

Light-triggered liposomal release most generally utilizes photons to alter the structure or properties of the lipid bilayer, either directly or indirectly through an intermediary agent. Broadly, these light-triggered release techniques can be categorized as either photochemical or photophysical in nature (25). Photochemical release utilizes energy delivered by light exposure to induce a chemical change in the lipid bilayer. The change could be isomerization of a molecule embedded in the bilayer that alters the bilayer structure upon conformational change (26), cleavage of an amphipathic molecule to separate bilayer entities by polarity (27), or polymerization to destabilize the bilayer (28). Photochemical techniques require high energies to induce chemical changes and thus generally rely on UV light (25). Exposure to UV is not ideal for biological

applications because of its toxicity and low penetration depth, and a near infrared alternative is desired.

Photophysical release mechanisms can be designed for use with near infrared light, and thus more attractive than UV triggered methods. These approaches utilize absorbers that convert light to thermal energy, and induce changes in bilayer diffusive properties or mechanically disrupt the membrane (25). Molecular absorbers can be encapsulated in the aqueous compartment or embedded in the lipid bilayer to generate heat upon irradiation (29). Alternatively, plasmon resonant gold nanoparticles can be used to achieve the same effect more efficiently (30). In either case, the thermal energy causes a phase transition of the lipids in the bilayer from an impermeable gel phase to a fluid phase, which has a higher permeability. This concept was demonstrated by embedding or tethering gold nanoparticles to a lipid bilayer and triggering release via irradiation (31). Each species of phospholipid has a specific transition temperature that increases with increasing hydrocarbon tail length, and is significantly higher for saturated than unsaturated lipids. Dipalmitoylphosphatidylcholine (DPPC) has a phase transition at 41ºC, and is often used for biological applications since it is slightly higher than physiological temperature.

Interestingly, plasmon resonant gold nanoparticles can also be used to cause liposomal release via light without significant thermal heating. The Zasadzinski laboratory first demonstrated that membrane disruption via cavitation could be induced by pulsed laser irradiation of hollow gold nanoshells (32). The overall bulk temperature of the solution increased by less than 1ºC during irradiation, as the thermal energy generate was sufficiently dissipated between laser pulses. The group confirmed that cavitation pressure was responsible for releases by irradiating with a continuous wave laser and observing no liposomal release. Thus, using plasmon resonant gold

nanoparticles with liposomes affords researchers two routes to triggered release; heat-induced increase in permeability or mechanical disruption of the vesicle. These routes are tunable based on the gold nanoparticle geometry (sphere, rod, shell, etc), proximity to the lipid bilayer, and irradiation source (continuous wave or pulsed laser).

Our strategy relies upon liposomes encapsulating gold nanorods to trigger vesicle release upon NIR irradiation, and calcium or chelators to modulate the crosslinking density of alginate gels. Previous work has demonstrated the ability to encapsulate and release divalent cations within liposomes. As early as 1977, O'Brien and colleagues incorporated rhodopsin into a lipid membrane and observed an increase in permeability of Mn^{2+}, Co^{2+}, and Eu^{3+} through the membrane upon exposure to light (28). Foundationally to our approach, Messersmith and coworkers were able to encapsulate calcium within temperature-sensitive vesicles (33, 34). The vesicles were composed of a majority DPPC and a variable fraction of DMPC to alter the melting temperature. The liposomes were shown to be metastable in a supersaturated solution of calcium phosphate due to the separation of the membrane. By increasing the temperature above the transition point, calcium was released and inorganic calcium phosphate was formed. Later, these temperature-sensitive liposomes were used to cause gelation of calcium-dependent hydrogel precursors (35, 36). The group demonstrated that after mixing the liposomes with an alginate solution at room temperature, no gelation occurs and the liposomes were stable for several days. By increasing the temperature, gelation occurred rapidly as calcium was released from the vesicles. Additionally, gelation through cleavage of fibrinogen to fibrin was induced by activating a Ca^{2+}-dependent enzyme, FXIII (35). Smith et al. developed a photosensitive liposomes within which calcium can be entrapped and released upon exposure to UV light via isomerization of the lipid tails (36, 37). Using this liposome system, the group demonstrated light-triggered gelation of alginate.

Viability of 3T3 fibroblasts was maintained during irradiation and gelation, and cells that were exposed to UV grew normally when recovered and plated on tissue culture plastic. In summary, prior work has established that calcium can be stably incorporated into lipid vesicles in sufficient concentrations to generate hydrogel formation. Increases in bilayer permeability through the gel-to-fluid phase-transition can provide a route for Ca^{2+} release. Our hypothesis is that combining these liposome advances with gold nanoparticle triggered liposome release would allow remotely triggered, temporal modulation of gel stiffness.

2.1.4 Chapter Overview

In this chapter, we will demonstrate stable loading and light-triggered release of calcium via gold nanorod induced permeabilization of DPPC liposomes. Using this calcium release platform, we induce light-triggered gelation of alginate, and more significantly, light-triggered modulation of 3D gel stiffness. By replacing $CaCl_2$ in the liposomes with a potent calcium chelator, DTPA, we show that alginate gels can be dynamically softened as well. This process is stable over time and highly tunable based on loading, liposome concentration, and irradiation time. Finally, we demonstrate the ability to spatially confine the stiffened gel regions using photolithographic techniques.

2.2 MATERIALS AND METHODS

2.2.1 Gold nanorod synthesis

Gold nanorods were synthesized by the seed-mediated growth mechanism. Cetyl trimethylammonium bromide (CTAB, 200 mM) was mixed with an equal volume of $HAuCl_4$ (0.5 mM) and stirred. Cold $NaBH_4$ (10 mM) was mixed into the solution at 6% v/v and stirred vigorously for 2 minutes, resulting in the seed solution. The growth solution was prepared by mixing 5 mL of CTAB with 200 μ $AgNO_3$ (4 mM), 5 mL of

$HAuCl_4$ (1 mM), and 70 µl of ascorbic acid (78.8 mM). The solution was mixed well at 30ºC. The seed solution was added (12 µl) to the growth solution and stirred for 2 hours. The gold nanorods were washed by centrifuging at 18,000 g for 45 minutes, rinsed in deionized water, and centrifuged again.

2.2.2 Liposome synthesis

1,2-dihexadecanoyl-sn-glycero-3-phosphocholine (DPPC, 50 mg) was dissolved in chloroform at 25 mg/ml in a round bottom flask. The chloroform was evaporated on a rotary evaporator to produce a lipid cake, which was stored in a desiccator overnight. The lipid cake was hydrated with 2 ml deionized water at 55ºC under rotation to yield multilamellar vesicles (MLV). The MLVs were sonicated for 30 minutes at 55ºC to form small unilamellar vesicles. Ethanol (4 M) was added to the SUV suspension to induce interdigitation of the lipid bilayer (38). The lipid sheets were centrifuged twice at 3000 g for 10 minutes and washed in deionized water to remove the ethanol. The pellet of lipid sheets was resuspended in the desired loading solution containing 5% gold nanorods and either 500 mM $CaCl_2$ or 500 mM DTPA. The solution was incubated for 2 hours at 55ºC with intermittent mixing to produce interdigitation fusion vesicles (IFV). After cooling, the IFVs were centrifuged 5 times at 200 g for 10 minutes to remove all the unencapsulated gold nanorods and $CaCl_2$ or DTPA.

2.2.3 Alginate Gels

Pronova UP MVG sodium alginate was dissolved in HEPES buffered 300 mM NaCl to 4% w/v. Uniformly crosslinked alginate gels were made using insoluble $CaCO_3$ as a calcium source, and glucono-δ-lactone (GdL), which hydrolyzes upon dissolution in water to release calcium ions (39). Gels were made from 10 mM $CaCO_3$ up to 30 mM $CaCO_3$ depending on the desired initial stiffness of the gel. The molar concentration of

GdL was always twice that of $CaCO_3$ to maintain a neutral pH. Liposomes were included at 20% of the volume of the gel unless otherwise stated within the experimental context. Gels for rheometry were formed by pipetting the alginate solution into 8 mm polydimethyl siloxane (PDMS) molds. After gelation, the gels were transferred to a 24 well plate and allowed to swell in 1 ml DPBS at least overnight.

2.2.4 Rheometry

Oscillatory shear stress rheometry was performed using an Anton-Paar MCR101 rheometer with an 8 mm parallel plate geometry. The gels were compressed until the entire surface of the measurement tool was covered. Excess gel was trimmed from the perimeter of the tool with a spatula to ensure uniform gel geometries. Frequency and amplitude sweeps (0.1 to 100 Hz, 0.1 to 10% strain) were performed to identify the linear viscoelastic regime, and all data was collected within those bounds. The storage modulus was reported in the text at 1.81 Hz and 1% strain for all samples.

2.2.5 Quantification of calcium loading and release

Arsenazo III was dissolved in 300 mM NaCl buffered with HEPES at 100 μM and used to determine the calcium concentration. $CaCl_2$-loaded liposomes were mixed in equal volume with 5% Triton-X-100 to lyse the vesicles or 300 mM NaCl as a control. 1 μl of this solution was mixed with 199 μl of arsenazo III in a 96-well plate. The absorbance was measured at 655 nm and a standard curve of $CaCl_2$ was used to quantify the release of calcium. The liposome suspension that was lysed with detergent was considered 100% release for comparisons with irradiated samples.

2.2.6 Quantification of DTPA loading and release

Arsenazo III was dissolved in 300 mM NaCl with HEPES buffer. DTPA liposomes were mixed in equal volume with either 5% Triton-X-100 or 300 mM NaCl

buffer. In a 96-well plate, 198 µl of arsenazo III solution was mixed with 1 µl of 20 mM $CaCl_2$ and 1 µl of the liposome solution or 1 µl of a DTPA standard. The absorbance was measured at 655 nm and the concentration of DTPA loaded was determined by comparison with a standard curve of a range of DTPA concentrations.

2.2.7 Transmission electron microscopy

Carbon coated copper 300 mesh grids were glow dischared then dipped into a solution of gold nanorods. The grids were removed and allowed to air dry. An FEI Tecnai transmission electron microscope with an AMT Advantage HR 1kx1k digital camera was used to image the gold nanorods.

2.2.8 Laser irradiation

An 808 nm continuous wave (CW) laser (Laser Lab Components, Inc., 1.4 W) was used to irradiate all the samples. The light was emitted from a 600 μm optical fiber. For 8 mm gels for rheometry, the fluence rate was 1.78 W/cm^2. The gels were irradiated for up to 5 minutes and placed into DPBS at least overnight before performing rheometry. For stiffness gradients, the laser spot size was increased to generate an intensity gradient spanning 1 mm to 3 mm. For stiffness patterning experiments, the light was focused using a plano-convex lens (Thorlabs LMR05). A motorized stage (Thorlabs Z825B) was used to translate a 3D gel slab through the beam at 0.05 mm/s.

2.2.9 Atomic force microscopy

The local stiffness of gels was assessed using an Asylum Research MFP-3D atomic force microscope (AFM). A cantilever with a nominal spring constant of 0.08 N/m and 10 μm borosilicate bead attached to the end was used to indent the samples. The exact spring constant was determined by thermal calibration. The gels were indented at 500 nm/s with a trigger force of 11 nN. The probe was translated across the gel, with

indentations performed every 100-200 μm. At each indentation location, 10-15 force curves were obtained. The elastic modulus was determined using the Hertz model for a sphere (Eq. 1).

$$F = \frac{4}{3} E R^{\frac{1}{2}} d^{\frac{1}{3}}$$

The applied force depends on the elastic modulus of the substrate (E), the radius of the indenting sphere (R), and the distance of indentation (d). The Poisson's ratio was assumed to be 0.5 since the hydrogels are predominantly composed of incompressible water.

2.2.10 Statistical Analysis

Data are presented as mean ± s.d. JMP 10 statistics software was used to analyze the data. Statistical significance was determined using either the Student's t test for comparisons between two groups, or a one-way ANOVA with *post-hoc* Tukey's HSD test for multiple comparisons. P values of less than 0.05 were considered significant.

2.3 Results and Discussion

2.3.1 Liposome Characterization

The overall scheme of the dynamic phototunable hydrogel system relies upon three critical components, (i) alginate, a biopolymer that crosslinks in the presence of divalent cations, (ii) temperature sensitive liposomes that encapsulate calcium and (iii) gold nanorods, which induce heating upon irradiation with NIR light (Fig. 2A,B). DPPC has a gel-to-fluid phase transition temperature of 41ºC. Below 41ºC, a DPPC bilayer will be impermeable to calcium cations; however, above this temperature this bilayer will adopt a fluid phase and allow diffusion of calcium across the membrane. Gold nanorods undergo surface plasmon resonance when irradiated near the absorption peak and this energy is given off as heat locally. Thus, the gold nanorods can be used as a light-

triggering agent so that upon irradiation with NIR light, the DPPC bilayer can be heated past the transition temperature and release calcium. In the presence of alginate, the calcium release will result in an increase in crosslinking density of the polymer chains, either inducing gelation of a solution or an increase in stiffness of a pre-formed gel.

Liposomes were formed using an adaptation of the interdigitation fusion (IF) methods (38) because this process forms for large, unilamellar vesicles within which gold nanorods can be encapsulated. Relatively large vesicles (greater than 1 μm) were desirable because the loading efficiency per lipid is high due to the large volume to surface area ratio. Additionally, the dimensions of the gold nanorods are approximately 15 x 55 nm, which makes passively loading them into smaller vesicles more unlikely.

Multilamellar vesicles (MLV) were formed from a DPPC lipid cake and sonicated to small unilamellar vesicles (SUV). Ethanol was added to the SUV suspension to induce interdigitation of the lipid bilayer. Interdigitation occurs when ethanol displaces water at the bilayer surface, and due to the larger size of ethanol, causes lateral shifting of the lipid head groups and interdigitation of the lipid tails. In this confirmation, it is not energetically favorable for the lipid bilayer to be bent into a tight radius of curvature of the SUV. Thus, the vesicles break apart and form large interdigitated lipid sheets. After removing the ethanol through centrifugation and heating the lipid sheets above the transition temperature, the sheets will form into large unilamellar vesicles, encapsulating the loading solution. In this manner, gold nanorods can be incorporated into these vesicles by suspending them in the heated loading solution.

The concentration of $CaCl_2$ during the loading phase was varied between 100 mM and 1 M to determine the optimal concentration. At 500 mM, the vesicles were found to be loaded with 56 mM $CaCl_2$ assessed with arsenazo III (Fig. 2.2). At this concentration, the only 2% of the calcium was leaked from the vesicle after incubation in DPBS

overnight (Fig. 2.2). Upon irradiation, 98% of the loaded calcium was released, indicating a highly efficient mechanism for stiffening hydrogels.

2.3.2 Gold nanorod characterization

The absorbance spectrum of the gold nanorods depends on the aspect ratio (40). The absorption peaks of the gold nanorods used in these experiments were between 735 and 790 nm (Fig. 2.3a). Transmission electron microscopy images of the gold nanorods shows the average size is 56 x 15 nm (Fig. 2.3b). A solution of the gold nanorods was irradiated with an 808 nm CW laser and the solution temperature was monitored with an IR camera. Irradiation induced a rapid temperature increase that closely follows the Arrhenius relation (Fig. 2.4).

2.3.3 Light-triggered gelation and stiffening

As a proof of concept to establish that calcium-loaded liposomes can be used to modulate the stiffness of alginate gels, the liposomes were mixed with an uncrosslinked alginate solution. Upon irradiation, calcium was released from the liposomes and induced gelation of the alginate solution (Fig. 2.5). Rheometry was performed on the resulting gel, showing a storage modulus of 554 Pa, significantly higher than the unirradiated solution (Fig. 2.5). This demonstrates the ability for light-triggered gelation of alginate via liposomal release of calcium. Prior work has demonstrated similar light-triggered alginate gelation by three distinct modes; (1) photochemical liposome release (41), light induced pH decrease to solubilize $CaCO_3$ via photoacid generator (42), or through photosensitive calcium caging molecules DM-nitrophen (43) or nitr-T (44). Unfortunately, DM-nitrophen is prohibitively expensive for bulk hydrogel studies and is relegated to microfluidic applications. Nitr-T is relatively less expensive, but still relies on UV light for activation and has not been demonstrate to be cytocompatible. More

importantly for our purposes, it does not lend itself to dynamic, temporal stiffness modulations that we are seeking to explore. The reduction of pH by photoacid generators will likely not be well tolerated by cells, and these molecules also rely on UV light to trigger gelation. The strategy presented here for remote-triggered calcium release to gel alginate addresses the limitations that have hampered previous work through the introduction of a NIR light triggering agent and a depot of high concentrations of calcium.

2.3.4 Dynamic stiffening of 3D hydrogels

We sought to utilize this system to not only induce gelation of alginate, but also dynamically modulate the gel stiffness with NIR light. Relatively compliant (91 Pa) three dimensional alginate hydrogels were formed in PDMS molds. Liposomes were included in the gels at 20% by volume. The gels were irradiated for various times up to 5 minutes and rheometry was perfomed after overnight swelling in DPBS (Fig. 2.6A). Irradiation of the gels caused a significant increase in storage modulus over unirradiated controls, which increased monotonically with irradiation time (Fig. 2.6B). The observed net change in storage modulus was 1108 Pa, which is spans the range seen in many fibrotic diseases (1-4 kPa change in elastic modulus). Further, by increasing the initial calcium present in the gels, and thus the initial stiffness, we observed an even greater net change in storage modulus upon irradiation. Gels formed with 20 mM or 30 mM $CaCO_3$ initial yielded significant increases in storage modulus of over 1500 Pa and 2500 Pa respectively upon irradiation (Fig. 2.6C).

Liposomes were loaded with NaCl and gold nanorods as a control to ensure increases in storage modulus were attributable only to calcium release from liposomes. Gels were formed with 20% NaCl-loaded liposomes and irradiated for up to 5 minutes.

We observed no increase in storage modulus over any irradiation time. Further, the stiffening effect is dependent on the concentration of liposomes present in the system. Gels were made with 5, 10, or 20% $CaCl_2$-loaded liposomes and irradiated for up to 3 minutes. In all cases, significant increases in storage modulus were observed. The net change in storage modulus increased with increasing liposome concentration from 276 to 1069 to 2389 Pa for 5, 10, and 20% liposome volume fraction respectively (Fig. 2.7).

For applications in 3D cell culture, there is a need to stiffen the gels at later timepoints to mimic physiological or pathological timelines. To demonstrate this capability, gels were made with $CaCl_2$ loaded liposomes (20% v/v) and incubated in DPBS for up to 7 days. The gels were irradiated after 1, 3, or 7 days and allowed to swell to equilibrium. Rheometry was performed to determine the resulting storage modulus of the gels. At all time points, the gels were significantly stiffer than unirradiated controls (Fig. 2.8A). The stiffening response does appear slightly diminished at day 7, though the irradiated gel stiffness is not significantly different than the other irradiation time points. Additionally, we demonstrated the ability to perform multistep stiffening by irradiating gels each day over the course of 3 days (Fig. 2.8B). The gels that were irradiated on all three days were stiffer than gels that were irradiated only on Day 1 or Days 1 and 2. All the irradiated gels were stiffer than controls that were not irradiated. This result indicates that this system is suitable for use in 3D cell culture applications that require stiffening at later time points.

2.3.5 Dynamic softening of 3D hydrogels

Alginate crosslinks, which are physical interactions between negatively charged guluronic acid regions and positively charged divalent cations, are inherently reversible. Crosslink reversibility is not common among popular hydrogel base polymers, but can be

particularly useful for dynamic systems. Chelators will compete for divalent cations with the alginate polymer chains, resulting in a decrease in crosslinking density and ultimately a softer gel. This phenomenon has been used previously to extract cells from alginate gels or beads (4). We hypothesized that loading a chelator into liposomes in place of calcium, and releasing it in a 3D alginate gel could result in a reduction of the gel storage modulus, or softening (Fig. 2.9A).

Liposomes loaded with DTPA were mixed with alginate to form 3D gels and irradiated, the storage modulus decreased, as expected (Fig. 2.9B). The storage modulus monotically decreased with increasing irradiation time, similar to the results with calcium release. The overall change in storage modulus seen here was muted compared to the results for stiffening via calcium release. This is likely due to competition for calcium from both the chelator and the alginate chains. For example, every calcium ion that is released from the liposomes in stiffening experiments is bound by alginate chains and contributes to an increase in crosslinking density. However, not every DTPA molecule is able to bind a calcium ion, as there is a competitive equilibrium with alginate. Additionally, DTPA is a much larger molecule (393 Da) than calcium, which may prevent diffusion through the lipid bilayer. Yet, these changes are still substantial on a cellular mechanotransduction scale, and changes of this magnitude are reported for pathological complications, making this suitable for modeling dynamical ECM.

Others have reported dynamic hydrogel softening in three-dimensional PEG systems that rely on photolabile groups to cleave upon UV irradiation (45). Several interesting results have been demonstrated with these dynamic gels, in both 2D and 3D, such as redirection of myofibroblasts to a dormant phenotype (46, 47) and very recently the presence of mechanical memory in stem cells (48). Since temporal softening hydrogels exist to explore relevant phenomenon, and because many interesting

pathologies involve temporal stiffening, for which there are no ideal systems, the focus of this dissertation will be primarily applied to stiffening hydrogels.

2.3.6 Spatial Stiffening

One unique advantage of using light-based techniques to modulate hydrogels is that light intensity can be easily profiled or patterned using a number of established optical techniques. Compared to other triggering modalities such as temperature or pH changes which occur globally throughout a gel, light can be focused to a particular region or across a gradient in a well control with theoretical resolution approaching the diffraction limit.

To capitalize on this advantageous, alginate gel slabs with $CaCl_2$-loaded liposomes were formed in PDMS molds. An approximation of a linear intensity gradient was created by using half of the laser beam output from the optical fiber, which is emitted in a Gaussian distribution. This gradient could be made more steep or shallow by varying the distance from the fiber source, as the beam diverges. Two gradients were formed with lengths of 1 mm and 3 mm, which would correlate to a full beam spot size of 2 mm and 6 mm respectively (Fig. 2.10A). An X-Y motorized stage was used to translate the gel slab through the intensity gradient at 0.05 mm/s. After irradiation, the gel stiffness was determined with AFM indentation. The elastic modulus of the gels increased from a relatively compliant 2 kPa outside of the intensity gradient to a maximum of over 20 kPa at the gradient peak (Fig. 2.10B). The slope of the stiffness increase trended with the slope of the intensity gradients as expected.

The light could also be focused to a small spot to local modulate the gel stiffness. This capability was demonstrated by translating gel slabs through a small, focused laser beam and probing the gel with AFM indentation (Fig. 2.11A). The gels were very

uniform in stiffness outside of the irradiated regions, with a large increase in stiffness in the irradiated region (Fig. 2.11B). These peaks within the irradiated regions closely resemble a narrow Gaussian distribution as expected from the fiber optic source. The resolution with this technique is approximately 500 μm based on the full-width half-max of the stiffness peaks. While this is certainly an improvement on global gel changes present in other triggered systems, it is not yet approaching the length scales over which a cell would sense a local change (~100 μm) (49).

2.4 CONCLUSIONS

We have developed a novel, photo-tunable 3D hydrogel cell culture system capable of modulating hydrogel stiffness both temporally and spatially. This system relies on three critical components; alginate, temperature sensitive liposomes, and gold nanorods. Similar designs to release calcium from liposomes with temperature or pH triggers (35) have been designed to cause gelation of alginate. Additionally, others have developed caged-calcium entities that are photo-cleavable, allowed for light-triggered alginate gelation (43). However, these molecules are cost-prohibitive on the bulk scale and are only suitable for microfluidic applications. Finally, the use of gold nanoparticles and NIR light to trigger release from liposomes has been thoroughly explored, particularly for release of therapeutic molecules. However, to our knowledge this is the first unification of these advances into a system to generate light-triggered alginate stiffening. Further, it is the first hydrogel stiffening system that allows for tunability over time, over physiological and pathological stiffness ranges, and with spatial tunability.

Additionally, by using the same hydrogel system, but replacing $CaCl_2$ with DTPA, 3D hydrogels can be softening upon irradiation with NIR light. While others have developed softening hydrogel systems previously, this is the first demonstration of a

bidirectionally tunable system. This feature is important for making accurate and robust comparisons in 3D hydrogel microenvironments, as the hydrogel platform can be maintained for either stiffening or softening experiments. Cell behavior is known to vary to a great extent between different hydrogel materials, especially between natural and synthetic polymers. Thus, conclusions drawn from softening experiments performed with PEG-based systems may not be seen with natural polymers such as alginate. However, using the same alginate system to perform both stiffening and softening experiments would provide greater confidence that the observed phenomenon is driven by matrix stiffness effects and not inherent material properties.

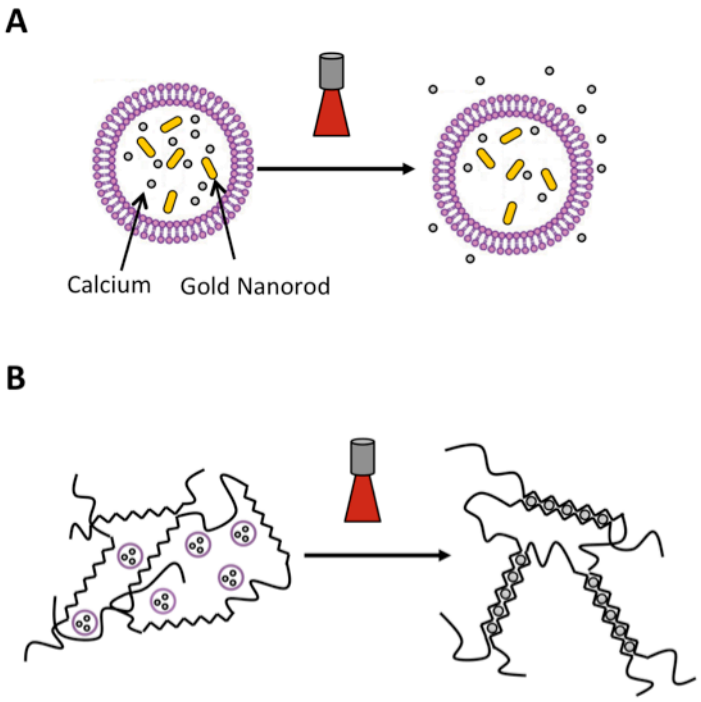

Figure 2.1: Mechanism for light-triggered release from liposomes. (A) Schmatic of temperature-sensitive liposome loaded with gold nanorods and $CaCl_2$. Upon irradiation, gold nanorods heat the lipid bilayer past its transition temperature, allowing calcium to diffuse out. (B) Irradiation of liposomes mixed with an alginate solution causes release of calcium and an increase in crosslinking density.

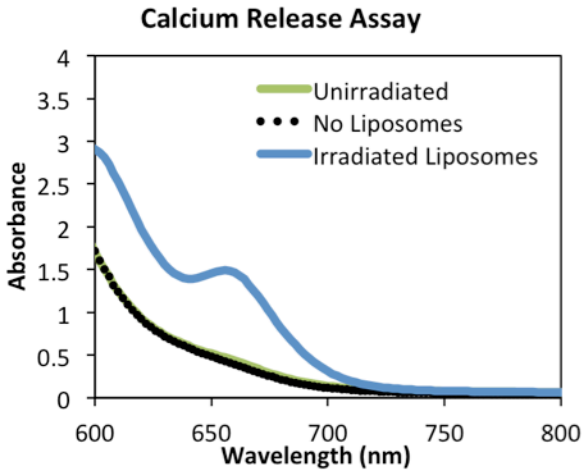

Figure 2.2: Calcium loading and release. Arsenazo III absorbance spectrum for unirradiated (green) and irradiated liposomes (blue), and arsenazo III alone (black dots). Upon irradiation, calcium is release and results in a peak at 655 nm.

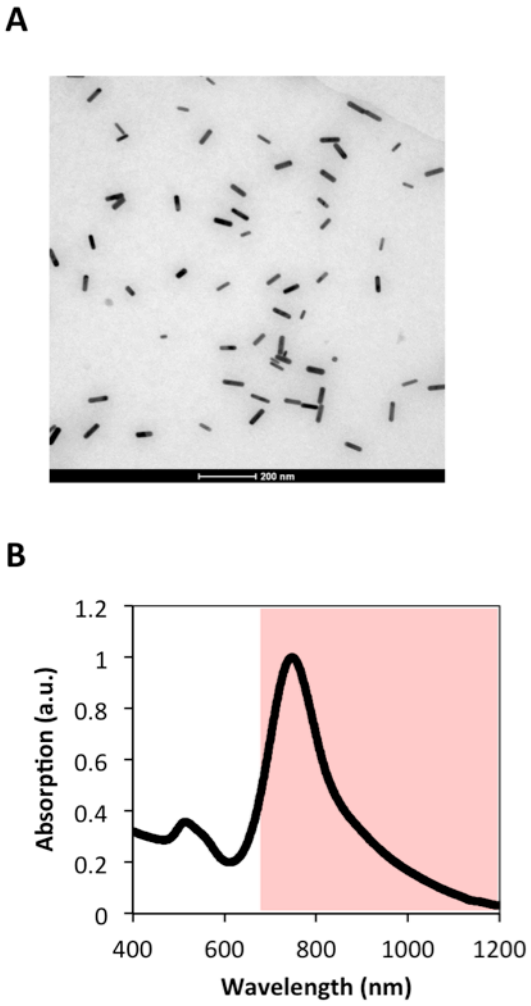

Figure 2.3: (A) Transmission electron micrograph of gold nanorods. Scale bar represents 200 nm. (B) Absorbance spectrum of gold nanorods, demonstrating the narrow peak in the NIR region. Shading denotes the optical window of highest penetration depth through tissue.

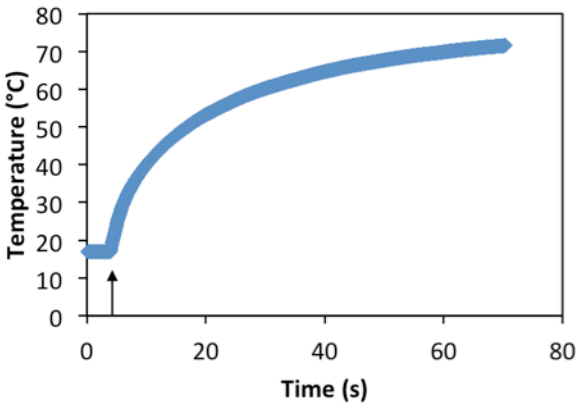

Figure 2.4: Temperature profile for gold nanorods in solution duration irradiation with an 808 nm CW laser at 1.78 W/cm^2. The arrow marks the time at which the irradiation was initiated. The temperature was monitored with an infrared camera.

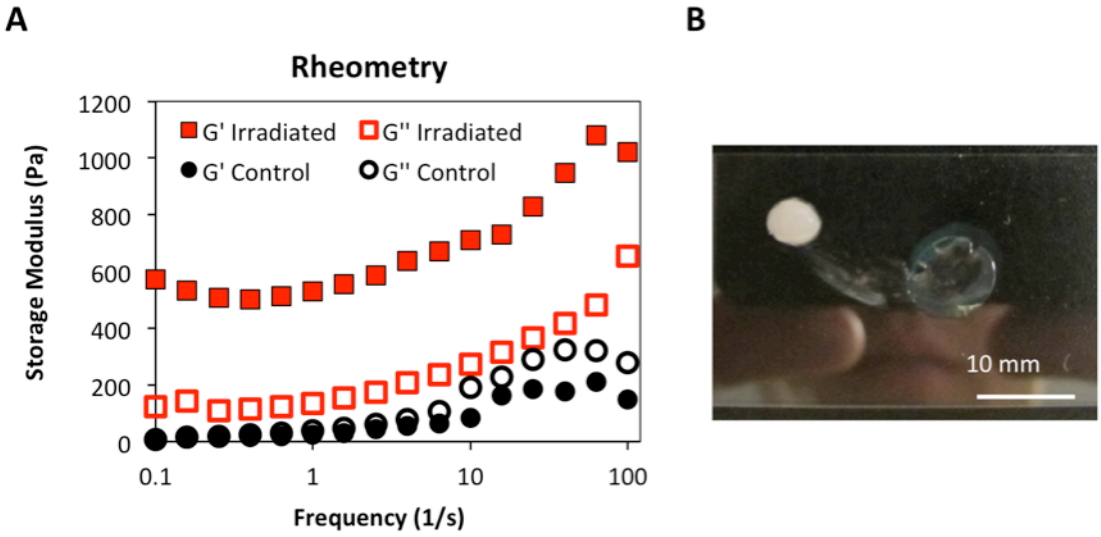

Figure 2.5: Light-triggered gelation of alginate. (A) Rheometry of a solution of alginate and calcium-loaded liposomes (20%). Irradiation causes calcium to be released and gel the alginate solution (red markers). Solutions that were not irradiated remained viscous solutions (black markers). (B) Photograph of alginate gel formed by NIR irradiation.

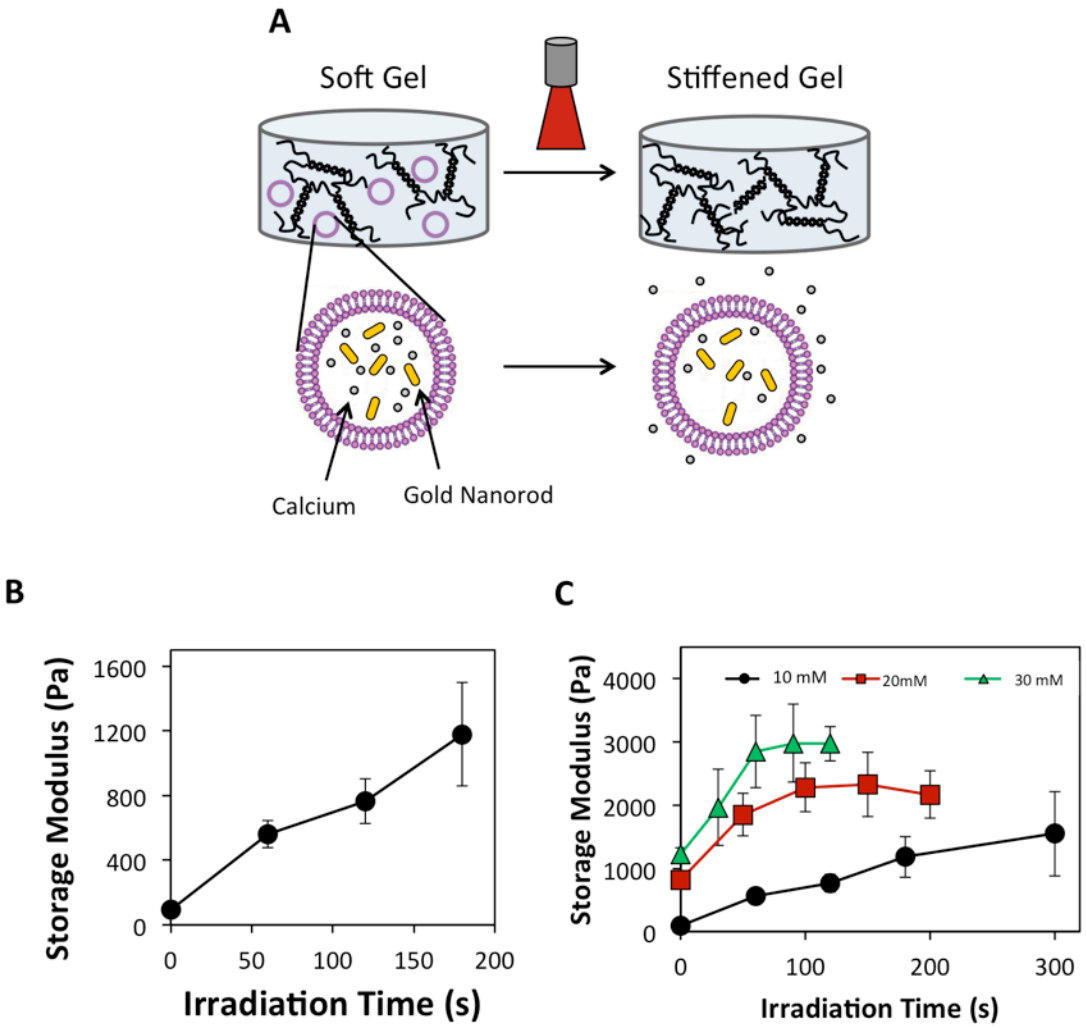

Figure 2.6: Light-triggered modulation of 3D alginate gels. (A) Schematic of 3D alginate gel with calcium loaded liposomes distributed throughout. (B) Irradiation induces release of calcium to stiffen the gels as a function of irradiation time. (C) Stiffening rate can be tuned based on initial gel stiffness.

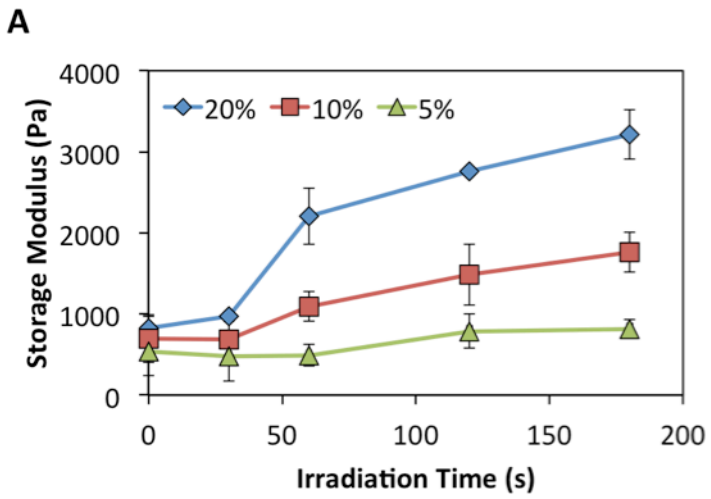

Figure 2.7: Stiffening rate depends on liposome concentration. Both the stiffening rate and magnitude of stiffening increase with increasing concentration of liposomes in 3D gels.

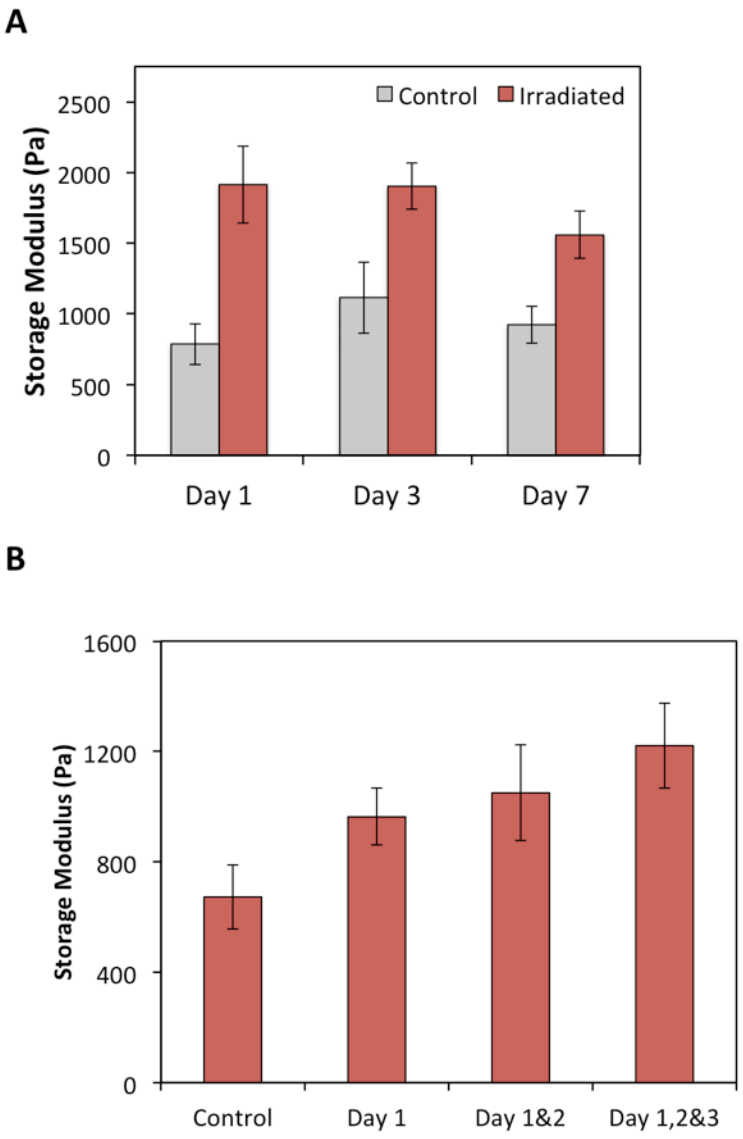

Figure 2.8: Longitudinal stiffening of 3D gels. (A) Alginate gels with calcium-loaded liposomes were irradiated after 1, 3, or 7 days. The irradiated gels were significantly stiffer than controls that were not irradiated across all timepoints. (B) Alginate gels were irradiated once, twice, or three times in 1 day intervals. Gel stiffness increases with the number of irradiations, demonstrating multi-step stiffening.

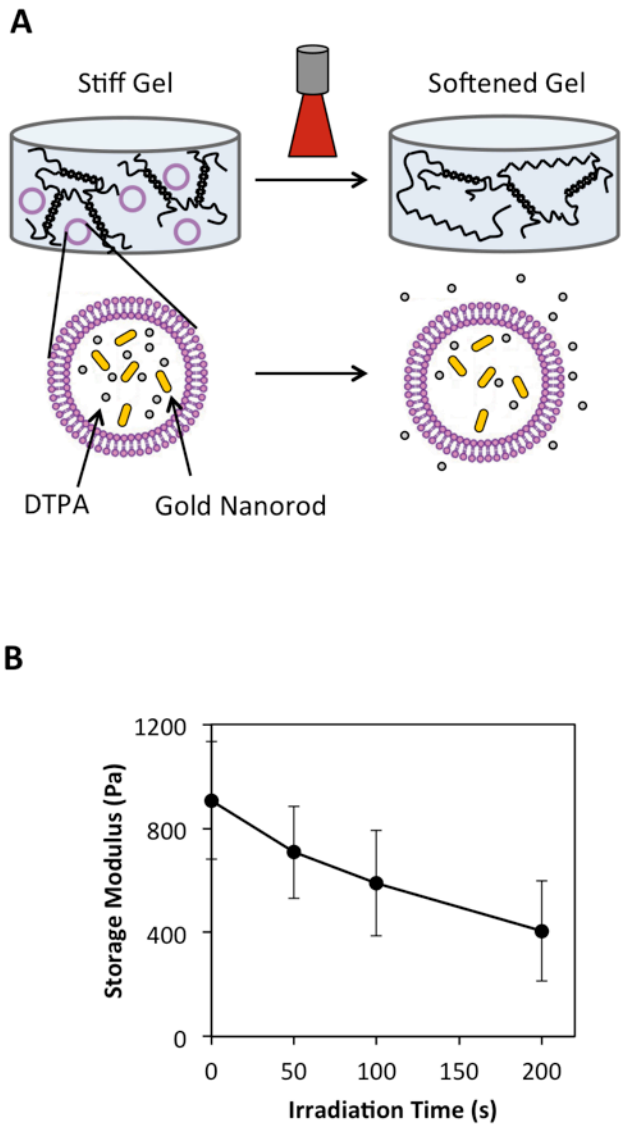

Figure 2.9: 3D alginate gel softening by chelation. (A) Schematic of loading and release of DTPA from liposomes in 3D alginate gels. (B) Storage modulus decreases with increasing irradiation time due to chelation from gel crosslinks by DTPA.

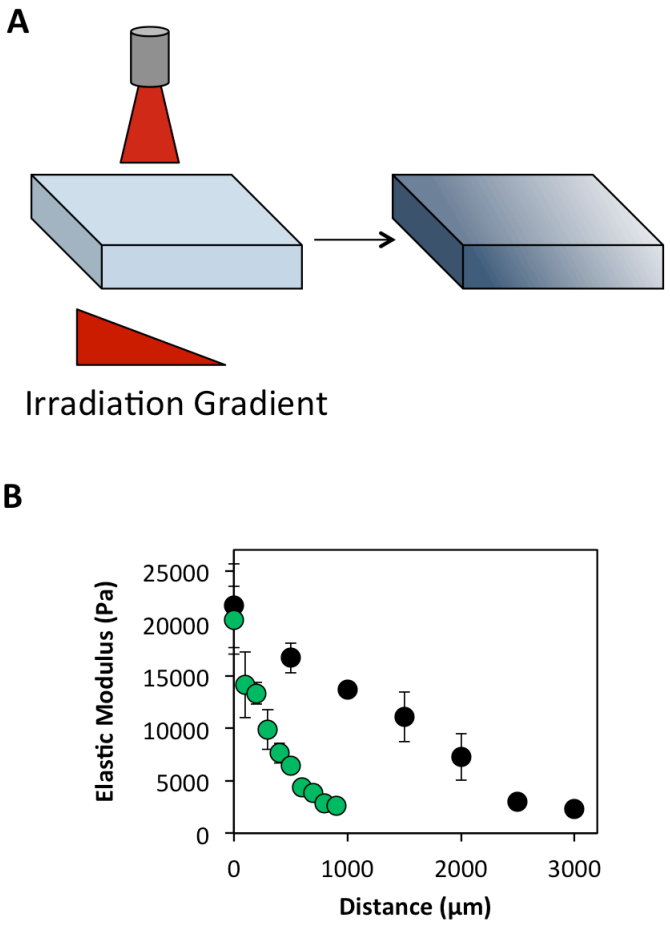

Figure 2.10: Stiffness gradients formed in initially uniform gels. (A) Schematic of gradient generation from an initially soft gel by formation of an intensity gradient of light. (B) Elastic moduli measured by AFM indentation of the resulting stiffness gradients. Steep (green) or shallow (black) stiffness gradients can be formed based on the light intensity profile.

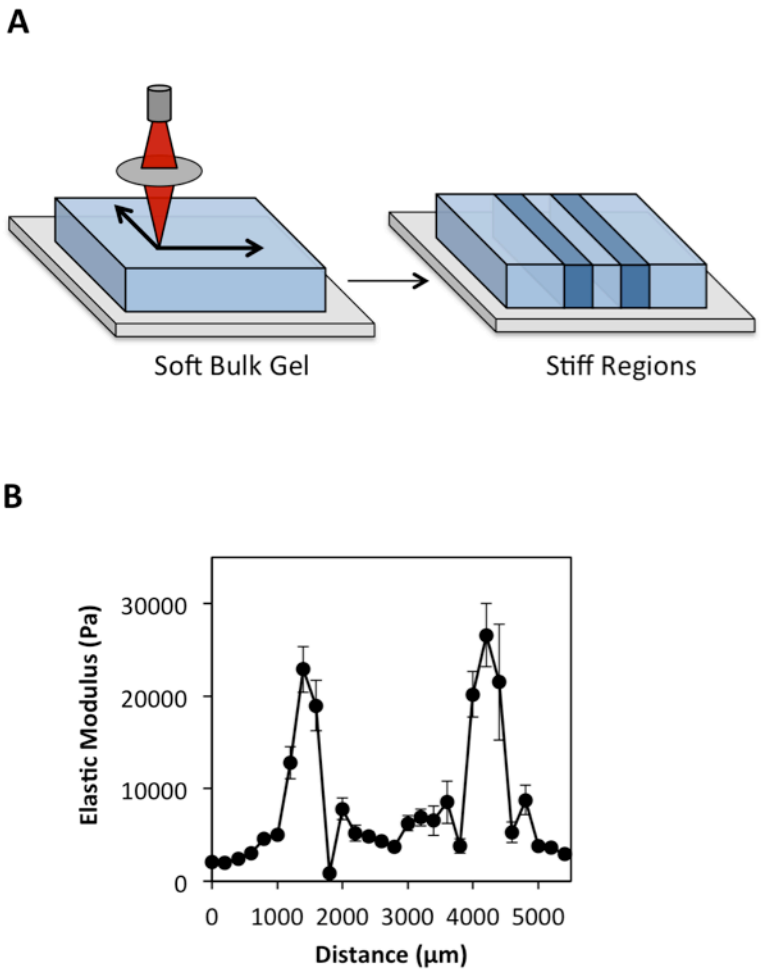

Figure 2.11: Stiffened regions formed from initially soft gels. (A) Schematic of lithographic patterning of stiffness. (B) Stiff regions in areas exposed to light were formed in an initially soft gel. Elastic moduli were measured by AFM indentation.

2.5 REFERENCES

1. Huebsch N, *et al*. (2010) Harnessing traction-mediated manipulation of the cell/matrix interface to control stem-cell fate. *Nature materials* 9(6):518-526.

2. Khetan S, *et al*. (2013) Degradation-mediated cellular traction directs stem cell fate in covalently crosslinked three-dimensional hydrogels. *Nature materials* 12(5):458-465.

3. Lee KY & Mooney DJ (2012) Alginate: properties and biomedical applications. *Progress in polymer science* 37(1):106-126.

4. Gombotz WR & Wee SF (1998) Protein release from alginate matrices. *Advanced drug delivery reviews* 31:267-285.

5. Lim F & Moss RD (1981) Microencapsulation of living cells and tissues. *J Pharm Sci* 70:351-354.

6. Soon-Shiong P, *et al*. (1993) Long-term reversal of diabetes by the injection of immunoprotected islets. *Proceedings of the National Academy of Sciences of the United States of America* 90:5843-5847.

7. Soon-Shiong P, *et al*. (1994) Insulin independence in a type 1 diabetic patient after encapsulated islet transplantation. *Lancet* 343:950-951.

8. Nunamaker EA, Purcell EK, & Kipke DR (2007) In vivo stability and biocompatibility of implanted calcium alginate disks. *Journal of biomedical materials research. Part A* 83(4):1128-1137.

9. Orive G, *et al*. (2002) Biocompatibility of microcapsules for cell immobilization elaborated with different types of alginates. *Biomaterials* 23:3825-3831.

10. Andersen T, Strand BL, Formo K, Alsberg E, & Christensen BE (2012) Alginates as biomaterials in tissue engineering. *Carbohydr Chem* 37:227-258.

11. Rowley JA, Madlambayan G, & Mooney DJ (1999) Alginate hydrogels as synthetic extracellular matrix materials. *Biomaterials* 20:45-53.

12. Dhoot NO, Tobias CA, Fischer I, & Wheatley MA (2004) Peptide-modified alginate surfaces as a growth permissive substrate for neurite outgrowth. *Journal of biomedical materials research. Part A* 71(2):191-200.

13. Mosahebi A, Wiberg M, & Terenghi G (2003) Addition of Fibronectin to Alginate Matrix Improves Peripheral Nerve Regeneration in Tissue-Engineered Conduits. *Tissue engineering* 9:209-218.

14. Branco da Cunha C, *et al*. (2014) Influence of the stiffness of three-dimensional alginate/collagen-I interpenetrating networks on fibroblast biology. *Biomaterials* 35(32):8927-8936.

15. Gillette BM, Jensen JA, Wang M, Tchao J, & Sia SK (2010) Dynamic hydrogels: switching of 3D microenvironments using two-component naturally derived extracellular matrices. *Advanced materials* 22(6):686-691.

16. Chaudhuri O, *et al*. (2014) Extracellular matrix stiffness and composition jointly regulate the induction of malignant phenotypes in mammary epithelium. *Nature materials* 13(10):970-978.

17. Bangham AD, Standish MM, & Watkins JC (1965) Diffusion of univalent ions across the lamellae of swollen phospholipids. *J Mol Biol* 13:238-252.

18. Bangham AD & Horne RW (1964) Negative staining of phospholipids and their structural modification by surface-active agents as observed in the electron microscope. *J Mol Biol* 8:660-668.

19. Allen TM & Cullis PR (2004) Drug delivery systems: entering the mainstream. *Science* 303(5665):1818-1822.

20. Gregoriadis G (1995) Engineering liposomes for drug delivery: progress and problems. *Trends in biotechnology* 13:527-537.

21. Malam Y, Loizidou M, & Seifalian AM (2009) Liposomes and nanoparticles: nanosized vehicles for drug delivery in cancer. *Trends in pharmacological sciences* 30(11):592-599.

22. Moscho A, Orwar O, Chiu DT, Modi BP, & Zare RN (1996) Rapid preparation of giant unilamellar vesicles. *Proceedings of the National Academy of Sciences of the United States of America* 93:11443-11447.

23. Tikshdeep C, Sonia A, Bharat P, & Abhishek C (2012) Liposomes Drug Delivery: A Review. *International Journal of Pharmaceutical and Chemical Sciences* 1:1103-1113.

24. Harris JM & Chess RB (2003) Effect of pegylation on pharmaceuticals. *Nature reviews. Drug discovery* 2(3):214-221.

25. Leung SJ & Romanowski M (2012) Light-activated content release from liposomes. *Theranostics* 2(10):1020-1036.

26. Kano K, Tanaka Y, Ogawa T, Shimomura M, & Kunitake T (1981) Photoresponsive artificial membrane. Regulation of membrane permeability of liposomal membrane by photoreversible cis-trans isomerization of azobenzenes. *Photochemistry and Photobiology* 34:323-329.

27. Anderson VC & Thompson DH (1992) Triggered release of hydrophilic agents from plasmalogen liposomes using visible light or acid. *Biochimica et biophysica acta*:33-42.

28. Bondurant B & O'Brien DF (1998) Photoinduced destabilization of sterically stablized liposomes. *Journal of the American Chemical Society* 120:13541-13542.

29. Mackanos MA, *et al*. (2009) Laser-induced disruption of systemically administered liposomes for targeted drug delivery. *Journal of biomedical optics* 14(4):044009.

30. Paasonen L, *et al*. (2007) Gold nanoparticles enable selective light-induced contents release from liposomes. *Journal of controlled release : official journal of the Controlled Release Society* 122(1):86-93.

31. Paasonen L, *et al*. (2010) Gold-embedded photosensitive liposomes for drug delivery: triggering mechanism and intracellular release. *Journal of controlled release : official journal of the Controlled Release Society* 147(1):136-143.

32. Wu G, *et al*. (2008) Remotely triggered liposome release by near-infrared light absorption via hollow gold nanoshells. *Journal of the American Chemical Society* 130:8175-8177.

33. Messersmith PB, Vallabhaneni S, & Nguyen V (1998) Preparation of calcium-loaded liposomes and their use in calcium phosphate formation. *Chem Mater* 10:109-116.

34. Messersmith PB & Starke S (1998) Thermally triggered calcium phosphate formation from calcium-loaded liposomes. *Chem Mater* 10:117-124.

35. Westhaus E & Messersmith PB (2001) Triggered release of calcium from lipid vesicles: a bioinspired strategy for rapid gelation of polysaccharide and protein hydrogels. *Biomaterials* 22:453-462.

36. Sanborn TJ, Messersmith PB, & Barron AE (2002) In situ crosslinking of a biomimetic peptide-PEG hydrogel via thermally activation of factor XIII. *Biomaterials* 23:2703-2710.

37. Smith AM, Harris JJ, Shelton RM, & Perrie Y (2007) 3D culture of bone-derived cells immobilised in alginate following light-triggered gelation. *Journal of controlled release : official journal of the Controlled Release Society* 119(1):94-101.

38. Ahl PL, *et al*. (1994) Interdigitation fusion: a new method for producing lipid vesicles of high internal volume. *Biochimica et biophysica acta* 1195:237-244.

39. Kuo CK & Ma PX (2008) Maintaining dimensions and mechanical properties of ionically crosslinked alginate hydrogel scaffolds in vitro. *Journal of biomedical materials research. Part A* 84(4):899-907.

40. Link S, Mohamed MB, & El-Sayed MA (1999) Simulation of the optical absorption spectra of gold nanorods as a function of their aspect ratio and the effect of the medium dielectric constant. *J Phys Chem B* 103:3073-3077.

41. Zhang ZY, Shum P, Yates M, Messersmith PB, & Thompson DH (2002) Formation of fibrinogen-based hydrogels using phototriggerable diplasmalogen liposomes. *Bioconjugate Chem* 13:640-646.

42. Javvaji V, Baradwaj AG, Payne GF, & Raghavan SR (2011) Light-activated ionic gelation of common biopolymers. *Langmuir : the ACS journal of surfaces and colloids* 27(20):12591-12596.

43. Chueh BH, *et al*. (2010) Patterning alginate hydrogels using light-directed release of caged calcium in a microfluidic device. *Biomedical microdevices* 12(1):145-151.

44. Cui J, Wang M, Zheng Y, Rodriguez Muniz GM, & del Campo A (2013) Light-triggered cross-linking of alginates with caged Ca2+. *Biomacromolecules* 14(5):1251-1256.

45. Kloxin AM, Kasko AM, Salinas CN, & Anseth KS (2009) Photodegradable hydrogels for dynamic tuning of physical and chemical properties. *Science* 324(5923):59-63.

46. Wang H, Haeger SM, Kloxin AM, Leinwand LA, & Anseth KS (2012) Redirecting valvular myofibroblasts into dormant fibroblasts through light-mediated reduction in substrate modulus. *PloS one* 7(7):e39969.

47. Wang H, Tibbitt MW, Langer SJ, Leinwand LA, & Anseth KS (2013) Hydrogels preserve native phenotypes of valvular fibroblasts through an elasticity-regulated PI3K/AKT pathway. *Proceedings of the National Academy of Sciences of the United States of America* 110:19336-19341.

48. Yang C, Tibbitt MW, Basta L, & Anseth KS (2014) Mechanical memory and dosing influence stem cell fate. *Nature materials* 13(6):645-652.

49. Sen S, Engler AJ, & Discher D (2009) Matrix strains induced by cells: computing how far cells can feel. *Cellular and Molecular Bioengineering* 2:39-48.

Chapter 3: In Vitro and In Vivo Applications of Dynamic Photo-Tuning

3.1 Introduction

3.1.1 Mechanotransduction

Mechanotransduction is most generally defined as the conversion of a mechanical force to a biochemical signal (1). Cells are able to sense external physical forces through transmembrane receptors, such as integrin, cadherins, selectins, amongst many others (2). Integrins, which bind to extracellular matrix (ECM) proteins, are the best understood of these receptors. Integrins are heterodimers composed of an α subunit and a β subunit. To date, eighteen different α subunits and eight different β subunits have been found, combining to form at least 24 unique integrins (3). Different integrin subunit combinations are specific for unique peptide sequences found on various ECM proteins. The β1 subunit is known to bind a to a variety of proteins including collagens, laminins, fibronectin and vitronectin (4). However, the β4 subunit is specific to laminin and generally only found on epithelial cells, which interact with a laminin-rich basement membrane (5). Through protein specific binding, the cell is able to activate appropriate signaling pathways based on the proteins it contacts within the ECM.

While the extracellular integrin domain binds ECM proteins, the intracellular domain is linked to the cellular cytoskeleton. The cytoskeleton is a network of polymerized filaments, formed from protein monomers that can be tensed or compressed. The cytoskeleton functions to transmit and generate forces across the cell, connect intracellular elements to extracellular proteins and neighboring cells, and finally to spatially organize the cell and maintain its shape (6). Actin microfilaments, microtubules, and intermediate filaments are the primary elements of the cytoskeleton, and function in separate but interrelated manners. Actin microfilaments are composed of monomers of

the globular protein, actin, which are polymerized into a linear filament. Actin filaments can be rapidly polymerized or depolymerized to allow the cell to quickly remodel its cytoskeleton in response to a stimulus (7). Tension can be generated across actin filaments by contraction of motor proteins like myosin (8). Actin filament elongation is involved in a multitude of cellular processes, including locomotion, anchorage, endocytosis, and cytokinesis (9, 10). Microtubules are much stiffer polymers than actin and can form long, linear filaments (6). Tubulin is polymerized into protofilaments, 13 of which adopt a helical conformation with a hollow center to form the microtubule. Microtubules are used as pathways for movement of intracellular vesicles and are highly involved in organization for cell division (11, 12). Finally, intermediate filaments are made up of many types of filament proteins that all share similarities, namely high extensibility and ability to crosslink to actin filaments and microtubules (6). Keratins and neurofilaments are two common families of cytoplasmic intermediate filaments, while lamins are a family of nuclear intermediate filaments. Intermediate filament function varies depending on the type, but generally they form networks to resist or respond to mechanical force, usually in concert with other cytoskeletal elements (13) .

From a mechanical standpoint, it has been proposed that the cellular cytoskeleton is arranged according to the structural principle of tensegrity, introduced to the biological field by Donald Ingber (1). Tensegrity refers to the balance of stress within a system of compressed struts and tensioned cables. In the case of the cell, microfilaments apply tension that is resisted in compression by microtubules. Tensegrity is seen across the length scales of biological systems, including the musculoskeletal system, organs, tissues, cells membranes, cytoskeletal networks, subcellular organelles, nuclei, mitotic spindles, vesicles, viruses, and proteins (14). Due to this arrangement in the cytoskeleton in particular, physical forces that are applied locally at a single integrin can be transmitted

throughout the cell globally, to neighboring cells, or to the ECM (15, 16). As an example, mitochondria in endothelial cells associate with microtubules. Strain on the cell membrane is transmitted to the mitochondria through the microtubule, which results in release of reactive oxygen species and activation of NF- κB and VCAM1 (17).

Transmembrane receptors, like integrins, are linked to the cytoskeleton through numerous signaling and adapter proteins. The signaling pathways from transmembrane mechanoreceptors are usually quite complex, multifaceted, dynamic, and force-dependent, making it difficult to fully understand how cells interpret physical forces. Nevertheless, a basic understanding of many of the signaling events has been distilled from much research in this area across a wide array of physical and life science fields. As an example, upon integrin binding to an ECM protein, talin, an adapter protein, bind the cytoplasmic integrin tail. Talin anchors the integrin directly to the actin cytoskeleton, and if sufficient tension is generated across talin, binding domains for vinculin are exposed (18, 19). Vinculin binds to talin and actin filaments, and is involved in focal adhesion maturation (20). Paxillin can also bind the cytoplasmic integrin tail, and can be bound by several proteins including vinculin, crk, and tyrosine kinases such as Src and FAK (21). Integrin binding also activates RhoGTPases through guanine nucleotide exchange factors (GEFs) (22). RhoA has been shown to phosphorylate ROCK, which in turn acts on LIM kinase to phosphorylate and deactivate actin depolymerizing cofilin, thus indirectly stabilizing actin filaments (20). Activated ROCK also phosphorylates myosin light chain which contributes to increased cellular contractility (23). RhoA can activate mDia1, which is known to promote nucleation and elongation of unbranched actin filaments necessary for stress fiber formation (24). Thus, even in simplified reductionist systems, care must be taken when interpreting observations in mechanotransduction. Further

adding to the complexity is variety of platforms on or in which cells are cultured for these studies, all of which differ in significant ways from the in vivo environment.

While it is clear that transmembrane receptors linked to the cellular cytoskeleton can transduce force and even influence signaling pathways, it is not immediately evident how this process regulates gene expression. Often, classical biochemical pathways are initiated through activation of proteins like extracellular signaling related kinase (ERK), which then activate transcription factors like p53, STAT1, MYC, or NF-κB (25-28). However, recently evidence has emerged that suggests a direct, mechanically coupling from the ECM to nuclear chromatin, which is regulated by tensegrity principles. Force is transmitted through the integrins and cytoskeleton to the nuclear membrane, where lamins transfer the force to change chromatin conformation or influence the activity of DNA remodeling enzymes (25, 29). Physical force can also effect histone acetylation and methylation through alteration of the enzyme histone deacetylase (30). While the exact mechanisms underlying these observations is yet to be revealed, it is clear that physical forces can regulate gene expression through modulation of DNA itself, or a remodeling enzyme.

2.1.2 Necessity of 3D hydrogel models

A broad knowledge base of general principles of mechanotransduction has been built primarily by utilizing 2D substrates with variable elastic moduli. These 2D models are quite useful for addressing basic biological questions, such as how cells interact with and transduce signal from adhering to a particular ligand of interest. However, as discussed previously, there are serious limitations to using static 2D models to study dynamic, 3D biology. As more studies are performed in 3D environments that more closely mimic in vivo physiology, it is becoming apparent that phenomena that occur in

2D models do not always translate to 3D. Unfortunately, it appears that sometimes, information gained from simple 2D models may not be relevant to real-world scenarios, or worse, that events in 3D actually contradict what would be expected from 2D model systems.

As an example of how studies in 2D systems may not yield physiologically meaningful results, consider the morphologic response of cells to a range of matrix stiffness. Pelham and Wang first established that cells spread more on stiff substrates and adopt rounded morphologies on softer substrates (31). This result has been replicated with a multitude of cell types, substrates, and adhesion molecules, and is conventional wisdom within the biomaterials field. Recently, several groups have shown that this relationship between cell shape and stiffness does not always hold in 3D gels however. Using alginate mixed with collagen I, da Cunha and coworkers formed gels in which the matrix stiffness could be varied with calcium sulfate concentration without influencing the collagen crosslinking density (32). Fibroblasts cultured in soft gels (50 Pa) elongated within the matrix, while cells in stiff gels (1200 Pa) remained rounded. Even in the presence of RGD-adhesion sequences on the alginate chains, the fibroblasts remained rounded in the stiff gels. A similar alginate-collagen I composite gel was used by Gillette et al to dynamically crosslink or de-crosslink the alginate by addition of calcium or chelators across a membrane. Fibroblasts in crosslinked gels remained rounded, but upon chelation to remove crosslinks, the cells formed elongations and were able to migrate. This behavior could be halted by addition of $CaCl_2$ to re-crosslink the alginate. While stiffness was not implicated directly by the authors, crosslinking density would correlate directly with gel stiffness. In these two studies, cells actually spread more in the soft gels and remain rounded in the stiff gels; exactly the opposite response that is observed on 2D substrates.

Stem cell differentiation in biomaterials environments is also an area that has been intensely investigated over the last decade. Work from the Discher laboratory showed that adult mesenchymal stem cells (MSCs) differentiated toward lineages that matched the stiffness of the underlying substrate (33). Collagen I coated polyacrylamide gels with elastic moduli between 0.1 and 40 kPa were used as cell culture substrates. MSCs cultured on soft substrates (0.1-1 kPa) differentiated toward neurogenic lineages, toward myogenic lineages on intermediately stiff substrates (8-17 kPa), and toward osteogenic lineages on stiff substrates (25-40 kPa). MSC morphology was also regulated by stiffness. On soft substrates, MSCs adopted highly branched morphologies reminiscent of neurons, while myoblast-like spindles were formed on intermediate substrates and highly spread osteoblast-like morphologies were observed on the stiffest substrates. The simple, yet elegant proposition that stem cell differentiation in vivo might be driven by the microenvironment it resides in spurred intense effort in nearly all biomaterials arenas to direct stem cell fate with microenvironmental cues.

The influence of stiffness on stem cell differentiation in 3D gels was investigated using a similar experimental design. The Mooney lab constructed RGD-conjugated alginate gels with elastic moduli ranging from 2.5 to 110 kPa. As expected, MSCs seeded within these gels differentiated toward adipocytes in soft gels (2.5 – 5 kPa) and osteoblasts in stiffer gels (11 – 30 kPa), though gels stiffer than 30 kPa were less effective at driving osteogenic differentiation (34). Interestingly, cell morphology was unchanged throughout the spectrum of elasticity. The cells remained rounded regardless of the gel stiffness or fate decision. Based on these experiments, it appears that stem cells are able to probe the mechanical properties of their microenvironment based on presentation of adhesion ligands and the ability to apply traction force. In addition to stiffness, dimensionality, and ligand presentation, recent evidence demonstrates that gel

crosslinking properties and degradability are also critical regulators of matrix-induced stem cell differentiation. In covalently crosslinked hyaluronic acid (HA) gels with stiffness from 4.4 to 92 kPa, the Burdick lab observed no changes in stem cell differentiation with respect to stiffness (35). The cells differentiated toward adipocytes and remained rounded regardless of the stiffness of the gel. When degradation sites were incorporated into these gels, osteogenesis was induced even in gels with low moduli (4.4 kPa), demonstrating that, at least in 3D covalently crosslinked hydrogels, degradation-mediated traction force was the primary driver in differentiation over gel stiffness. The group designed a secondary crosslinking chain to sterically block the degradation sites that could be introduced immediately or at later timepoints. They show the immediate blockage of the degradation site prevents cell elongation and osteogenesis, and promotes rounded morphologies and adipogenesis. Interestingly, if degradation is blocked after 7 days, when the cells have already adopted an elongated morphology, adipogenic differentiation is still favored but cell shape remains elongated. Thus, depending on the presentation of degradation sites, both adipocytes and osteocytes could be generated with either elongated or rounded morphologies, all in gels with relatively low stiffness. In other words, at least for this covalently crosslinked hydrogel, neither gel stiffness nor cell morphology is predictive of stem cell fate. Clearly, as a field we have much to learn about how cells interact with their microenvironments. It is only through development of novel cell culture platforms that more closely mimic the native ECM that we can come to more fully understand mechanotransduction.

3.1.3 Hydrogels to study temporal biology

One area where progress has been made through advancements in hydrogel technology is in understanding how cells temporally interpret dynamic stiffness. The

Anseth lab developed a photocleavable PEG-based hydrogel that could be softened upon UV irradiation (36). The dynamic platform was used to explore the effects of substrate (2D) stiffness on valvular interstitial cell activation to myofibroblasts. Kloxin and coworkers demonstrated that VICs are activated to myofibroblasts on stiff substrates, but can be deactivated by softening the substrate modulus (37, 38). Later work demonstrated that the deactivation could be detected in gene signatures as soon as six hours after softening (39). This dynamic hydrogel platform was also used to investigate the effects of stiffness of previous substrates on stem cells, known as mechanical memory. Yang and colleagues found that long term culture of MSCs on tissue culture plastic biases the cells toward osteogenic lineages (40). When cultured on 10 kPa gels that were softened to 2 kPa, the cells exhibited different responses depending on the length of time they were cultured on the stiffer substrate. YAP/TAZ and RUNX2 expression were increased on 10 kPa gels, but could be fully reduced if the modulus was decreased after 1 day. If the softening occurred after 5 days, a partial reversion was observed, while softening after 10 days had no effect. Thus, stem cells appear to have a memory of previous physical microenvironments that can carry over into new environment, depending on the length of time and magnitude of stiffness of the first environment. In light of recent work with stem cells differentiation in 3D gels, it would be interesting to investigate this phenomenon in more representative 3D environments. Additionally, the capability to dynamic stiffen the microenvironment would allow for many more experiments to be conducted in this vein. As stem cells typically reside in soft microenvironments like bone marrow or adipose tissue, and migrate to stiffer environments for differentiation, stiffening gels may be a more realistic scenario for applications as well.

3.1.4 Hydrogels for in vivo use

Hydrogels are widely used in vivo for cell and drug delivery, cell encapsulation, and tissue engineering scaffolds, and many have reached widespread clinical use (41, 42). Hydrogels are beneficial for cell delivery applications because they protect the cells from harsh, inflammatory wound environments. The cells are able to assist in wound healing through paracrine secretion of soluble factors, and can migrate out of the gel to interact at the wound site. Pancreatic islets have been encapsulated in hydrogels to produce insulin in patients with type 1 diabetes mellitus for up to 10 months without immunosuppression (43). Drug delivery through hydrogel matrices can be finely controlled, and many clinical products employ this strategy for drug delivery up to several months (44). While there has been much success from the use of hydrogels in vivo, there are still opportunities for improvement in development of injectable therapies, remote control of hydrogel properties, and development of tissue engineering scaffolds.

3.1.6 Injectable hydrogels

There is a clinical need for development of injectable or minimally invasive hydrogel platforms for in vivo use. Injectable systems are desirable because of the minimal damage done during injection compared to implantation surgery, and because they freely flow and gel around physiological structures to provide good adhesion at the injection site. Conventional strategies to develop injectable hydrogels generally rely on solvent exchange, photopolymerization, and temperature or pH changes (45). In solvent exchange systems, a polymer is solubilized in an organic solvent and injected. In the body, the solvent is replaced with water, which causes precipitation of the polymer and induces gelation. Unfortunately, many organic solvents are known to be toxic, and can cause protein denaturation, which limits their usage. Temperature or pH switch methods work with polymers that have bimodal hydrogen bonding preferences. For instance,

below the lower critical solution temperature (LCST) of a thermogelator, hydrogen bonding between water and the polymer chain is energetically favorable. Above the LCST temperature though, polymer-polymer interactions are favored over polymer-water interactions, and a gel is formed. Many different polymer types have been used for injectable hydrogels based on temperature changes, including: polysaccharides such as cellulose derivatives, chitosan, and xyloglucan, N-isopropylacrylamide (PNIPAM)-based systems such as PNIPAM-co-acrylic acid (AA), and PNIPAM-co-poly ethylene oxide (PEO), poloxamer based systems such as PEO-PPO-PEO, and PEO/poly (D,L-lactic acid-co-glycolic acid) copolymer systems (45). As described in Chapter 2, Messersmith et al developed a temperature-sensitive liposome system to gel alginate above 37ºC. Additionally, many peptide-based materials have been developed to undergo self-assembly after injection in vivo, either driven by temperature or pH changes (46).

3.1.7 Remotely-triggered in vivo hydrogels

The use of light to remotely trigger gelation is attractive because of its ease of use, biocompatibility, and direct control of gelation timing. Light has been used to induce gelation of a pre-polymer solution in vivo. Elisseeff et al first demonstrated in situ photo-polymerization of a PEG-based gel (47). The polymer solution was injected with a photo-initiator and irradiated with UV light to form a gel. UV light does not penetrate skin with high efficiency, however the group was able to transmit enough light to successfully form gels loaded with chondrocytes for cartilage regeneration. This study also demonstrated the potential for controlled drug release from a photo-polymerized gel system. Others have since developed transdermal gelation systems based on similar concepts with UV triggered photoinitiators (48). Ideally however, light based systems would be designed with photo-initiators or triggering mechanisms that are excited by NIR light wavelengths to allow for maximum penetration depth.

There is a desire to engineer systems that provide continuous or long-term control of gel properties, instead of simply the ability to cause gelation on-demand. Remote control strategies have been developed with light, ultrasound, magnetic fields and radio waves as in vivo triggering modalities (49-53). Using mitoxantrone-loaded alginate discs, Huebsch et al demonstrated remote controlled, high dosage burst releases by temporally disrupting alginate crosslinks (53). In vivo, the crosslinks were rapidly reformed by calcium present in the vicinity of the gel. The controlled, burst release of drug was more effective at killing breast cancer cells in vitro and reducing tumor size and increasing survival in vivo than a steadily releasing control gel.

3.1.8 Near infrared light and the optical window

Near infrared light is an ideal modality for remote triggering of hydrogel system for in vivo applications due to its high penetration depth. Light absorption by tissue components is high in the UV and visible spectrum due to strong absorbance of hemoglobin, and in the infrared region due to absorption by water. However, the near-infrared region has relatively low absorption. This region is known as the optical window, and is generally defined between 700 nm and 1200 nm (54, 55). Several gold nanoparticles, including gold nanorods, have absorption peaks in the optical window and make excellent candidates for in vivo applications. Gold nanorods have been used to induce cell death of tumor cell via laser irradiation, either through heating of the tissue or mechanical disruption (56-58). Gold nanorods have also been used for on-demand delivery and release of doxorubicin (59). Liposomes loaded with gold nanorods have also been employed in vivo deliver doxorubicin in mice to successfully treat a mouse model of glioblastoma (60). Results to date with gold nanorods and near infrared light have shown good biocompatibility and low cytotoxicity from the irradiation and presence of gold nanorods. Obviously, as irradiation of gold nanorods can be used to induce cell

death, the concentration of the gold nanorods in the presence of cells and the irradiation dosage must be maintained below a threshold. The Burdick lab has successfully employed gold nanorods to trigger gelation in a temperature-sensitive gel while maintaining cell viability (61), demonstrating that this is a feasible strategy.

3.1.9 Chapter overview

Here, we present a system that utilizes NIR light to modulate the crosslinking density and stiffness of alginate gels. This process offers supreme control of gelation timing and matrix crosslinking. Matrix stiffness can also be independently tuned with constant cell adhesion ligand density. Here, the platform will be used to examine morphological changes of 3T3 fibroblasts in 3D dynamic stiffening gels. Additionally, a strategy to employ dynamic phototunable hydrogels in vivo will be presented. The strategy utilizes NIR light to induce gelation or modulate gel stiffness. To our knowledge, this is the first presentation of the ability to tune hydrogel mechanical properties in situ.

3.2 MATERIALS AND METHODS

3.2.1 Cell culture

Human mammary epithelial cells (MCF10A) were obtained from American Type Culture Collection (ATCC). MCF10A were cultured with DMEM/F12 basal media containing 5% horse serum, 20 ng/ml epidermal growth factor, 0.5 mg/ml hydrocortisone, 100 ng/ml cholera toxin, 10 μg/ml insulin, and 1% penicillin-streptomycin (P-S) (62). Media was changed every 2 days and cells were passaged before reaching confluency.

NIH 3T3 fibroblasts were obtained from ATCC and cultured in DMEM with 10% fetal bovine serum, and 1% P-S. Media was changed every 2 days and the cells were passaged at 70% confluency.

3.2.2 3D cell culture

Pronova UP MVG sodium alginate was dissolved in DPBS to 4% w/v. High molecular weight MVG alginate with GRGDS peptide sequences conjugated to the polymer chains were purchased and used in a subset of experiments. Uniformly crosslinked alginate gels were made using insoluble $CaCO_3$ as a calcium source, and glucono-δ-lactone (GdL), which hydrolyzes upon dissolution in water to release calcium ions (2) Gels were made from 10 mM $CaCO_3$ up to 40 mM $CaCO_3$ depending on the desired initial stiffness of the gel. The molar concentration of GdL was always twice that of $CaCO_3$ to maintain a neutral pH. Liposomes were included at 20% of the volume of the gel. Cells were mixed with the alginate solution prior to gelation to ensure a uniform distribution throughout the gel. Gels were pipetted into chambered coverglasses or well plates and allowed to gel at 37ºC for 30 minutes. Culture media was then carefully pipetted over the gels and changed every other day.

Matrigel was added to some gels to provide cell adhesion moieties. For these studies, Matrigel was mixed with the alginate solution just prior to plating for gelation. Matrigel was included at 25% by volume from a stock that ranged from 8.8 to 9.6 mg/ml total protein content. The Matrigel was well mixed prior to gelation to ensure uniform distribution within the alginate gels.

3.2.3 Viability assays

Calcein AM (Life Technologies) was used to assess cell viability and ethidium homodimer was used to detect non-viable cells. For microscopy, gels were formed in 8

well chambered cover glasses. The gels were irradiated and incubated at 37ºC for 24 hours. Then, the gels were washed 3 times with DPBS followed by incubation in 4 μM Calcein AM and 2 μM ethidium homodimer solution for 1 hour at 37ºC. The gels were rinsed 3 times with DPBS to remove the excess staining solution and fixed with 2% formaldehyde for 15 minutes. The gels were imaged on a Leica DM 3000B fluorescent microscope equipped with a digital camera. Viability was quantified by counting the number of green (live) and red (dead) fluorescently labeled cells as a fraction of the total number of cells. A minimum of 200 cells were counted per condition.

3-(4,5-dimethylthiazol-2-yl)-5-(3-carboxymethoxyphenyl)-2-(4-sulfophenyl)-2H-tetrazolium (MTS, Promega) was used to assess cell proliferation. The assay was first validated with alginate gels of varying cell number. Gels were made in a 48 well plate with cell concentations from 15,000 to 250,000 cells per mL. After 24 hours in culture, the MTS solution was diluted in phenol-red free media to 20% v/v and incubated with the gels for 4 hours. The solution was removed and plated in a 96 well plate and the absorbance was read at 490 nm. The absorbance increased linearly in cell number.

To assess the effects of irradiation, gels were made in 8 mm diameter PDMS molds and transferred into at 24 well plate with media. The gels were irradiated for varying times between 0 and 5 minutes. MTS solution was diluted in media to 20% v/v and added to the gels 24 hours after irradiation. After 4 hours of incubation, 200 μl of the solution was pipetted in triplicate to a 96-well plate. The absorbance was read at 490 nm and normalized to control gels that were unirradiated. Two different liposome groups were assessed by the MTS assay. First, DPBS loaded liposomes were used to isolate any effects of calcium release that may affect viability and focus solely on the effects from

the liposomes and heating of the gold nanorods under irradiation. Next, $CaCl_2$-loaded liposomes were loaded and irradiated to assess the viability of the system as a whole.

3.2.4 Effects of stiffening on fibroblast morphology

3T3 fibroblasts were mixed with alginate solutions prior to gelation. In one experiment, Matrigel was used as the cell adhesive moieties, while in another experiment, RGD-conjugated alginate was purchased from Novamatrix and used without any cell-adhesive protein. One day after gelation, the gels were irradiated for 30, 60, or 120 s or left unirradiated as soft controls. The cells were allowed to growth for another 3 days in the stiffened gels. Phase contrast microscopy images were taken of cells in each stiffness group (25-30 images per group). The cell outline was traced in Image J and a best-fit ellipse was generated. Cell area, perimeter, aspect ratio, and circularity were calculated from the cell trace. Circularity is defined here as the square of the perimeter divided by the product of the cell area and 4π.

Calcein AM was used to stain the cells after the phase-contrast images were captured, as described in section 3.2.3. Two photon excitation laser scanning microscopy was used to image the 3D gels. The samples were excited at 820 nm with a Spectra Physics Mai Tai pulsed laser source. A Prairie View Ultima multiphoton microscopy system with a 20X objective was used to capture images. Image J was used to convert the image sequences into a Z-projection.

3.2.5 Transdermal irradiation

All animal studies were performed on previously euthanized nude mice donated from the laboratory of Dr. Stanislav Emelianov. For gelation studies, a 100 μl solution of 4% alginate (80% v/v) and liposomes (20% v/v) was injected into the dorsal region of the mouse. The region was irradiated for 5 minutes. Liposomes without gold nanorods were

used as controls. After irradiation, the gels were harvested and rheometry was performed to determine the resulting matrix stiffness. The solution containing liposomes without gold nanorods never gelled, and thus could not be harvested. In place of these samples, a fresh solution of alginate and liposomes was pipetted onto the rheometer plate and tested.

For transdermal stiffening studies, a solution of alginate, $CaCO_3$, GdL, and liposomes was prepared as described in the previous chapter. The solution was injected into the dorsal region of the mouse and allowed to gel for 30 minutes. Half of the gels were irradiated for 5 minutes, and the remaining gels were used as controls. The gels were harvested and stiffness was determined by rheometry.

3.2.6 Infrared imaging

To monitor the temperature change during irradiation, an infrared camera (FLIR A325sc) was focused on the injection site and video was recorded during irradiation. The camera was calibrated with a blackbody calibration source (Mikron M310) over the temperature range of interest (15-65^{o}C). The pixel intensity was then converted into temperature. The change in temperature at the irradiation site was determined by tracking the average pixel intensity of the irradiated region for each image in the video sequence. The still frame images were converted to video files in Image J.

3.2.7 Rheometry of explanted gels

Oscillatory shear stress rheometry was performed after explantation of the gels using an Anton-Paar MCR101 rheometer with an 8 mm parallel plate geometry (1% strain, 0.5 – 10 Hz). The strain and frequency range were determined to be within the linear viscoelastic range of the gels by amplitude and frequency sweeps from previous studies. All host tissue was cleared from the gels before rheometry. Any excess gel was

trimmed from the periphery of the measurement tool to ensure consistent gel sizes. The storage modulus was reported in the text at 1.81 Hz for all samples.

3.2.8 Statistical Analysis

Data are presented as mean ± s.d. JMP 10 statistics software was used to analyze the data. Statistical significance was determined using either the Student's t test for comparisons between two groups, or a one-way ANOVA with *post-hoc* Tukey's HSD test for multiple comparisons. P values of less than 0.05 were considered significant.

3.3 RESULTS AND DISCUSSION

3.3.1 Cell viability

There is a concern for cell viability in this system due to the presence of gold nanorods, liposomes, calcium release and heating from irradiation. We sought to assess the impact of the gold nanorod loaded liposomes under irradiation in isolation from calcium release initially. By replacing $CaCl_2$ in the liposomes with DPBS, there would be no negative effects upon release of the liposomal cargo, and any detrimental effects could be attributed to either the liposome components or heating. However, we saw no decrease in cell viability as assessed by the MTS assay up to 5 minutes of irradiation compared to control gels that were not irradiated (Fig. 3.1A). $CaCl_2$-loaded liposomes were then used to test the system as a whole, and again, there was no decrease in viability for up to 5 minutes of irradiation (Fig. 3.1B).

The MTS assay generally tests cell proliferation globally throughout the gel. To look at individual cell viability, the Live/Dead staining assay was used. Cells in gels loaded with $CaCl_2$ liposomes that were irradiated showed no significant differences compared to unirradiated control gels in terms of percent viability (Fig. 3.2).

While an excess of extracellular calcium or heat could be cytotoxic, there was no significant decrease in viability in our system. We hypothesize that released calcium is bound by G-blocks in alginate chains on such a short timescale that it is not readily available to cells, despite the millimolar level of release. Whether calcium signaling pathways are perturbed in our system is unknown, and an interesting topic for future pursuit.

The negligible impact of heat in our system is likely due to the fact that the gold nanorods locally heat their environment, but the bulk gel temperature does not rise above a critical threshold for cell death. In other words, while locally the lipid membrane is heated above 41°C to allow for calcium release, the total heat introduced to the system is not substantial enough to raise the bulk temperature of the gels to a cytotoxic level. Certainly, if irradiation was carried out for an extended duration, the gel temperature would rise high enough to cause cell death. In fact, many groups have utilized this feature of gold nanorods to induce hyperthermic cell death in tumors (54).

3.3.2 3T3 fibroblast morphology in stiffening gels

3T3 fibroblasts were used as a model cell to determine the ability of cells to sense and respond to temporal changes in matrix stiffness. Alginate was mixed with Matrigel to provide a cell adhesion moiety. The cells were uniformly distributed within the gels in 8-well chamber slides. The gels were stiffened to various degrees after 24 hours by irradiation for 0, 30, 60, or 120 s.

In unirradiated control gels that were soft throughout the experiment, fibroblasts adopted an elongated morphology. However, as the gel stiffness increased, the cells became more rounded and less elongated (Fig. 3.3A). The cell perimeter, aspect ratio, and circularity all show significant decreases as irradiation time, and thus stiffness,

increases compared to unirradiated controls (Fig. 3.3B-E). Calcein AM staining reveals that the rounded cells in the stiffened gels are still viable. These morphological changes in response to a stiffened matrix are likely the result of a decreased ability of the cell to deform and elongate throughout the matrix. However, the exact mechanism through which cells exert traction force and sense stiffness in alginate-Matrigel interpenetrating networks is not well understood. To allow for a more direct analysis of cell morphology in response to stiffening matrices, we performed similar experiments with RGD-conjugated alginate.

First, to verify cell adhesion and stiffness sensing in our stiffening gels, 2D RGD-alginate substrates were formed. These gels were made with 20% $CaCl_2$-loaded liposomes. 3T3s seeded on soft RGD-alginate gels had minimal spreading but were adherent to the gel. One day after irradiation to stiffen, the cells were spread over a significantly larger area than unirradiated control gels (Fig. 3.4). Thus, as seen in many other 2D experiments, fibroblasts spread more of stiffer substrates, even when the substrate stiffness is changed dynamically.

Next, 3T3s were seeded within 3D RGD-alginate gels. After 24 hours in the gels, irradiation was performed for 0, 30, 60, or 120 s. Elongation was observed in control gels that were not irradiated, and similar to the alginate-Matrigel composites, the cells became more rounded as irradiation time increased (Fig. 3.5). This indicates that the cells are able to dynamically respond to changes in matrix stiffness. At low crosslinking density in alginate, the cells are able to deform the matrix by applying traction force to the polymer chains to elongate. However, as crosslinking density, and thus stiffness increase, the cells are no longer able to deform the network enough to migrate or elongate. It should be noted that elongation in this case cannot be the result of cell-mediated degradation of the matrix, but simply a remodeling of the alginate network.

These results are quite different from the commonly reported response of fibroblasts to spread more on stiffer 2D substrates and remain rounded on soft substrates. However, we have validated the conventional 2D response here, and others have observed similar morphologies of fibroblasts or mesenchymal stem cells in 3D gels that are either soft or stiff (i.e. not dynamic) (32, 35). This highlights the need to investigate the effects of microenvironmental properties in the most faithful recapitulation of native physiology possible, and especially in 3D contexts. Much work has been done to establish the relationship between cell phenotype and stiffness on 2D substrates. As the field advances into three-dimensional work however, it is unfortunately becoming apparent that much of the knowledge gained in 2D may not be of much value in understanding *in vivo* phenomenon.

3.3.3 Transdermal gelation

Hydrogels are used in many in vivo applications for drug delivery, wound healing, and tissue engineering constructs. A minimally invasive delivery method is particularly beneficial for cell delivery, as it prevents mechanical damage (63) and a detrimental inflammatory response (64). Light-triggered gelation or modulation would allow for excellent temporal and spatial control of the gel properties in vivo, which to date remains challenging. Standard hydrogel photo-polymerization techniques employ UV or visible light wavelengths, which are highly absorbed by the skin and blood, preventing transdermal excitation of the photoinitiator. An optical window exist through which light in the near-infrared region can maximally penetrate tissue however, and light in these wavelengths has been used for many imaging and therapeutic applications. The hydrogel system presented here is particularly well suited for translation to transdermal

applications because of its reliance on NIR light to trigger gelation and stiffness modulation.

To demonstrate this utility, a solution of alginate and $CaCl_2$-loaded liposomes was injected into the dorsal region of a nude mouse (Fig. 3.6A). The injection site was irradiated with an 808 nm CW laser for 5 minutes (Fig. 3.6B). The inclusion of gold nanorods in the liposomes resulted in substantial heating of the irradiation site; monitored by an IR camera. The temperature increased by over 23°C with gold nanorods compared to 12°C in control solutions without gold nanorods after 5 minutes of irradiation (Fig. 3.7, 3.8). The increase in temperature in the controls is due to non-specific absorption of light by the tissue. After just 1 minute of irradiation, the samples containing gold nanorods had heated by 15°C, while the controls had increased by just 5°C (Fig. 3.7, 3.8).

In solutions with gold nanorods, crosslinked gels were formed after irradiation (Fig. 3.6C). These gels were explanted from the mouse and rheometry was performed. Solutions that did not contain gold nanorods did not form gels and remained viscous solutions in the mouse. These solutions could not be recovered for rheometry, and a fresh alginate-liposome mixture was tested in place of these samples. The samples containing gold nanorods formed gels with a storage modulus of 675 Pa, much higher than the viscous solution (31 Pa) of uncrosslinked alginate and liposomes (Fig. 3.9A).

3.3.4 Transdermal stiffening

We next assessed the ability to modulate the stiffness of an alginate hydrogel via transdermal irradiation. A slow-gelling solution of alginate and $CaCl_2$ and gold nanorod loaded liposomes was injected into the dorsal region of a nude mouse again. The solutions were allowed to gel for 30 minutes prior to irradiation. Half of the gels were left unirradiated as controls, and the other half were irradiated for 5 minutes. The gels were explanted and rheometry was performed. The unirradiated gels were moderately

crosslinked and had a storage modulus of 797 Pa. After irradiation, the gels were stiffened significantly to 2363 Pa (Fig. 3.9B), which is within the range seen in our in vitro studies previously reported. To our knowledge, this is the first demonstration of transdermal modulation of hydrogel stiffness.

The capability to modulate stiffness transdermally allows for direct control of mechanical properties of hydrogels during in vivo experiments. This technology could provide a route to investigate the role and mechanisms of matrix stiffness on tumor development and metastasis, which will be discussed further in chapter 5. Many tissue engineering constructs are designed to passive obtain particular mechanical properties at various timepoints to match new tissue formation. Using our system, the properties of the hydrogel could be directly tuned in real time. Additionally, this system could be applied in other hydrogel arenas. Drug release is generally a function of crosslinking density and irradiating the gel to release calcium could easily modulate release rates of an encapsulated solute.

3.4 CONCLUSIONS

In this chapter, we sought to demonstrate the applicability of the dynamic photo-tuning hydrogel system presented in chapter 2 toward *in vitro* investigations of cellular mechanotransduction. Cell morphology with respect to substrate stiffness is well defined on 2D gels, however the recent exploration of morphology in 3D has generated interesting results that are not well-explained with 2D models. Here, we demonstrate that on 2D RGD-conjugated alginate, 3T3 fibroblasts are rounded on soft gels and spread after the gels are stiffened, as expected. Interestingly, in 3D gels, the cells were observed to elongate in soft matrices, and remain rounded in gels that were stiffened. This result was seen in both RGD-conjugated alginate gels and alginate-Matrigel composite gels.

Our findings, along with other similar observations of mesenchymal cells in static 3D gels, point to a need for new models of cell morphology in 3D matrices. Additionally, it is quite likely that the type of gel will influence the degree of elongation observed. Further, and similar to findings in 2D, ligand density, type, and tethering are probably influential in promoting cell elongation in 3D. Dynamic hydrogel systems like the one presented here should be employed to assist in elucidating the mechanisms and driving forces for changes to 3D cell morphology.

We also sought to present a strategy for implementing light-triggered alginate gelation and dynamic stiffness modulation in vivo in this chapter. Our approach utilizes NIR light, which maximally penetrates tissue and is ideal for in vivo applications. We show the ability to form gels from injected alginate solutions via transdermal irradiation, which would allow for a minimally invasive mode of delivery for therapeutics or cells. Additionally, we demonstrate the capability to modulate gel stiffness transdermally. This technology would allow for interesting and previously untestable hypotheses to be assessed, such as the contribution of matrix stiffening to tumorigenesis. Modulation of gel crosslinking density would also allow for changes to the delivery rate of soluble therapeutics entrapped in a gel. Such a system could potentially be used to obtain a remote controlled, tunable drug delivery profile for therapeutics that should be administered in periodic dosages (e.g. insulin).

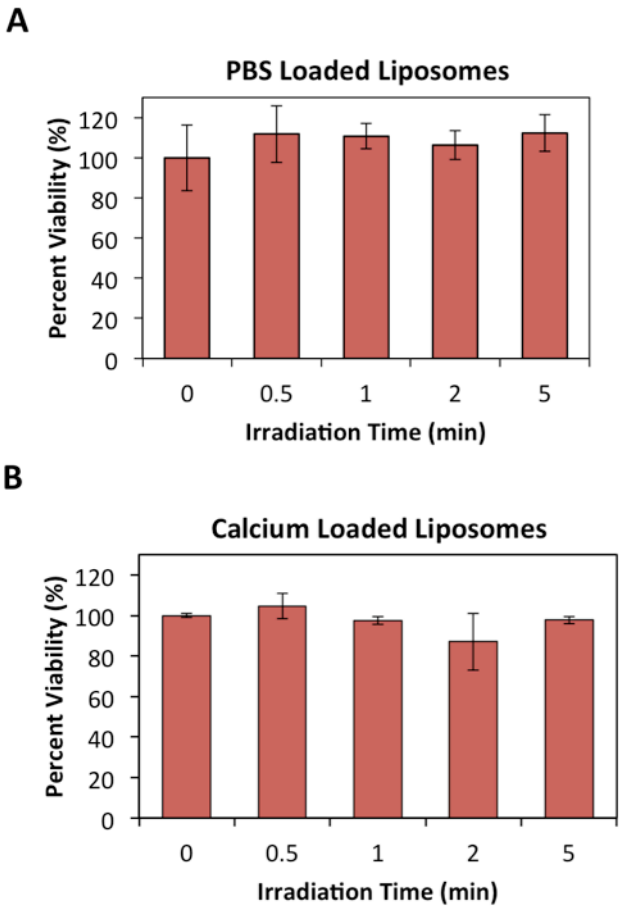

Figure 3.1: MTS assay for cell viability. (A) Liposomes loaded with PBS to assess the effects of irradiation, heating, and presence of gold nanorods on cell viability. No decrease in viability was observed up to 5 minutes of irradiation. (B) $CaCl_2$-loaded liposomes also demonstrated no decrease in viability up to 5 minutes of irradiation.

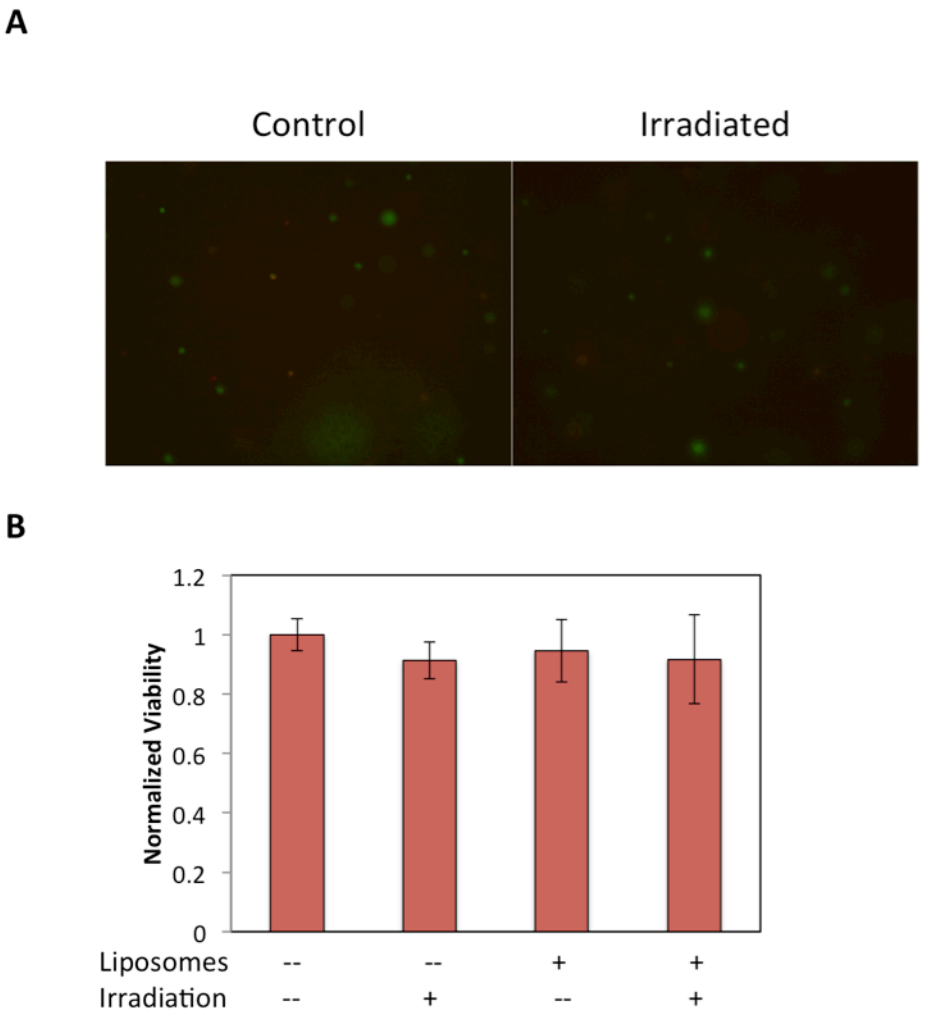

Figure 3.2: Live/Dead assay for cell viability. (A) Cells in alginate gels loaded with $CaCl_2$-liposomes predominantly stained for calcein AM (viable) in control or irradiated gels. (B) Quantification of images from Live/Dead staining. No differences were observed from the presence of liposomes or irradiation.

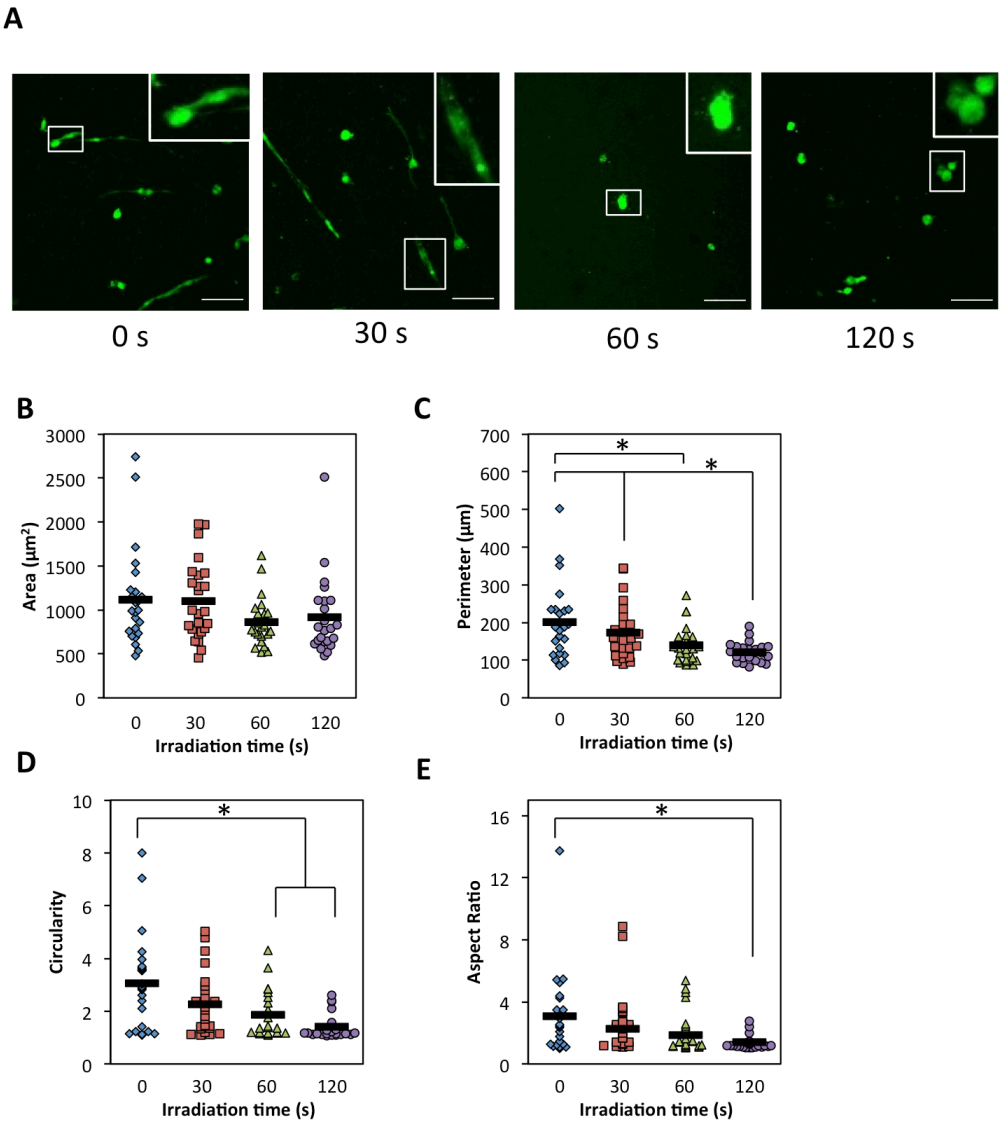

Figure 3.3: Influence of stiffening on cell morphology. (A) NIH 3T3 fibroblasts were encapsulated in alginate gels and increasingly irradiated to induce stiffening. After a total of 72 hours, the cells were imaged. (B) Z-projections of calcein-AM stained cells demonstrate more rounded cells in gels that were stiffened by irradiaiton. Scale bar represents 100 μm. (C-F) Metrics based on traces of at least 25 cells from each group. Cells became more rounded as irradiation time (stiffness) increased. Circularity was calculated as $P^2/4\pi A$ and equals 1 for a perfect circle. * indicates statistical significance of $p < 0.05$.

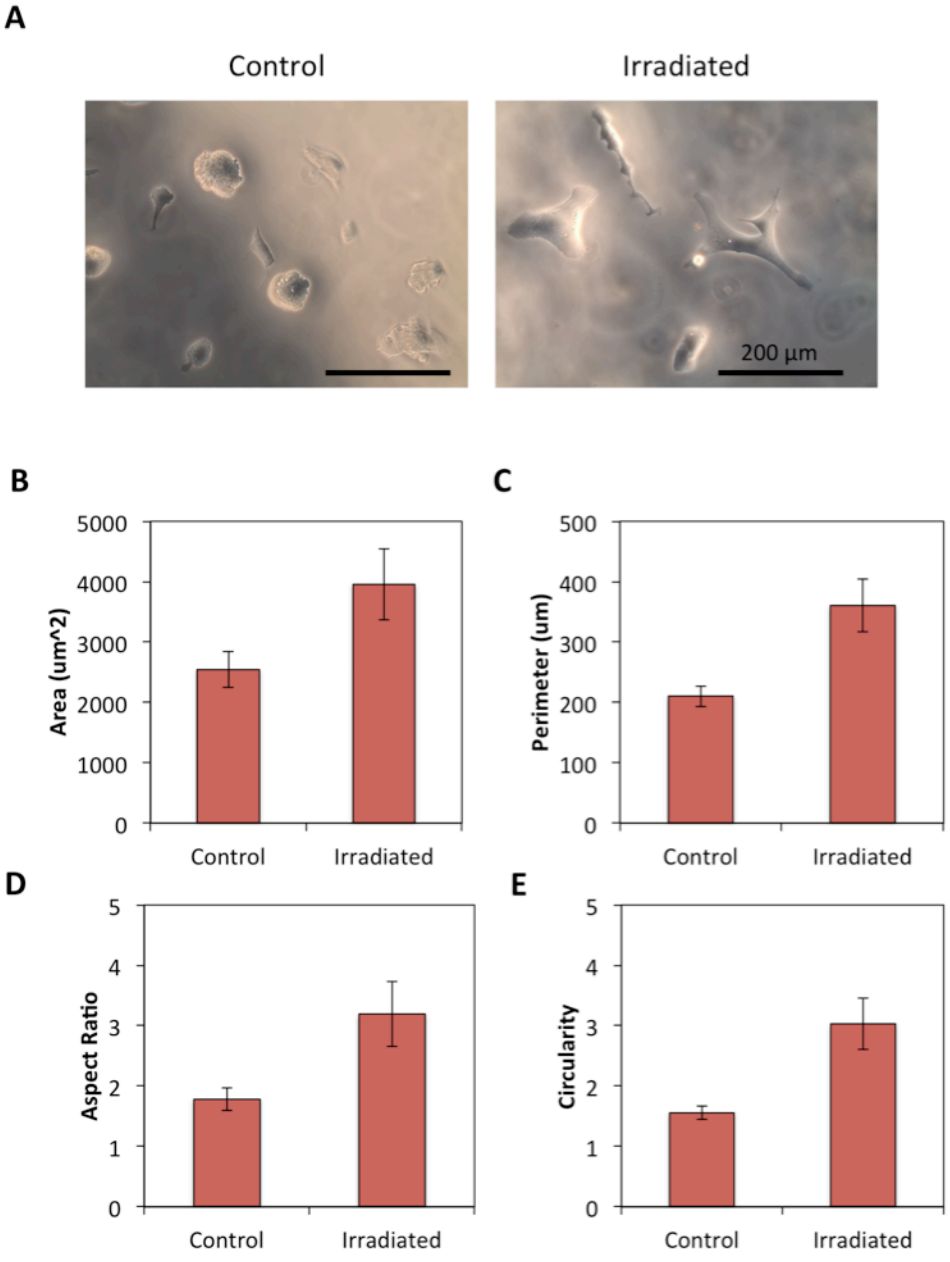

Figure 3.4: 2D validation of cellular response to stiffening. (A) 3T3 fibroblasts seeded on RGD-alginate gels that were initially soft remain rounded. After irradiation to stiffen, the cells spread on the substrates. (B-D) Quantification of image traces of 3T3 fibroblasts on 2D stiffening gels for area, perimeter, aspect ratio, and circularity ($P^2/4\ \pi A$).

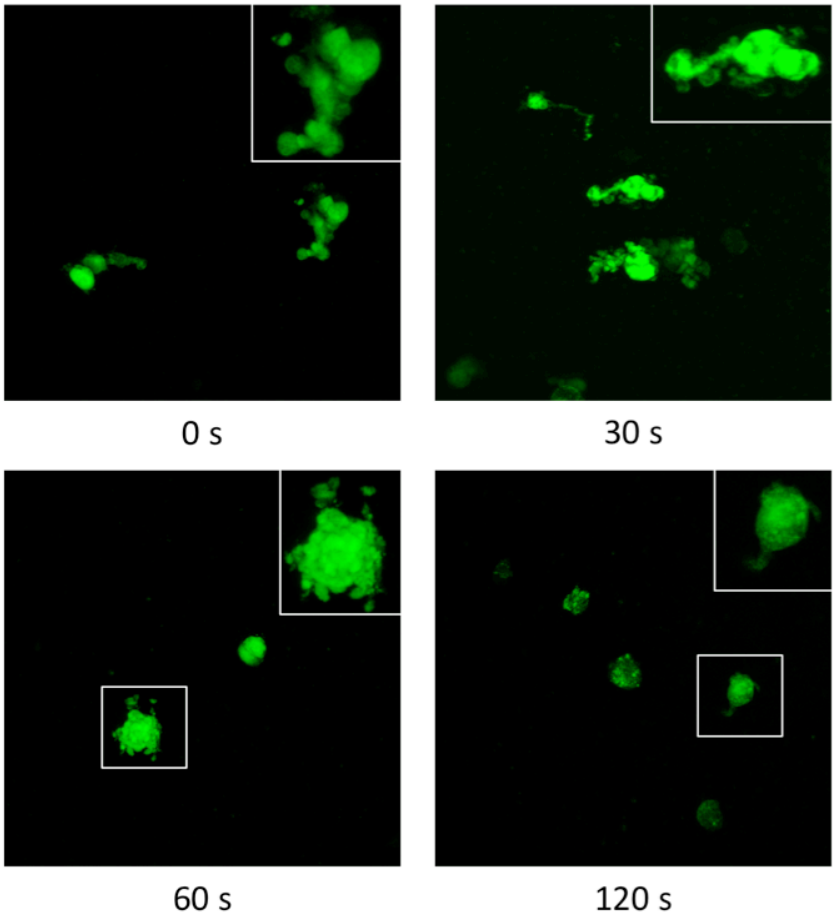

Figure 3.5: Morphology of fibroblasts in 3D RGD-alginate gels. 3T3 fibroblasts elongate in soft matrices, and become increasing rounded as stiffness is increased via irradiation.

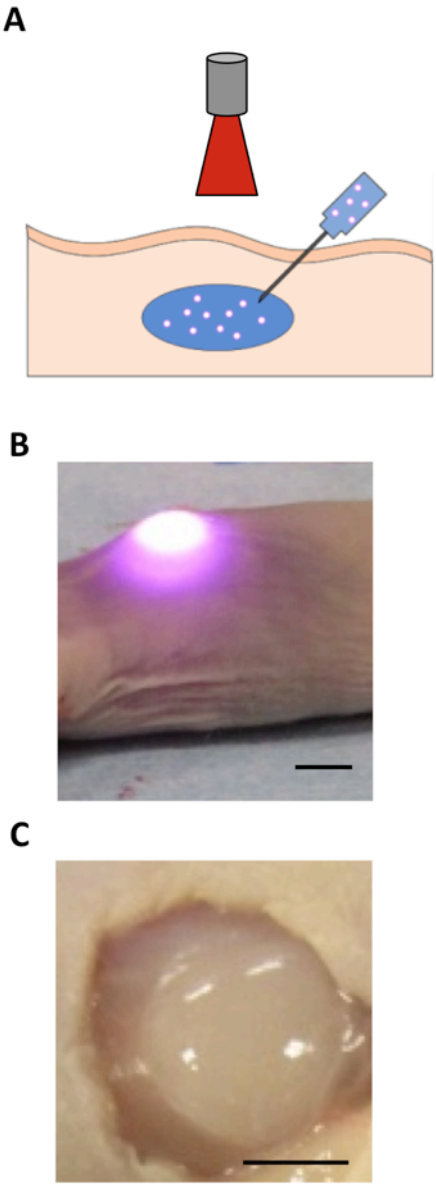

Figure 3.6: Transdermal irradiation induces alginate gelation. (A) Schematic of minimally invasive injection of alginate solution containing $CaCl_2$. (B) Photograph during transdermal irradiation. (C) Photograph of gel produced by transdermal irradiation.

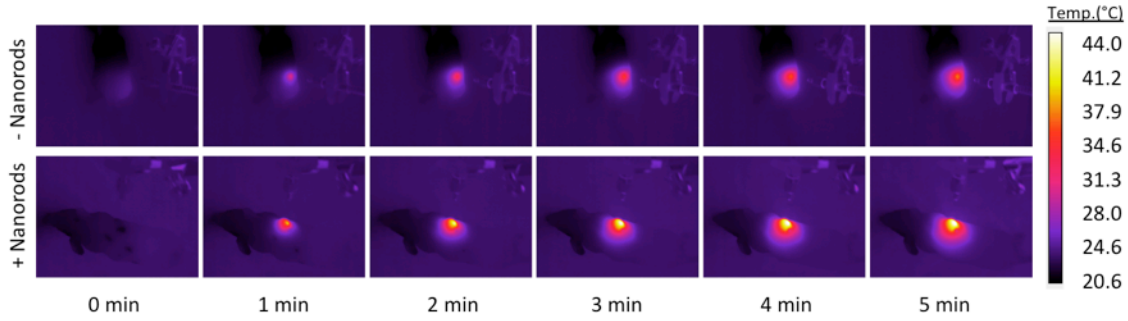

Figure 3.7: Infrared heatmaps along the timecourse of irradiation show significantly faster heating in gold nanorod containing gels.

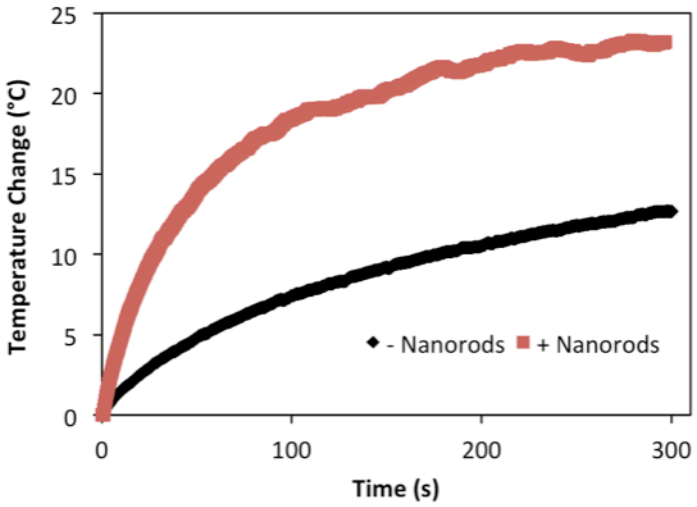

Figure 3.8: Temperature profile of the irradiated region over time. The presence of gold nanorods induces significantly faster heating.

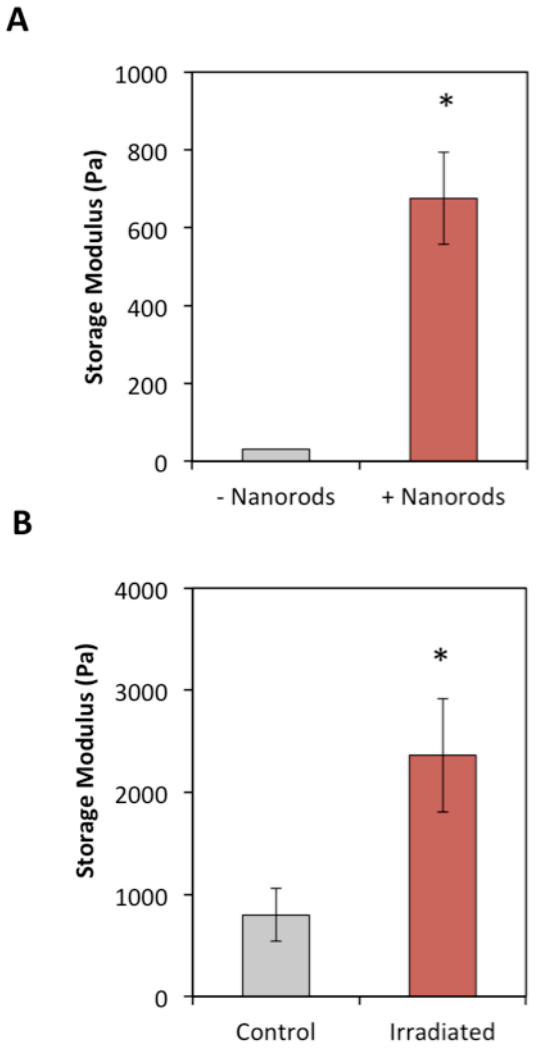

Figure 3.9: Rheometry of explanted gels. (A) Irradiated alginate solutions form gels, indicated by the increase in storage modulus. (B) Soft gels were significantly stiffened after irradiation transdermally as well.

3.5 REFERENCES

1. Ingber DE (1997) Tensegrity: The architectural basis of cellular mechanotransduction. *annu Rev Physiol* 59:575-599.
2. Aplin AE, Howe A, Alahari SK, & Juliano RL (1998) Signal transduction and signal modulation by cell adhesion receptors: the role of integrins, cadherins, immunoglobulin-cell adhesion molecules, and selectins. *Pharmacological reviews* 50(2):197-263.
3. Juliano RL (2002) Signal transduction by cell adhesion receptors and the cytoskeleton. *Annu. Rev. Pharmacol. Toxicol.* 42:283-323.
4. Barczyk M, Carracedo S, & Gullberg D (2010) Integrins. *Cell and tissue research* 339(1):269-280.
5. Niessen CM, *et al*. (1994) The alpha-6 beta-4 integrin is a receptor for both laminin and kalinin. *Experimental cell research* 211:360-367.
6. Fletcher DA & Mullins RD (2010) Cell mechanics and the cytoskeleton. *Nature* 463(7280):485-492.
7. Korn ED, Carlier MF, & Pantaloni D (1987) Actin polymerization and ATP hydrolysis. *Science* 238:638-644.
8. Huxley HE (1969) The mechanism of muscular contraction. *Science* 164:1356-1366.
9. Chaudhuri O, Parekh SH, & Fletcher DA (2007) Reversible stress softening of actin networks. *Nature* 445(7125):295-298.

10. Pollard TD & Cooper JA (2009) Actin, a central player in cell shape and movement. *Science* 326(5957):1208-1212.

11. Karki S & Holzbaur ELF (1999) Cytoplasmic dynein and dynactin in cell division and intracellular transport. *Current opinion in cell biology* 11:45-53.

12. Holy TE & Leiber S (1994) Dynamic instability of microtubules as an efficient way to search in space. *Proceedings of the National Academy of Sciences of the United States of America* 91:5682-5685.

13. Sivaramakrishnan S, DeGiulio JV, Lorand L, Goldman RD, & Ridge KM (2008) Micromechanical properties of keratin intermediate filament networks. *Proceedings of the National Academy of Sciences of the United States of America* 105(3):889-894.

14. Ingber DE (2006) Cellular mechanotransduction: putting all the pieces together again. *FASEB journal : official publication of the Federation of American Societies for Experimental Biology* 20(7):811-827.

15. Wang N & Suo Z (2005) Long-distance propagation of forces in a cell. *Biochemical and biophysical research communications* 328(4):1133-1138.

16. Maniotis AJ, Chen CS, & Ingber DE (1997) Demonstration of mechanical connections between integrins, cytoskeletal filaments, and nucleoplasm that stabilize nuclear structure. *Proceedings of the National Academy of Sciences of the United States of America* 94:849-854.

17. Ali MH, Pearlstein DP, Mathieu CE, & Schumacker PT (2004) Mitochondrial requirement for endothelial responses to cyclic strain: implications for mechanotransduction. *Am J Physiol Lung Cell Mol Physiol* 287:L486-L496.

18. Gilmore AP, *et al*. (1993) The cytoskeletal protein talin contains at least two distinct vinculin binding domains. *The Journal of cell biology* 122(337-347).

19. del Rio A, *et al*. (2009) Stretching single talin rod molecules activates vinculin binding. *Science* 323:638-641.

20. Holle AW & Engler AJ (2011) More than a feeling: discovering, understanding, and influencing mechanosensing pathways. *Current opinion in biotechnology* 22:1-7.

21. Turner CE, Glenney Jr. JR, & Burridge K (1990) Paxillin: A new vinculin-binding protein present in focal adhesions. *The Journal of cell biology* 111:1059-1068.

22. Lim Y, *et al*. (2008) PyK2 and FAK connections to p190Rho guanine nucleotide exchange factor regulate RhoA activity, focal adhesion formation, and cell motility. *The Journal of cell biology* 180(1):187-203.

23. Amano M, *et al*. (1996) Phosphorylation and activation of myosin by Rho-associated kinase. *The Journal of biological chemistry* 271:20246-20249.

24. Palazzo AF, Cook TA, Alberts AS, & Gundersen GG (2001) mDia mediates Rho-regulated formation and orientation of stable microtubules. *Nature cell biology* 3:723-729.

25. Butcher DT, Alliston T, & Weaver VM (2009) A tense situation: forcing tumour progression. *Nature reviews. Cancer* 9(2):108-122.

26. Reichelt J (2007) Mechanotransduction of keratinocytes in culture and in the epidermis. *European journal of cell biology* 86(11-12):807-816.

27. Chien S (2008) Effects of disturbed flow on endothelial cells. *Annals of biomedical engineering* 36(4):554-562.

28. Avvisato CL, *et al*. (2007) Mechanical force modulates global gene expression and beta-catenin signaling in colon cancer cells. *Journal of cell science* 120(Pt 15):2672-2682.

29. Bloom S, Lockard VG, & Bloom M (1996) Intermediate filament-mediated stretch-induced changes in chromatin: A hypothesis for growth initiation in cardiac myocytes. *Journal of molecular and cellular cardiology* 28:2123-2127.

30. Lelievre S, *et al*. (1998) Tissue phenotype depends on reciprocal interactions between the extracellular matrix and the structural organization of the nucleus. *Proceedings of the National Academy of Sciences of the United States of America* 95:14711-14716.

31. Pelham RJ & Wang Y-L (1997) Cell locomotion and focal adhesions are regulated by substrate flexibility. *Proceedings of the National Academy of Sciences of the United States of America* 94:13661-13665.

32. Branco da Cunha C, *et al*. (2014) Influence of the stiffness of three-dimensional alginate/collagen-I interpenetrating networks on fibroblast biology. *Biomaterials* 35(32):8927-8936.

33. Engler AJ, Sen S, Sweeney HL, & Discher DE (2006) Matrix elasticity directs stem cell lineage specification. *Cell* 126(4):677-689.

34. Huebsch N, *et al*. (2010) Harnessing traction-mediated manipulation of the cell/matrix interface to control stem-cell fate. *Nature materials* 9(6):518-526.

35. Khetan S, *et al*. (2013) Degradation-mediated cellular traction directs stem cell fate in covalently crosslinked three-dimensional hydrogels. *Nature materials* 12(5):458-465.

36. Kloxin AM, Kasko AM, Salinas CN, & Anseth KS (2009) Photodegradable hydrogels for dynamic tuning of physical and chemical properties. *Science* 324(5923):59-63.

37. Kloxin AM, Benton JA, & Anseth KS (2010) In situ elasticity modulation with dynamic substrates to direct cell phenotype. *Biomaterials* 31(1):1-8.

38. Wang H, Haeger SM, Kloxin AM, Leinwand LA, & Anseth KS (2012) Redirecting valvular myofibroblasts into dormant fibroblasts through light-mediated reduction in substrate modulus. *PloS one* 7(7):e39969.

39. Wang H, Tibbitt MW, Langer SJ, Leinwand LA, & Anseth KS (2013) Hydrogels preserve native phenotypes of valvular fibroblasts through an elasticity-regulated PI3K/AKT pathway. *Proceedings of the National Academy of Sciences of the United States of America* 110:19336-19341.

40. Yang C, Tibbitt MW, Basta L, & Anseth KS (2014) Mechanical memory and dosing influence stem cell fate. *Nature materials* 13(6):645-652.

41. Peppas NA, Hilt JZ, Khademhosseini A, & Langer R (2006) Hydrogels in Biology and Medicine: From Molecular Principles to Bionanotechnology. *Advanced materials* 18:1345-1360.

42. Annabi N, *et al*. (2014) 25th anniversary article: Rational design and applications of hydrogels in regenerative medicine. *Advanced materials* 26(1):85-123.

43. Ludwig B, *et al*. (2013) Transplantation of human islets without immunosuppression. *Proceedings of the National Academy of Sciences of the United States of America* 110(47):19054-19058.

44. Hoare TR & Kohane DS (2008) Hydrogels in drug delivery: Progress and challenges. *Polymer* 49:1993-2007.

45. Ruel-Gariepy E & Leroux JC (2004) In situ-forming hydrogels--review of temperature-sensitive systems. *European journal of pharmaceutics and biopharmaceutics : official journal of Arbeitsgemeinschaft fur Pharmazeutische Verfahrenstechnik e.V* 58(2):409-426.

46. Matson JB, Zha RH, & Stupp SI (2011) Peptide Self-Assembly for Crafting Functional Biological Materials. *Current opinion in solid state & materials science* 15(6):225-235.

47. Elisseeff JH, *et al*. (1999) Transdermal photopolymerization for minimally invasive implantation. *Proceedings of the National Academy of Sciences of the United States of America* 96:3104-3107.

48. Lin RZ, Chen YC, Moreno-Luna R, Khademhosseini A, & Melero-Martin JM (2013) Transdermal regulation of vascular network bioengineering using a photopolymerizable methacrylated gelatin hydrogel. *Biomaterials* 34(28):6785-6796.

49. Kearney CJ & Mooney DJ (2013) Macroscale delivery systems for molecular and cellular payloads. *Nature materials* 12:1004-1017.

50. Stanley SA, *et al*. (2012) Radio-wave heating of iron oxide nanoparticles can regulate plasma glucose in mice. *Science* 336(6081):604-608.

51. Zhao X, *et al*. (2011) Active scaffolds for on-demand drug and cell delivery. *Proceedings of the National Academy of Sciences of the United States of America* 108(1):67-72.

52. Zhang J & Peppas NA (2000) Synthesis and characterization of pH- and temperature-sensitive poly(methacrylic acid)/poly(N-isopropylacrylamide) interpenetrating polymeric networks. *Macromolecules* 33:102-107.

53. Huebsch N, *et al*. (2014) Ultrasound-triggered disruption and self-healing of reversibly cross-linked hydrogels for drug delivery and enhanced chemotherapy. *Proceedings of the National Academy of Sciences of the United States of America* 111(27):9762-9767.

54. Alkilany AM, Thompson LB, Boulos SP, Sisco PN, & Murphy CJ (2012) Gold nanorods: their potential for photothermal therapeutics and drug delivery, tempered by the complexity of their biological interactions. *Advanced drug delivery reviews* 64(2):190-199.

55. Weissleder R (2001) A clearer vision for in vivo imaging. *Nature biotechnology* 19:316-317.

56. Huang X, El-Sayed IH, Qian W, & El-Sayed MA (2006) Cancer cell imaging and photothermal therapy in the near-infrared region by using gold nanorods. *Journal of the American Chemical Society* 128(6):2115-2120.

57. von Maltzahn G, *et al*. (2009) Computationally guided photothermal tumor therapy using long-circulating gold nanorod antennas. *Cancer research* 69(9):3892-3900.

58. von Maltzahn G, *et al*. (2011) Nanoparticles that communicate in vivo to amplify tumour targeting. *Nature materials* 10(7):545-552.

59. Venkatesan R, *et al*. (2013) Doxorubicin conjugated gold nanorods: a sustained drug delivery carrier for improved anticancer therapy. *J Mater Chem B* 1:1010-1018.

60. Agarwal A, Mackey MA, El-Sayed MA, & Bellamkonda RV (2011) Remote triggered release of doxorubicin in tumors by synergistic application of thermosensitive liposomes and gold nanorods. *ACS nano* 5(6):4919-4926.

61. Gramlich WM, Holloway JL, Rai R, & Burdick JA (2014) Transdermal gelation of methacrylated macromers with near-infrared light and gold nanorods. *Nanotechnology* 25(1):014004.

62. Debnath J, Muthuswamy SK, & Burgge JS (2003) Morphogenesis and oncogenesis of MCF-10A mammary epithelial acini grown in three-dimensional basement membrane cultures. *Methods* 30:256-268.

63. Aguado BA, Mulyasasmita W, Su J, Lampe KJ, & Heilshorn SC (2012) Improving viability of stem cells during syringe needle flow through the design of hydrogel cell carriers. *Tissue engineering. Part A* 18(7-8):806-815.

64. Zeng Q & Chen W (2010) The functional behavior of a macrophage/fibroblast co-culture model derived from normal and diabetic mice with a marine gelatin-oxidized alginate hydrogel. *Biomaterials* 31(22):5772-5781.

Chapter 4: Influence of Matrix Stiffening on Mammary Acini

4.1 Introduction

4.1.1 Tumor stiffness

In many cancers, tumors are much stiffer than the surrounding tissue. Palpation, the process of manually examining the body for abnormalities, relies upon the contrast in tissue stiffness and is the most basic and predominant screening method in current medical practice for tumor detection. Tumor stiffness directly correlates with the stage of cancer progression and metastases are more likely to originate from stiff tumors (1). This clinical evidence has led researchers to evaluate whether stiff matrices contribute to malignant progression or are simply innocuous byproducts of aberrant cell proliferation and ECM remodeling mechanisms. In order to address these fundamental questions regarding the influence of biophysical factors on tumor initiation and progression, in vitro models are needed that reproduce the structure and function of the mammary gland. Additionally, these models need to recapitulate the native microenvironment, including the temporal stiffening that occurs during tumorigenesis.

4.1.2 Mammary gland architecture

The mammary gland is a branching ductal system composed of a single cell layer of polarized epithelial cells surrounding a hollow lumen (2). Located on the basal side of the epithelial cells are contractile myoepithelial cells. The mammary gland branches terminate in alveoli, which is the basic unit of mammary tissue. Around the ducts is the intralobular stroma, which is composed of loose connective tissue and a variety of cell types including microvasculature, lymph vessels, adipocytes, fibroblasts, and inflammatory cells. The bulk of breast tissue is made up of the interstitial stroma, which is denser connective tissue than the intralobular stroma. The interstitial stroma contains

adipose tissue and ECM and is less cellular than the intralobular stroma. The ECM components of each breast tissue component are quite varied. The basement membrane, which is adjacent to the polarized epithelial cells, is comprised of laminins, collagen IV, heparin proteoglycans, and perlecans among other minor components. The intralobular stroma is maintained by stromal fibroblasts and is mostly made of structural ECM proteins such as collagen I and III, elastin, glycosaminoglycans and glycoproteins. Overall, this structure forms a complex network of ECM scaffolding and multiple cell types. The ECM acts as a structure to maintain and direct gland architecture, bind and release growth factors, and signal both biochemically and biophysically to the neighboring cells. One can easily imagine the difficulty in recapitulating this complex and dynamic microenvironment in vitro, even before considering the changes, both cellular and architectural, to the niche upon disease onset.

Mammary tumor progression is accompanied by an infiltration of inflammatory cells, an increase in microvasculature surrounding the tumor, differentiation of stromal fibroblasts, and major changes to the structure and composition of the ECM. Specifically the ECM is remodeled by deposition of fibronectin, tenascin, collagen I, III, IV, and proteoglycans and an increase in matrix metalloproteinase (MMP) expression. MMP 3, 11, 12, and 13 are overexpressed in the tumor stroma while MMP2 is upregulated in transformed epithelial cells (3). Further, induced overexpression of MMP3 has been shown to induce tumor formation or increase tumor incidence, suggesting that MMP overexpression may contribute to disease initiation instead of being merely a correlated effect. Lysyl oxidase (LOX), an enzyme that crosslinks collagen fibers, is overexpressed in the tumor stroma, resulting in a stiffer tumor stroma, in addition to a change in collagen fiber morphology and mechanics (4). The significant changes that occur during

tumor progression hint that ECM stiffening and remodeling could contribute to disease progression, and recent evidence has bolstered this hypothesis.

4.1.3 Microenvironmental stiffness regulates MCF10A phenotype

Initially, three-dimensional models of breast cancer arose out of a need to distinguish between normal and transformed epithelial cells, which was not possible on 2D plastic substrates (2). Normal mammary epitheial cells (MECs) distributed in floating collagen gels formed a multicellular spheroid structure termed an acinus (5). Further inspection of the acinus revealed the cells had polarized and formed a hollow lumen in the center, assembled a basement membrane of laminin around the acinus, and could produce milk proteins when stimulated with hormones (6-8). This demonstrated that tissue specific morphologies and functions could be modeled *in vitro* by providing the appropriate microenvironmental context. Currently, basement membrane extract (BME), commercially available as Matrigel, is the gold standard for generating mammary acini from MEC populations (9). The primary components of Matrigel are laminin-111, collagen IV, entactin, and heparan sulfate proteoglycan (10), which provide structural and biochemical signaling cues to the developing mammary acinus. Matrigel forms a hydrogel when it is warmed to room temperature or above, providing a simple method to encapsulate cells in 3D gels (10).

In many protein gel based systems, matrix stiffness is tunable only within a small range based on the protein concentration. To understand the effects of varied stiffness on mammary acini, polyacrylamide (PA) gels with tunable elastic moduli and coated with adhesion proteins like collagen I or Matrigel can be employed. The Weaver lab used the non-transformed immortalized breast epithelial cell line MCF10A to explore the influence of 2D substrate stiffness ranging from 100-5000 Pa on MCF10A phenotype

(11). On compliant substrates, MCF10A formed spherical, hollow acini with apicobasal polarity and were phenotypically normal. However, on stiffer substrates, the apicobasal polarity was lost, cells began to proliferate in the center of the acini, and cells were even observed to migrate on the stiffest substrates. This study provided substantial evidence that microenvironmental stiffness can regulate epithelial cell phenotype, even in the absence of oncogenic signaling. A significant limitation of this study, aside from its 2D nature, is that the cells cultured on stiff substrates would never adopt the normal acinar structure, making the interpretation of the abnormal phenotype difficult in the physiological context. The research group later sought to improve upon this work by culturing MCF10As in 3D collagen matrices that were of physiological compliance initially and could be further crosslinked by the addition of ribose (4). They found that secondary crosslinking disrupted normal acinar structures, and when combined with oncogene activation (ErbB2), could induce invasion. However, the stiffness of the matrices was increased by only 40 Pa (130 initially to 170 Pa). For comparison, the same authors reported the difference in modulus between healthy tissue and a mammary tumor as 3882 Pa. Thus, the cellular changes observed in this study were likely due to increased collagen crosslinking density and not specifically from an increase in stiffness. Increased collagen crosslinking could increase integrin occupancy and is known to influence cell fate independently of matrix stiffness (12). Additionally, collagen I is not a basement membrane component in normal tissue, thus MECs would only interact with it after breaching the basement membrane. MCF10A interaction with collagen I could prime the cells toward an invasive phenotype simply through cell-ECM binding interactions (13). For these reasons, it is imperative to evaluate the role of ECM stiffening in tumor progression and metastasis by utilizing a tunable hydrogel with stiffness changes of the same magnitude seen in tumorigenesis and with appropriate ECM composition.

Recently, MCF10A were shown to adopt an invasive phenotype in stiff gels composed of alginate and Matrigel interpenetrating networks (14). This study is intriguing because the stiffness can be controlled independently of ECM composition and architecture, which are typically highly correlated in protein gels. The group was able to convincingly demonstrate that matrix stiffness per se can drive conversion to a malignant phenotype. Again however, these cells are seeded within matrices that are either soft or stiff initially and maintain constant mechanical properties throughout the experiments. Thus, the malignant phenotype does not arise from a phenotypically normal population of cells. A dynamic platform is needed to address these outstanding questions. Nonetheless, signaling through the Rac1 and PI3K pathways were identified as critical to the maintenance of the malignant phenotype. Indeed, these and other mechanotransduction pathways may be critical to establishing and reinforcing a dynamic reciprocity between a stiffening microenvironment and tumor progression.

4.1.4 Epithelial to Mesenchymal Transition

The epithelial-to-mesenchymal transition (EMT) is a latent embryonic program that can be induced in tumors and causes migratory and invasive behavior from cancer cells. EMT has been postulated as a mechanism by which cancerous epithelial cells could disseminate from the primary tumor and metastasize. Markers for EMT inducers correlate with poor clinical outcomes across a variety of cancer and metrics (15). Until very recently however, researchers were unable to confirm the presence of EMT in clinical samples. This is partially due to the fact that mesenchymal cells derived from epithelial tumors are nearly indistinguishable from tumor stromal fibroblasts. Recently, several studies have demonstrated the presence of mesenchymal cells leading the invasive front in migration away from the primary tumor (16). E-cadherin expression in these cells was not found (17) or downregulated (15), while the mesenchymal marker vimentin was

upregulated at the invasive front. Loss of E-cadherin is a critical event in EMT, and can be induced by repressors of E-cadherin promoters like Snail, Zeb, E47, or KLF8 (18, 19) or indirect repression of E-cadherin transcription through Twist, Goosecoid, E2.2 and FoxC2 (20, 21). Induction of EMT in tumor cells leads to dissemination of the cells from the primary tumor, breach of the basement membrane and interaction with the stromal microenvironment. Thus, these cells will be the first to interact with the alter ECM present around the tumor. Further, as mesenchymal cells, they are likely more responsive to changes in matrix stiffness. For these reasons, we are interested in assessing how matrix stiffening may contribute to EMT induction and how induced cells respond in stiffened matrices.

4.1.6 Chapter overview

Here, we show that MCF10A cultured in initially soft alginate-Matrigel composites that are stiffened after acinus formation undergo a phenotypic switch to a malignant or protrusive phenotype. Gene analysis for an array of EMT associated genes shows upregulation in a number of critical EMT markers across several stiffening time points. Morphologically, we observed an increase in protrusive colonies and colony size after stiffening at day 14 and imaging at day 17. Expression of Ki-67, a proliferative cell marker, was increased in the nuclei of acini in irradiated gels. These changes associated with stiffening were abrogated when small molecule inhibitors of PI3K and Rac1 were added to the cultures upon stiffening. Inhibition of MAPK did not prevent protrusive acini but did result in smaller acini.

4.2 MATERIALS AND METHODS

4.2.1 Cell culture

Human mammary epithelial cells (MCF10A) were obtained from American Type Culture Collection (ATCC). MCF10A were cultured with DMEM/F12 basal media containing 5% horse serum, 20 ng/ml epidermal growth factor, 0.5 mg/ml hydrocortisone, 100 ng/ml cholera toxin, 10 μg/ml insulin, and 1% penicillin-streptomycin (9). Media was changed every 2 days and cells were passaged before reaching confluency.

4.2.2 3D cell culture

Assay media was used for all 3D cell cultures. The assay media was composed of DMEM/F12 basal media, 2% horse serum, 5 ng/ml epidermal growth factor, 0.5 mg/ml hydrocortisone, 100 ng/ml cholera toxin, 10 ug/ml insulin, and 1% penicillin-streptomycin (9).

Pronova UP MVG sodium alginate was dissolved in 300 mM NaCl buffered with HEPES to 4% w/v. Uniformly crosslinked alginate gels were made using insoluble $CaCO_3$ as a calcium source, and glucono-δ-lactone (GdL), which hydrolyzes upon dissolution in water to release calcium ions. Gels were made with 5 mM $CaCO_3$ and 10 mM GdL. Liposomes were included at 20% of the volume of the gel. Growth factor reduced Matrigel was included at stock concentration as 25% of the volume of the gels. Cells were mixed with the alginate solution prior to gelation to ensure a uniform distribution throughout the gel. Gels were pipetted into chambered coverglasses or well plates and allowed to gel at 37ºC for 30 minutes. Culture media was then carefully pipetted over the gels and changed every other day.

The gels were irradiated after 4, 7, 14, and 21 days in culture for RNA analysis and on day 14 for all other experiments. The culture media was removed prior to irradiation and replaced immediately afterward. An 808 nm CW laser was positioned above the well plate or chamber slide and exposed for 1 minute.

4.2.3 Phase contrast microscopy

A Leica DM IRB microscope was used to capture phase contrast images of the MCF10A acini in 3D gels. Images were taken throughout the time period of culture to ensure proper development of the mammary acini. To quantify the number of protrusive colonies, images were taken at day 17, three days after stiffening. A minimum of 30 acini were imaged per experimental condition. Acini were manually identified as protrusive if there was a non-continuous curvature of the acinus perimeter (14). Acinus size was determined by tracing the outline of the acini in ImageJ and determining the area.

4.2.4 Multi-photon and confocal microscopy

Multi-photon excitation or confocal laser scanning microscopy was used to image the 3D gels. Multi-photon imaging was performed at 770 nm excitation wavelength. Confocal samples were excited with both 405 nm and 561 nm lasers. The samples were excited with a Spectra Physics Mai Tai pulsed laser source. A Prairie View Ultima multiphoton microscopy system with a 20X or 40X objective was used to capture images. ImageJ was used to convert the image sequences into a Z-projection or 3D projections.

4.2.5 F-actin staining

F-actin was stained using an AlexaFluor 488 conjugated phalloidin. The media was removed from the gels and then the gels were rinsed three times for 5 minutes with DPBS with Ca^{2+}, Mg^{2+} to maintain the alginate crosslinks. The gels were then fixed in 2% formaldehyde with 2.5 mM $CaCl_2$ for 15 minutes. The gels were rinsed again with DPBS

three times. The cells were permeabilized with 0.1% Triton-X-100 in DPBS for 15 minutes, then incubated with 50 uM phalloidin for 30 minutes. The phalloidin solution was removed and the gels were washed three times for 5 minutes in DPBS again. Finally, a 5 uM solution of DAPI in Anti-fade solution was added and the gels were imaged.

4.2.6 Immunocytochemistry

Antibodies against Ki-67 (Thermo Scientific, RM-9106) and β catenin (BD Transduction 610154) were purchased. To prepare gels for antibody labeling, they were fixed fixed in 2% paraformaldehyde for 15 minutes. The alginate gel porosity is on the nanometer scale, and substantially limits the diffusion of antibodies. The gels were broken up by gentle pipette mixing to reduce the distance the antibodies must diffuse to reach their antigen. The cells were permeabilized with 0.5% Triton-X-100 in DPBS for 10 minutes at 4ºC and then rinsed three times with DPBS with glycine for 5 minutes each. The gels were incubated in a blocking solution of 10% goat serum in DPBS for 1 hour. The primary antibody was incubated overnight at 4ºC at a dilution of 1:100 in 10% goat serum. The following day, the gels were rinsed three times with DPBS with 0.1% Triton-X-100 for 20 minutes. The secondary antibody was diluted 1:100 in 10% goat serum in DPBS and incubated at room temperature in the dark for 90 minutes. The gels were rinsed three times in DPBS. DAPI was diluted to 5 ug/ml in DPBS and incubated with the gels for 15 minutes. The gels were then rinsed three times with DPBS for 15 minutes. Finally, the gel suspension was pipetted onto coverslips depressed into petri dishes or glass slides, coverslipped and sealed. The slides were imaged immediately or stored at 4ºC in the dark until imaging.

4.2.7 RNA isolation and PCR arrays

Twenty-four hours after irradiation, cells were isolated from alginate-Matrigel composites by carefully removing the gels from the well plates and placing them into 50 mM EDTA in DPBS on ice for 5 minutes. The tubes were gently shaken to dissolve the gels and the solution was centrifuged at 150 g for 5 minutes to pellet the cells. The cell pellet was resuspended in Qiagen RLT Buffer and centrifuged through a QIAShredder column to lyse the cells. The flow-through was collected and RNA was isolated with the RNeasy Mini Kit according to the manufacturer's instructions. The RNA was quantified with a NanoDrop Spectrophotometer.

Equal amounts of RNA from the irradiated and control conditions were used in a First Strand reverse transcription kit, according to the manufacturer's instructions. After reverse transcription, the cDNA was mixed with SybrGreen Master Mix and RNase free water. This solution was plated into a 96-well PCR array for epithelial-to-mesenchymal transition (EMT) markers (PAHS-090Z). The plates were run on Viia 7 PCR machines. Thresholds for amplification curves were manually set to be equal between control and irradiated samples. The $\Delta\Delta C_t$ values were calculated by normalizing to the best fit of five housekeeping genes in the plate, and then normalizing to the control condition. Heatmaps were generated from the PCR array data using JMP. The heatmaps were sorted in descending order for day 7, 14, and 21 for comparison.

4.2.8 Small Molecule Inhibition

Small molecule inhibitors of mechanotransduction pathways were added on day 14 after irradiation of the gels. The gels were fixed on day 17 and images of acini were captured. The acini size and number of protrusive colonies was determined as in section 4.2.3. The specific inhibitors used were a FAK inhibitor (PF573228, 5 uM), a ROCK inhibitor (Y27632, 10 uM), a MAPK inhibitor (PD98059, 10 uM), a Rac1 inhibitor

(NSC23766, 70 uM), and a PI3K inhibitor (LY294002 20 uM). The inhibitors and concentrations were selected based on previous work (14, 22, 23).

4.2.9 Quantification of Ki-67 labeled nuclei

Acini stained for Ki-67 and DAPI were imaged with a Leica DM 3000B fluorescence microscope. The nuclei positive for Ki-67 and DAPI were analyzed in ImageJ. Briefly, the images were converted to black and white and a watershed algorithm was applied to separate adjacent nuclei. A size threshold for a nucleus was applied and the particles were counted using the automated feature. The number of Ki-67 positive nuclei was divided by the total number of nuclei labeled with DAPI to give the fraction of proliferating cells.

4.2.10 Statistical Analysis

Data are presented as mean ± s.d. JMP 10 statistics software was used to analyze the data. Statistical significance was determined using either the Student's t test for comparisons between two groups, or a one-way ANOVA with *post-hoc* Tukey's HSD test for multiple comparisons. P values of less than 0.05 were considered significant.

4.3 RESULTS AND DISCUSSION

4.3.1 MCF10A acinus formation in alginate-Matrigel composites

MCF10A seeded within alginate-Matrigel composite gels formed mammary acini similar to MCF10A embedded in Matrigel alone. Single cells proliferated over the course of two weeks to form multicellular aggregates (Fig. 4.1). It should be noted that while hollow and polarized acini were observed, not all acini were fully mature in these gels. It is possible that more time was needed for full maturation. Additionally, the initial gel crosslinking density, spatial distribution of Matrigel, or other features of the alginate gel

may have prevented full maturation in some cases. Using similar soft alginate-Matrigel interpenetrating networks, others have demonstrated that normal morphogenesis of MCF10A occurs in these gels (14). Unlike previous studies where single cells were seeded either in soft or stiff matrices, here we are able to assess the impact of a stiffened microenvironment on a multicellular mammary acinus.

4.3.2 Effect of stiffening on acinus morphology

MCF10A acini in alginate-Matrigel composites were cultured for 14 days and irradiated to stiffen the matrix (Fig. 4.2A). The storage modulus of the gels prior to irradiation was 50 Pa, and after irradiation the gels stiffened to 357 Pa (Fig. 4.2B). These values are within the range reported for normal mammary gland tissue, and malignant tumors (11). Within 3 days after stiffening the gels, protrusions or branches were observed emanating from the acini (Fig. 4.3A). The protrusions were multicellular structures that maintained cell-cell contacts, as evidenced by β catenin expression between neighboring cells (Fig. 4.4). These protrusive structures resemble collective cell migrations from tumor fragments embedded in in vitro gels (24). Interestingly, collective cell migration from carcinoma samples was previously seen predominately in collagen I gels, and abrogated in Matrigel. In both gel conditions, the matrix stiffness was relatively low. Here, we observe collective cell protrusions in environmental contexts where MCF10A can only interact with proteins contained in Matrigel, and not collagen I. Therefore, we conclude that matrix stiffening, as well as ECM composition can promote protrusive behavior.

We next sought to quantify the effect of matrix stiffening on MCF10A acinus morphology. Acini were imaged 3 days after stiffening and classified as protrusive or normal. The cross-sectional area was also quantified by tracing the perimeter of the

acinus. We observed a statistically significant increase in the number of protrusive acini after stiffening (55.5 ± 5.8% protrusive) compared to controls that were not irradiated (14.0 ± 8.5%) (Fig. 4.3A,B). The cross-sectional area of acini in stiffened gels was also significantly larger, by 2.7 times, than acini in control gels (Fig. 4.3C), suggesting a loss of growth-arrest and an increase in proliferation. This was confirmed by a significant increase in Ki-67 positive nuclei in acini from irradiated gels. While Ki-67 labeled nuclei were rarely observed in acini from control gels, nearly one third of nuclei in the irradiated gels were positive for Ki-67 (Fig. 4.4). Staining of cellular F-actin allowed for the visualization of the cytoskeleton of the protrusive cells. Multiple cells were observed to collectively migrate away from the perimeter of acini with hollow lumens (Fig. 4.5, 4.6). It should be noted that not all acini had hollow lumens in both the control and irradiated groups. In the stiffened gels, protrusions were seen in both hollow and filled acini.

Previous work has demonstrated that MCF10A seeded as single cells on stiff 2D substrates or in stiff 3D gels adopt a malignant phenotype (11, 14). How stiff environments affect acini was an outstanding question, largely because of the lack of hydrogel platforms for 3D dynamic stiffening. In prior attempts to dynamically stiffen rBM-collagen gels through glycation of collagen with ribose, MCF10A were only observed to invade matrices when the oncogene ErbB2 was concurrently activated (4). In the absence of oncogenic signaling, the MCF10A adopted an abnormal morphology but were not observed to invade the matrix. However, the increase in stiffness in this system was quite low; a net change in elastic modulus of only 40 Pa was induced. It is possible that a larger stiffness change may have triggered invasion in the absence of ErbB2 activation. Our observation of MCF10A converting to an protrusive phenotype from a mammary acinus addresses the question of ECM stiffening in a more physiologically relevant context, both in terms of timing and magnitude of stiffening. These findings

confirm the hypothesis that matrix stiffening, in isolation from changes in matrix composition or ligand density, can promote an aberrant, protrusive phenotype from a quiescent population of nontransformed mammary epithelial cells.

A branching or protrusive phenotype might arise from a mammary acinus by a change in matrix stiffness through several routes. Matrix stiffness is known to alter biochemical signaling through several mechanotransduction pathways. We assessed the influence of several of these signaling enzymes (PI3K, Rac1, MAPK, ROCK, FAK) in this chapter. Other intriguing possibilities include alterations in the sensitivity of MCF10A to growth factor signaling and the distribution of mechanical stress in soft and stiffened gels. TGF-β signaling in Madin-Darby canine kidney (MDCK) epithelial cells depends greatly on the stiffness of the substrate on which the cells are cultured. On compliant substrates, TGF-β induces apoptosis, while on stiff substrates, TGF-β promotes EMT (25). Additionally, Kim and Asthagiri showed MDCK cells are 100-fold more sensitive to EGF on stiffer substrates than on compliant substrates (26). On stiff substrates, even EGF doses as low at 0.1 ng/ml caused significant increases in proliferation of the cell clusters. It is possible that similar mechanical switches exist in MCF10A acini in 3D gels, where an increase in matrix stiffness can cause an increase in sensitivity or a change in response to particular cytokines.

The distribution of stress throughout mammary ducts has also been implicated in driving invasion. Using micropatterned acini, Boghaert et al placed a single tumor cells in acini of non-transformed cells at areas of high or low mechanical stress. The cells in regions of high stress were much more invasive than cells in areas of low stress, despite having similar cell-cell contacts. Overall, the distribution of stress was shown to dictate whether cells invade or remain in the duct. Similarly, a change in matrix stiffness in the system presented here could change the overall stress in a mammary acini, as cells are

able to exert higher traction forces against stiffer matrices. Areas where stress is concentrated may prime cells for protrusion into the matrix.

4.3.3 Matrix stiffening induces upregulation of EMT markers

The emergence of a protrusive population of cells from the mammary epithelial cell spheroids suggested a possible EMT event occurring after matrix stiffening. We sought to screen a panel of EMT markers using a commercially available EMT PCR array to determine the gene expression signature of MCF10A after stiffening. MCF10A were cultured in alginate-Matrigel composites and stiffened at day 4, 7, 14, or 21. The RNA content was isolated 24 hours after stiffening and analyzed with an EMT PCR array. Compared to cells in unirradiated control gels, stiffening of the matrix caused upregulation of a number of genes associated with EMT with good agreement across stiffening timepoints (Fig. 4.7). It should be noted that replicates within timepoints were not performed for these experiments, as the intent was to broadly screen gene expression trends and not quantitatively assess statistically significant changes. Nonetheless, the general correlation of values across timepoints affords some confidence that the observed trends are indicative of gene expression changes in response to matrix stiffening, and not simply random variations.

Notably, ZEB2 and to a lesser extent ZEB1 and TWIST1, critical mediators of EMT, are upregulated after matrix stiffening. VIM, which encodes for vimentin, a specific marker of mesenchymal cells, is moderately upregulated as well. In addition, the RNA production after stiffening on day 14 of several other genes that are implicated or associated with EMT was at least twice that of controls including WNT5A, SOX10, IGFBP4, and AHNAK. Notably, expression of the Snail family of transcription factors as well as GSC was unchanged from controls or even mildly downregulated. Thus, it

appears that matrix stiffening induces upregulation of a number of critical EMT markers, but does not fully reproduce the classical EMT gene expression profile. Interestingly, many invasive cancers are marked by a partial-EMT character, wherein cells of epithelial origin are involving in or leading invasion and migration, while maintain some epithelial traits such as E-cadherin junctions (27).

4.3.3 Inhibition of Rac1, PI3K, and MAPK abrogate protrusive behavior

To understand the mechanisms involved in stiffening-induced invasion, small molecule inhibitors of Rac1, PI3K, MAPK, FAK, and ROCK were added to culture media after stiffening. The acini were imaged 3 days after stiffening and application of the inhibitors. Acini treated with Rac1 and PI3K showed marked reduction size and number of protrusive colonies compared to untreated, stiffened acini (Fig. 4.8). Only 27.5% of acini treated with the PI3K inhibitor were protrusive (Fig. 4.9A). Similarly, only 28.5% of colonies treated with the Rac1 inhibitor were protrusive. Both of these groups were significantly lower than untreated cells in stiffened gels, and neither were significantly different from control gels that were not stiffened. The average acinus size in gels treated with either PI3K or Rac1 inhibitors was also significantly lower than the stiffened but untreated acini (Fig. 4.9B). In fact, the acinus size in the PI3K treatment group was statistically similar to unirradiated control gels. The proportion of protrusive acini in gels treated with ROCK and MAPK inhibitors decreased slightly, however the changes were not statistically significant. The average size of acini treated with the MAPK inhibitor was significantly smaller than untreated acini in stiffened gels however. This points to a possible role for MAPK in promoting proliferation or loss of normal acinus morphology, but not directly in initiation of invasion. Acini treated with the FAK inhibitor showed no change from the untreated acini. These results suggests that ROCK and FAK may not be directly involved in initiation of invasion of mammary acini. That is

not to say that ROCK and FAK are not involved in transducing mechanical signals to drive tumor progression and invasion in vivo. In tumors, genetic changes may cause aberrant FAK or ROCK signaling that could promote invasion. Indeed, disruption of FAK has been shown to prevent invasion of in situ carcinomas in mouse models (28).

Rac1 and PI3K were also found to be essential mediators of MCF10A invasion in static, stiff alginate-Matrigel networks (14). Inhibition of these molecules lead to a reduction in invasion and colony size in stiff gels, similar to our finding that the effects of stiffening reduce the phenotypic conversion of MCF10A. This study suggested that maintenance of a normal phenotype is mediated through clustering of β4 integrins. In stiff gels, the cells were unable to cluster the integrins and the cytoplasmic tails were available for phosphorylation by receptor tyrosine kinases, which lead to activation of PI3K and Rac1. Our findings are consistent with this PI3K and Rac1 mediated pathway.

Weaver and colleagues sought to determine the effects of matrix stiffness on multicellular epithelial cell spheroids by transplanting them from soft, rBM gels to collagen gels of varied stiffness (29). They observed altered morphology, but not invasion, of MCF10A spheroids 48 hours after transplantation to a stiffer (1.5 kPa) collagen gel. Invasion was observed only with Ha-ras transformed MCF10AT spheroids, and was mediated by PI3K signaling. This finding was consistent with previous work from this group that demonstrated invasion occurred only when stiff matrices were coupled with oncogenic signaling (4). Here, we show a protrusive phenotype arising from a non-transformed population of MCF10A in 3D architectures upon stiffening of the matrix. Interestingly, promotion of the invasive phenotype by matrix stiffening is also driven by the PI3K pathway.

4.4 CONCLUSIONS

We have demonstrated that MCF10A form mammary acini in 3D alginate-Matrigel composite hydrogels. Stiffening these gels by irradiation promotes dissemination of cell clusters from the acinus and protrude into the matrix. Matrix stiffening also induces increased cellular proliferation, resulting in larger acini. Further, the effects of stiffening are abrogated by inhibiting the PI3K or Rac1 pathways. Finally, several EMT markers are upregulated upon matrix stiffening, indicating a partial EMT event by which MCF10A become protrusive.

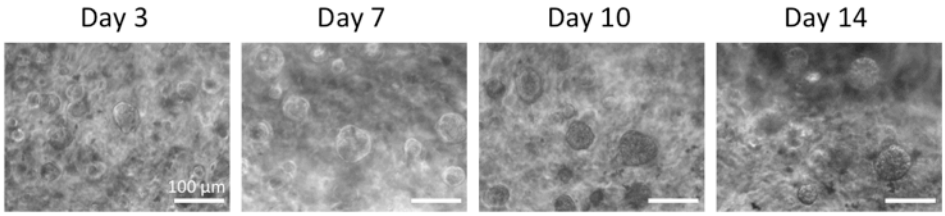

Figure 4.1: MCF10A morphogenesis in alginate-Matrigel composite gels over 14 days. Scale bar represents 50 µm.

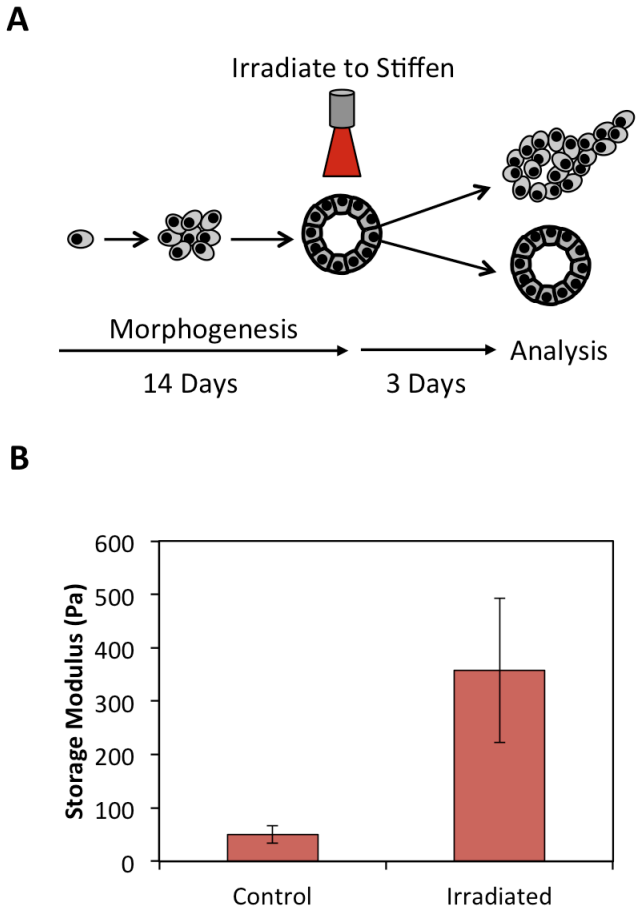

Figure 4.2: (A) Scheme of experimental timeline. MCF10A will be cultured in alginate-Matrigel composites to undergo morphogenesis. The gels will be irradiated to stiffen the matrix around the cells and analysis will be performed. (B) Storage modulus of alginate-Matrigel composites increases upon irradiation.

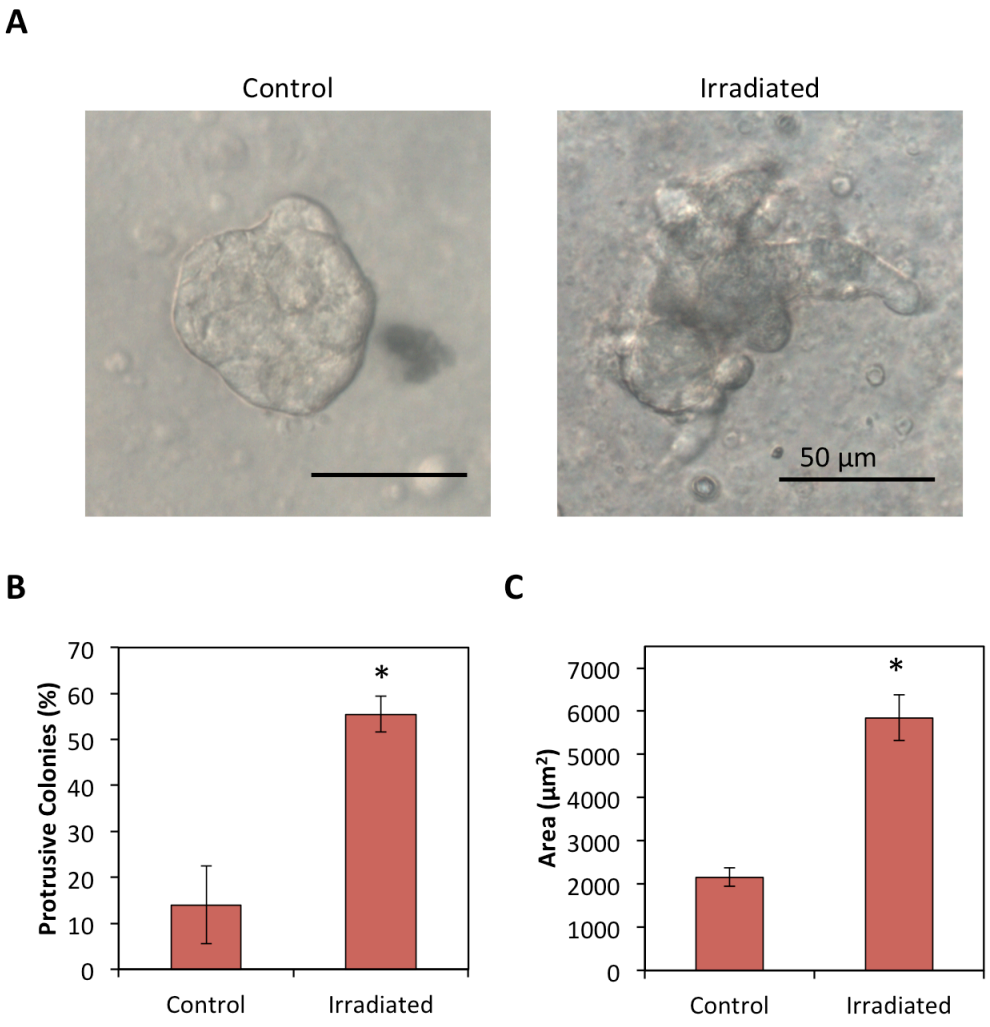

Figure 4.3: Effect of stiffening on MCF10A morphology and phenotype. (A) Morphology of MCF10A after 17 days in culture in static, soft alginate-Matrigel composites (left) and gels that were stiffened on day 14 (right). Protrusions arise after stiffening. (B) The number of protrusive colonies significantly increases upon stiffening the gels. (C) Acinus area significantly increases are stiffening as well.

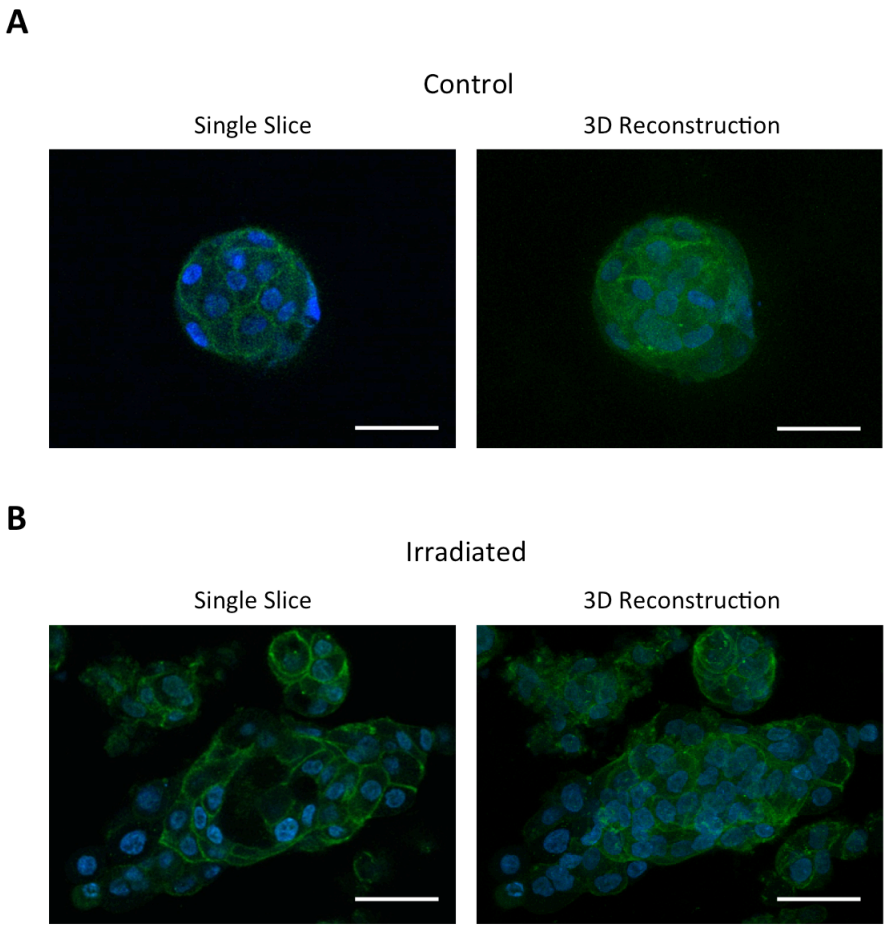

Figure 4.4: β catenin expression in MCF10A in control and stiffened gels. (A) Single image (left) from the middle of MCF10A acinus in control gels labeled with anti-β catenin antibody (green) and DAPI (blue). 3D reconstruction of Z-series of images (right). (B) Single slice (left) and 3D reconstruction (right) of protrusive acinus in irradiated gels. Scale bar represents 50 μm in all images.

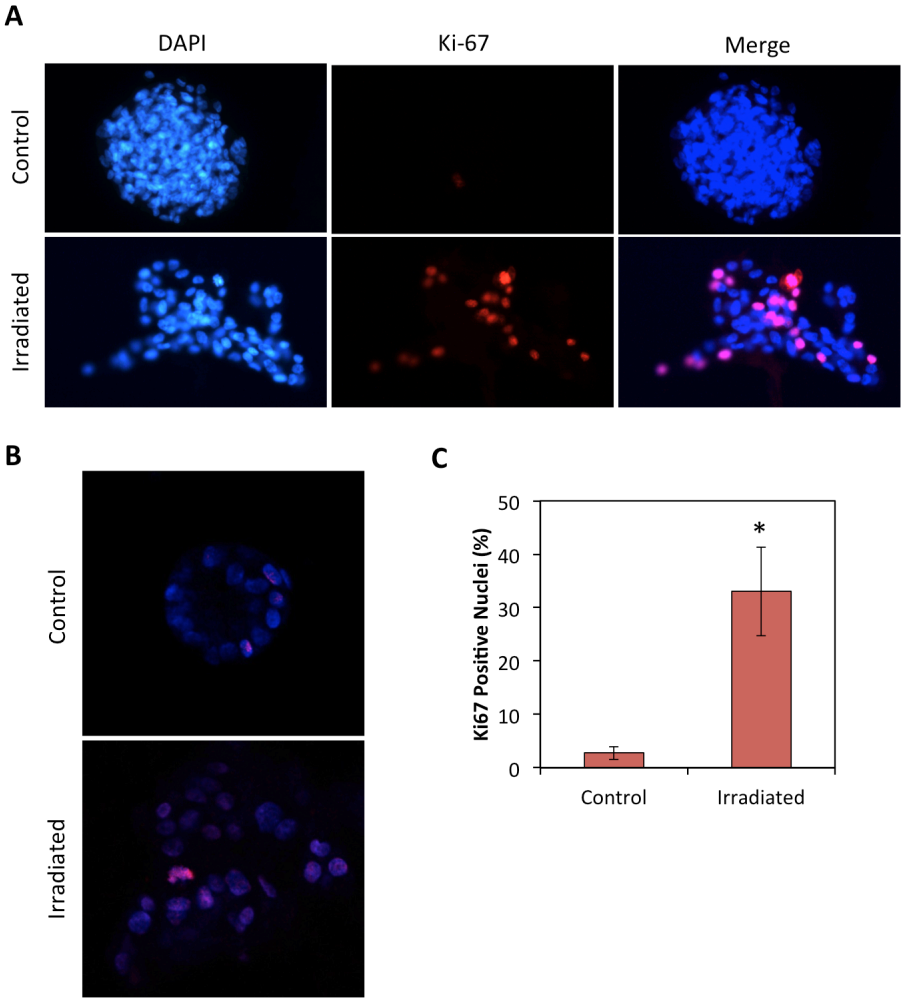

Figure 4.5: Effect of stiffening on MCF10A proliferation in acini. (A) Immunofluorescence of whole MCF10A nuclei for DAPI and Ki67. (B) Confocal microscopy slices demonstrate a hollow lumen in control gels with little Ki67 expression. Irradiated acini were disorganized and proliferative. (C) Quantification of nuclei labeled with Ki67 as a fraction of total nuclei. At least 10 acini (350-700 nuclei) were analyzed for each group.

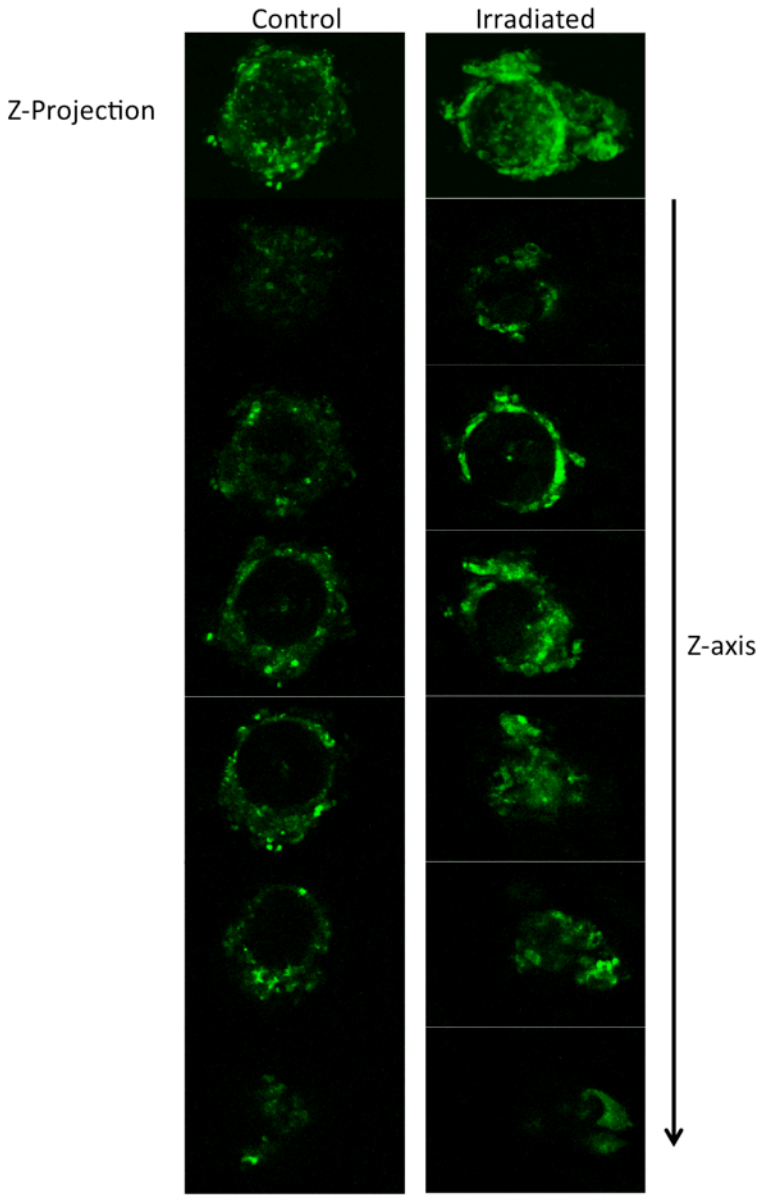

Figure 4.6: 3D morphology of MCF10A acini in stiffened gels. Z-projections of MCF10A stained with AlexaFluor 488-phalloidin for F-actin (top row). Series of images through the z-direction of the acini demonstrates formation of a hollow lumen in the control condition and protrusions emanating from the acinus in the irradiated condition.

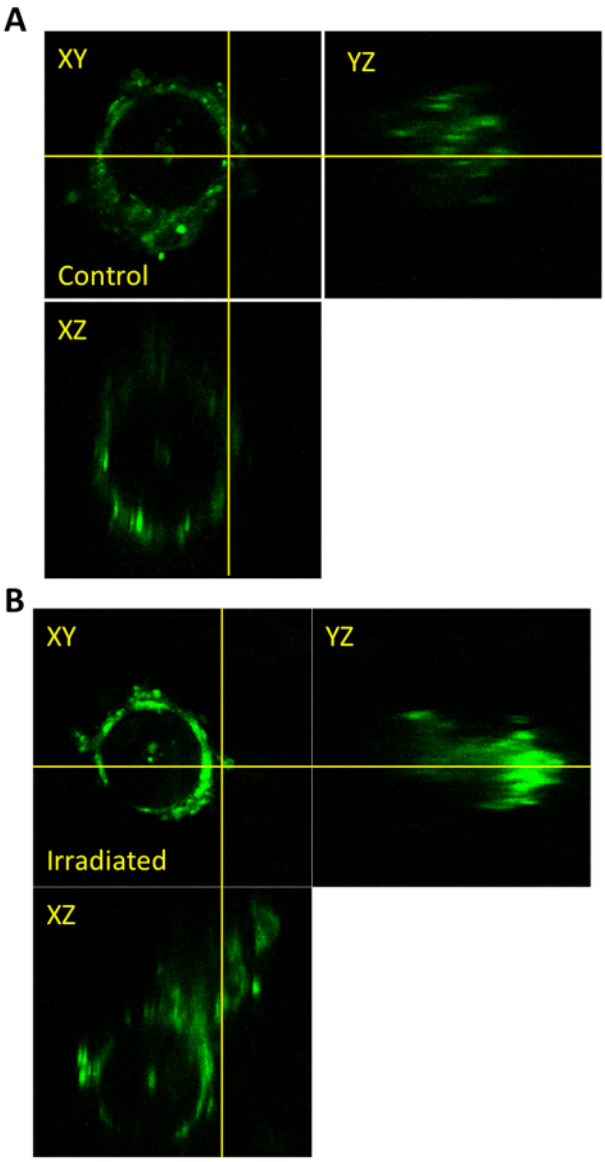

Figure 4.7: Orthogonal views of F-actin stained MCF10A. (A) MCF10A acinus in static, soft gels showing an XY, XY and YZ plane. (B) MCF10A acinus in a stiffened gel showing an XY, XZ, and YZ plane. The protrusion is evident in XZ and YZ planes.

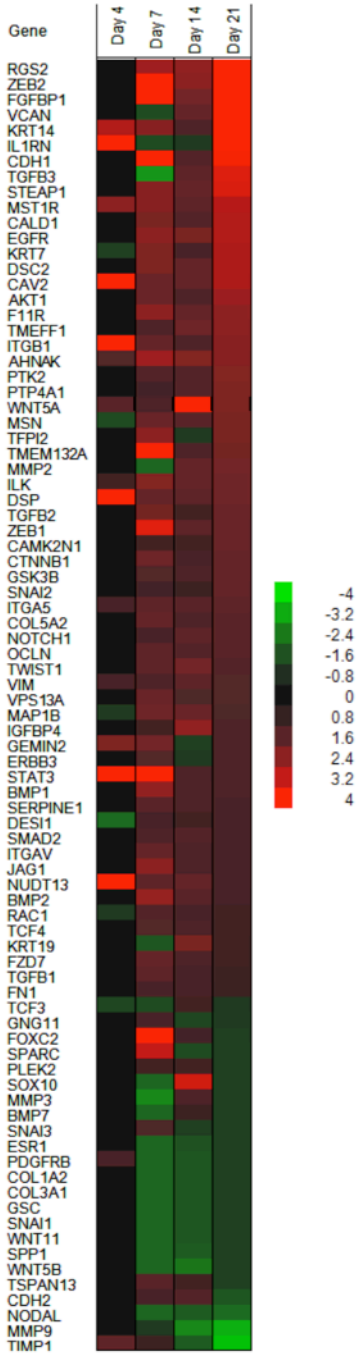

Figure 4.8: Heatmap of epithelial-to-mesenchymal PCR array. Genes are sorted in descending order for gels irradiated at Day 21.

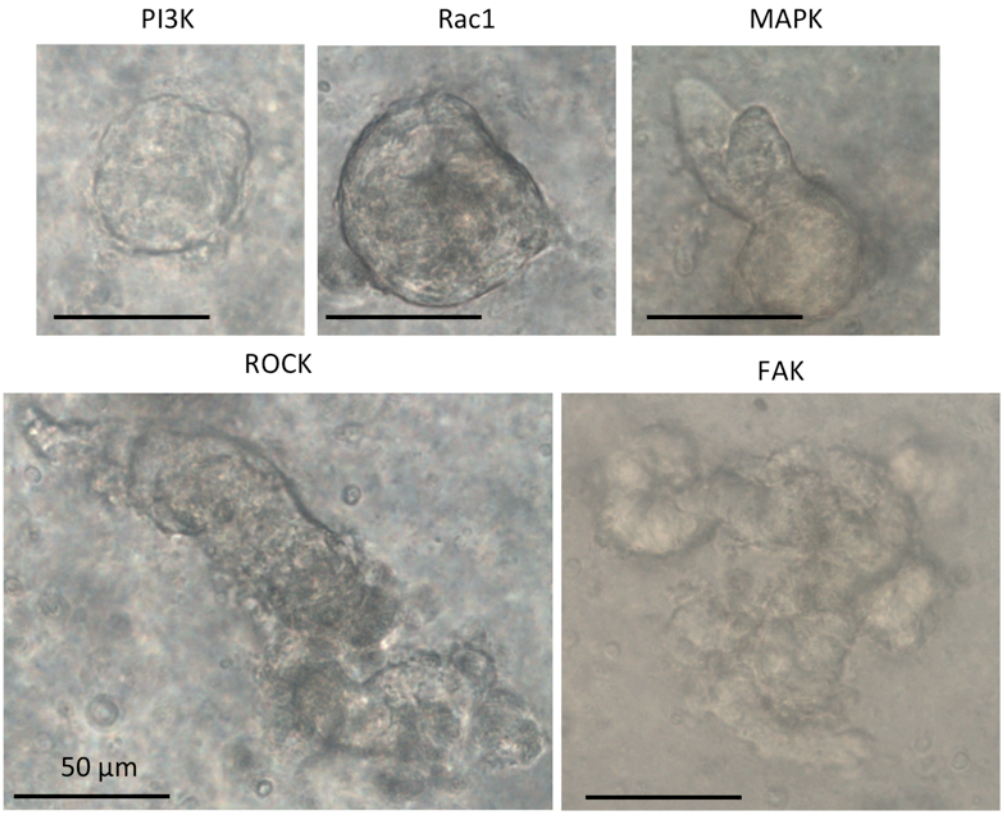

Figure 4.9: Morphology of MCF10A after stiffening and treatment with inhibitors. Inhibition of PI3K and Rac1 yielded smaller, less protrusive acini. Treatment with MAPK resulted in smaller acini that were still protrusive, while ROCK and FAK treatment produced no discernable effect.

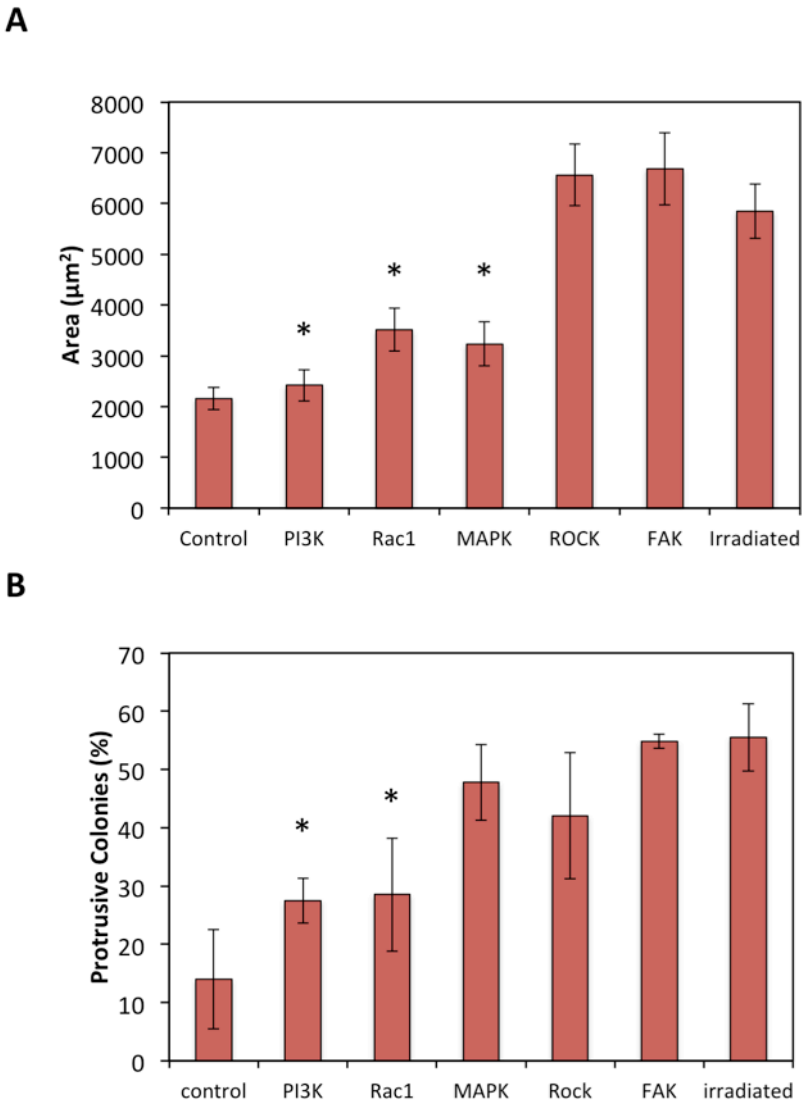

Figure 4.10: Effect of small molecule inhibitors on MCF10A after stiffening. (A) Acinus area in gels that were stiffened and treated with small molecule inhibitors of PI3K, Rac1, MAPK, ROCK, and FAK, or irradiated with no treatment, or in statically soft control gels. Acinus area significantly decreases from irradiated gels for PI3K, Rac1, and MAPK treatments. (B) The percentage of protrusive acini after inhibitor treatment. Inhibition of PI3K and Rac1 reduce the number of protrusive colonies significantly compared to irradiated but untreated gels.

4.5 REFERENCES

1. Wirtz D, Konstantopoulos K, & Searson PC (2011) The physics of cancer: the role of physical interactions and mechanical forces in metastasis. *Nature reviews. Cancer* 11(7):512-522.
2. Nelson CM & Bissell MJ (2005) Modeling dynamic reciprocity: engineering three-dimensional culture models of breast architecture, function, and neoplastic transformation. *Seminars in cancer biology* 15(5):342-352.
3. Yu H, Mouw JK, & Weaver VM (2011) Forcing form and function: biomechanical regulation of tumor evolution. *Trends in cell biology* 21(1):47-56.
4. Levental KR, *et al*. (2009) Matrix crosslinking forces tumor progression by enhancing integrin signaling. *Cell* 139(5):891-906.
5. Emerman JT & Pitelka DR (1977) Maintenance and induction of morphological differentiation in dissociated mammary epithelium on floating collagen membranes. *In vitro* 13(5):316-328.
6. Emerman JT, Enami J, Pitelka DR, & Nandi S (1977) Hormonal effects on intracellular and secreted casein in cultures of mouse mammary epithelial cells on floating collagen membranes. *Proceedings of the National Academy of Sciences of the United States of America* 74(10):4466-4470.
7. Lee EY, Parry G, & Bissell MJ (1984) Modulation of secreted proteins of mouse mammary epithelial cells by the collagenous substrata. *The Journal of cell biology* 98(1):146-155.

8. Lee EY, Lee WH, Kaetzel CS, Parry G, & Bissell MJ (1985) Interaction of mouse mammary epithelial cells with collagen substrata: regulation of casein gene expression and secretion. *Proceedings of the National Academy of Sciences of the United States of America* 82(5):1419-1423.

9. Debnath J, Muthuswamy SK, & Burgge JS (2003) Morphogenesis and oncogenesis of MCF-10A mammary epithelial acini grown in three-dimensional basement membrane cultures. *Methods* 30:256-268.

10. Benton G, Arnaoutova I, George J, Kleinman HK, & Koblinski J (2014) Matrigel: From discovery and ECM mimicry to assays and models for cancer research. *Advanced drug delivery reviews*.

11. Paszek MJ, *et al*. (2005) Tensional homeostasis and the malignant phenotype. *Cancer cell* 8(3):241-254.

12. Pathak A & Kumar S (2011) Biophysical regulation of tumor cell invasion: moving beyond matrix stiffness. *Integrative biology : quantitative biosciences from nano to macro* 3(4):267-278.

13. Egeblad M, Rasch MG, & Weaver VM (2010) Dynamic interplay between the collagen scaffold and tumor evolution. *Current opinion in cell biology* 22(5):697-706.

14. Chaudhuri O, *et al*. (2014) Extracellular matrix stiffness and composition jointly regulate the induction of malignant phenotypes in mammary epithelium. *Nature materials* 13(10):970-978.

15. Thiery JP, Acloque H, Huang RY, & Nieto MA (2009) Epithelial-mesenchymal transitions in development and disease. *Cell* 139(5):871-890.

16. Prall F (2007) Tumour budding in colorectal carcinoma. *Histopathology* 50(1):151-162.

17. Brabletz T, *et al*. (2001) Variable beta-catenin expression in colorectal cancers indicates tumor progression driven by the tumor environment. *Proceedings of the National Academy of Sciences of the United States of America* 98(18):10356-10361.

18. Peinado H, Olmeda D, & Cano A (2007) Snail, Zeb and bHLH factors in tumour progression: an alliance against the epithelial phenotype? *Nature reviews. Cancer* 7(6):415-428.

19. Wang X, *et al*. (2007) Kruppel-like factor 8 induces epithelial to mesenchymal transition and epithelial cell invasion. *Cancer research* 67(15):7184-7193.

20. Yang J & Weinberg RA (2008) Epithelial-mesenchymal transition: at the crossroads of development and tumor metastasis. *Developmental cell* 14(6):818-829.

21. Sobrado VR, *et al*. (2009) The class I bHLH factors E2-2A and E2-2B regulate EMT. *Journal of cell science* 122(Pt 7):1014-1024.

22. Muranen T, *et al*. (2012) Inhibition of PI3K/mTOR leads to adaptive resistance in matrix-attached cancer cells. *Cancer cell* 21(2):227-239.

23. Guo CL, *et al*. (2012) Long-range mechanical force enables self-assembly of epithelial tubular patterns. *Proceedings of the National Academy of Sciences of the United States of America* 109(15):5576-5582.

24. Nguyen-Ngoc KV, *et al*. (2012) ECM microenvironment regulates collective migration and local dissemination in normal and malignant mammary epithelium. *Proceedings of the National Academy of Sciences of the United States of America* 109(39):E2595-2604.

25. Leight JL, Wozniak MA, Chen S, Lynch ML, & Chen CS (2012) Matrix rigidity regulates a switch between TGF-beta1-induced apoptosis and epithelial-mesenchymal transition. *Molecular biology of the cell* 23(5):781-791.

26. Kim JH & Asthagiri AR (2011) Matrix stiffening sensitizes epithelial cells to EGF and enables the loss of contact inhibition of proliferation. *Journal of cell science* 124(Pt 8):1280-1287.

27. Friedl P & Gilmour D (2009) Collective cell migration in morphogenesis, regeneration and cancer. *Nature reviews. Molecular cell biology* 10(7):445-457.

28. Lahlou H, *et al*. (2007) Mammary epithelial-specific disruption of the focal adhesion kinase blocks mammary tumor progression. *Proceedings of the National Academy of Sciences of the United States of America* 104(51):20302-20307.

29. Rubashkin MG, *et al*. (2014) Force Engages Vinculin and Promotes Tumor Progression by Enhancing PI3K Activation of Phosphatidylinositol (3,4,5)-Triphosphate. *Cancer research* 74(17):4597-4611.

Chapter 5: Conclusions and Future Directions

5.1 Summary of findings

The ECM serves as a medium in which cells grow, organize, move and function. Properties of the ECM vary based on tissue type and specific location, and are known to be influential in nearly all areas of cell biology. The ECM can dictate cellular locomotion, differentiation, proliferation, and morphogenesis. Many diseases are associated with abnormal ECM properties. For example, ECM that is stiffer than normal is found in cancer, atherosclerosis, and all fibrotic diseases. In order to understand disease progression more fully in tissues that undergo dynamic remodeling of the ECM, it is necessary to developing 3D model systems that recapitulate the mechanical properties of the tissue in a temporally relevant manner.

In this dissertation, we present the development of such a model using a photo-tunable 3D alginate hydrogel system. The system is based on three essential components; (i) alginate, a naturally derived biopolymer that is crosslinked by divalent cations, (ii) temperature-sensitive liposomes encapsulating calcium, and (iii) gold nanorods, which convert NIR light to heat through the photothermal effect. Altogether, gold nanorods and $CaCl_2$ are encapsulated in the liposomes and distributed within an alginate gel. Irradiation with NIR light generates heat and causes a phase change in the lipid bilayer, which allows diffusion of the calcium ions out of the liposome and into the alginate. The introduction of calcium into the gel causes an increase in crosslinking density and thus an increase in gel stiffness. In Chapter 2, the optimization and characterization of the system are presented. We demonstrate the ability to stiffen 3D hydrogels over a range that encompasses many fibrotic tissue levels. The calcium is stably stored in the liposomes until irradiation is induced. Further, this system can be adapted to photolithographic

techniques to generate spatially confined stiffening. Finally, by loading chelators in place of calcium in the liposomes, the 3D gels can be dynamically softened by decreasing the crosslinking density of the gels.

In Chapter 3, this system is adapted for investigations of time-dependent biology. We first investigated the biocompatibility of the system and found that no loss of cell viability was induced by calcium release, irradiation, gold nanorods, or heating. We then probed the influence of a dynamically stiffening matrix on 3T3 fibroblast morphology. Contrary to observations on 2D substrates, we observed an increase in cell elongation in soft gels, and an increase in cell roundedness when the gels were stiffened. The effect was observed regardless of the nature of cell adhesions (alginate-Matrigel composite or RGD-conjugated alginate). Next, we sought to translate the photo-tuning technology to in vivo transdermal models. We demonstrate the ability to induce gelation of an alginate solution or stiffening of an alginate gel through the skin of a mouse.

Chapter 4 focuses on the application of the dynamic stiffening model to understand the influence of matrix stiffening on epithelial cells as a model of tumor stiffening. Using non-transformed MCF10A breast epithelial cells as a model of a mature, healthy mammary gland, we observed a phenotypic change in these cells after stiffening the surrounding matrix. The acini became larger and more protusive after stiffening, and lost several markers of epithelial character. Further, several critical genes associated with epithelial to mesenchymal transition were upregulated after stiffening. We determined that the morphological changes could be abrogated by inhibiting the PI3K and Rac1 pathways. Thus, utilizing dynamic stiffening to mimic changes to the ECM during breast cancer, we observed a novel phenomenon; the emergence of a protrusive phenotype from MCF10A in mammary acini.

5.2 FUTURE DIRECTIONS

5.2.1 Stiffening induced phenotypic changes

Here, we have identified matrix stiffening as a mechanism to drive a phenotypic change in MCF10A breast epithelial cells. After formation of the mammary acinus, matrix stiffening promotes upregulation of mesenchymal genes, protrusive acinar morphology, and aberrant expression of canonical protein markers. Further, we show that this behavior is abrogated when Rac1 and PI3K pathways are inhibited, indicating that phenotypic switching is induced through these pathways.

Future investigation in this topic should look at the critical threshold of stiffening to induce this phenotypic switch. Using our system, gels could be tuned to stiffen to various moduli by varying irradiation time or liposome concentration. Additionally, it would be interesting to determine if this behavior is observed in the presence of high concentrations of laminin. Chaudhuri et al showed that MCF10A in stiff gels undergo a malignant conversion to an invasive phenotype, similar to our observations (1). However, when the concentration of laminin in the gels was increased, the cells remained phenotypically normal regardless of matrix stiffness. The effect was attributed to the ability of the cells to cluster integrins. In soft microenvironments with a low concentration of laminin, the cells were able to pull the ligands together to form desmosomes. However, in stiff matrices, the polymer network resisted deformation and ligand clustering, causing the invasive phenotype. If sufficient quantities of laminin were present in stiff environments, the intergrins were able to cluster ligands without deforming the matrix, prevent the malignant switch. Our system could be used to test this hypothesis by varied the concentration of laminin initially present in the gels and inducing stiffening. Notably, since our hydrogel platform is capable of temporal

stiffening, mature acini could be generated prior to stiffening to probe a more physiologically relevant timeline of tumor progression.

Another interesting set of experiments could be performed by utilizing the softening modality presented in chapter 2. Weaver and Bissell have demonstrated that malignant T4-2 cells cultured in 3D basement membrane gels adopt a malignant morphology (2). However, if β1 integrin sites are blocked in these gels, the cells revert to a normal acinar phenotype. It is not clear the extent to which matrix stiffness could drive phenotypic reversion of malignant cells. Using our hydrogel system with DTPA loaded liposomes, malignant cells could be cultured in 3D gels and subsequently softened. The decrease in matrix stiffness might lead to less cellular traction force, and less signaling through β1 integrin pathways.

5.2.2 Effects of matrix stiffening on tumor initiation and progression in vivo

A potentially impactful application of the dynamic phototunable hydrogel platform presented here would be investigating the effects of microenvironmental stiffness on tumor initiation and progression in vivo. Utilizing the transdermal capabilities of the system, tumorigenic cells could be injected into mice in alginate gel plugs along with $CaCl_2$-loaded liposomes. These gels could be stiffened at various time periods to artificially stiffen the cellular microenvironment. There are a number of mouse models with well-established disease timelines and metastatic properties. It would be extremely interesting and clinically relevant to determine if the effects seen in vitro are mirrored in vivo. For these experiments, the gels could be stiffened at various timepoints and to various magnitudes to determine optimal timing and level of microenvironmental stiffness for promoting tumor progression and metastasis. Further, many chemotherapeutics act by inhibiting molecules that are involved in mechanotransduction pathways. It would be valuable to determine which of these inhibitors are effective at

abrogating the response to increased microenvironmental stiffness. Also of relevance to the breast cancer research community is at what stage of tumor progression stiffness plays the most impactful role. It is quite likely that highly malignant tumors, or very tumorigenic cells, will metastasize regardless of the gel stiffness, and may even be hindered by a stiffened gel. However, at earlier timepoints, the tumor may be induced into a migratory or invasive form by an increase in stiffness. Clinicians ideally would match treatments to the most effective tumor stage for the patient. Therefore it would be beneficial to understand if mechanotransduction inhibitors are more effective at early or late stages.

5.2.3 Probing the mechanical memory of stem cells in 3D microenvironments

As discussed in chapter 3, there is some debate over the influence of matrix stiffness on stem cell differentiation in 3D environments. Cell behavior and fate decisions are strikingly different depending on the gel type used in the experiments, making it difficult to understand the influence of stiffness in isolation of other confounding factors. Further, stem cells possess mechanically memory, or the plasticity to reverse effects of prior substrates to a point. This is an emerging concept in stem cell biology and is currently not well understood.

Experiments could be designed using the dynamic phototunable hydrogel platform presented here to explore the effects of matrix stiffening on stem cell differentiation and mechanical memory. These experiments could be conducted in three-dimensional, physically crosslinked gels that have been shown to promote stiffness-dependent stem cell fate decisions previously (3). Stem cell mechanical memory has only been demonstrated on 2D substrates, and only on gels that dynamically soften. These studies could be extended to determine if mechanically memory is maintained in 3D

environments, and could be explored in the context of dynamic stiffening and softening using our system.

5.3 REFERENCES

1. Chaudhuri O, *et al*. (2014) Extracellular matrix stiffness and composition jointly regulate the induction of malignant phenotypes in mammary epithelium. *Nature materials* 13(10):970-978.
2. Weaver VM, *et al*. (1997) Reversion of the Malignant Phenotype of Human Breast Cells in Three-Dimensional Culture and In Vivo by Integrin Blocking Antibodies. *The Journal of cell biology* 137:231-245.
3. Huebsch N, *et al*. (2010) Harnessing traction-mediated manipulation of the cell/matrix interface to control stem-cell fate. *Nature materials* 9(6):518-526.

Bibliography

Agarwal, A., M. A. Mackey, M. A. El-Sayed and R. V. Bellamkonda (2011). "Remote triggered release of doxorubicin in tumors by synergistic application of thermosensitive liposomes and gold nanorods." ACS Nano **5**(6): 4919-4926.

Ahl, P. L., L. Chen, W. R. Perkins, S. R. Minchey, L. T. Boni, T. F. Taraschi and A. S. Janoff (1994). "Interdigitation fusion: a new method for producing lipid vesicles of high internal volume." Biochim Biophys Acta **1195**: 237-244.

Alberts, B. J., A. Lewis, J. Raff, M. Roberts, K. Walter, P. (2007). Molecular Biology of the Cell, Garland Science.

Ali, M. H., D. P. Pearlstein, C. E. Mathieu and P. T. Schumacker (2004). "Mitochondrial requirement for endothelial responses to cyclic strain: implications for mechanotransduction." Am J Physiol Lung Cell Mol Physiol **287**: L486-L496.

Alkilany, A. M., L. B. Thompson, S. P. Boulos, P. N. Sisco and C. J. Murphy (2012). "Gold nanorods: their potential for photothermal therapeutics and drug delivery, tempered by the complexity of their biological interactions." Adv Drug Deliv Rev **64**(2): 190-199.

Allen, T. M. and P. R. Cullis (2004). "Drug delivery systems: entering the mainstream." Science **303**(5665): 1818-1822.

Amano, M., M. Ito, K. Kimura, Y. Fukata, K. Chihara, T. Nakano, Y. Matsuura and K. Kaibuchi (1996). "Phosphorylation and activation of myosin by Rho-associated kinase." J Biol Chem **271**: 20246-20249.

Andersen, T., B. L. Strand, K. Formo, E. Alsberg and B. E. Christensen (2012). "Alginates as biomaterials in tissue engineering." Carbohydr Chem **37**: 227-258.

Anderson, V. C. and D. H. Thompson (1992). "Triggered release of hydrophilic agents from plasmalogen liposomes using visible light or acid." Biochim Biophys Acta: 33-42.

Avvisato, C. L., X. Yang, S. Shah, B. Hoxter, W. Li, R. Gaynor, R. Pestell, A. Tozeren and S. W. Byers (2007). "Mechanical force modulates global gene expression and beta-catenin signaling in colon cancer cells." J Cell Sci **120**(Pt 15): 2672-2682.

Bangham, A. D. and R. W. Horne (1964). "Negative staining of phospholipids and their structural modification by surface-active agents as observed in the electron microscope." J Mol Biol **8**: 660-668.

Bangham, A. D., M. M. Standish and J. C. Watkins (1965). "Diffusion of univalent ions across the lamellae of swollen phospholipids." J Mol Biol **13**: 238-252.

Barczyk, M., S. Carracedo and D. Gullberg (2010). "Integrins." Cell Tissue Res **339**(1): 269-280.

Bloom, S., V. G. Lockard and M. Bloom (1996). "Intermediate filament-mediated stretch-induced changes in chromatin: A hypothesis for growth initiation in cardiac myocytes." J Mol Cell Cardiol **28**: 2123-2127.

Bondurant, B. and D. F. O'Brien (1998). "Photoinduced destabilization of sterically stablized liposomes." J Am Chem Soc **120**: 13541-13542.

Brabletz, T., A. Jung, S. Reu, M. Porzner, F. Hlubek, L. A. Kunz-Schughart, R. Knuechel and T. Kirchner (2001). "Variable beta-catenin expression in colorectal cancers

indicates tumor progression driven by the tumor environment." Proc Natl Acad Sci U S A **98**(18): 10356-10361.

Branco da Cunha, C., D. D. Klumpers, W. A. Li, S. T. Koshy, J. C. Weaver, O. Chaudhuri, P. L. Granja and D. J. Mooney (2014). "Influence of the stiffness of three-dimensional alginate/collagen-I interpenetrating networks on fibroblast biology." Biomaterials **35**(32): 8927-8936.

Bunnell, B. A., M. Flaat, C. Gagliardi, B. Patel and C. Ripoll (2008). "Adipose-derived stem cells: isolation, expansion and differentiation." Methods **45**(2): 115-120.

Butcher, D. T., T. Alliston and V. M. Weaver (2009). "A tense situation: forcing tumour progression." Nat Rev Cancer **9**(2): 108-122.

Chaudhuri, O., S. T. Koshy, C. Branco da Cunha, J. W. Shin, C. S. Verbeke, K. H. Allison and D. J. Mooney (2014). "Extracellular matrix stiffness and composition jointly regulate the induction of malignant phenotypes in mammary epithelium." Nat Mater **13**(10): 970-978.

Chaudhuri, O., S. H. Parekh and D. A. Fletcher (2007). "Reversible stress softening of actin networks." Nature **445**(7125): 295-298.

Chien, S. (2008). "Effects of disturbed flow on endothelial cells." Ann Biomed Eng **36**(4): 554-562.

Chueh, B. H., Y. Zheng, Y. S. Torisawa, A. Y. Hsiao, C. Ge, S. Hsiong, N. Huebsch, R. Franceschi, D. J. Mooney and S. Takayama (2010). "Patterning alginate hydrogels using light-directed release of caged calcium in a microfluidic device." Biomed Microdevices **12**(1): 145-151.

Critchley, D. R. (2000). "Focal adhesions- the cytoskeletal connection." Curr Opin Cell Biol **12**: 133-139.

Cui, J., M. Wang, Y. Zheng, G. M. Rodriguez Muniz and A. del Campo (2013). "Light-triggered cross-linking of alginates with caged Ca2+." Biomacromolecules **14**(5): 1251-1256.

Debnath, J., S. K. Muthuswamy and J. S. Burgge (2003). "Morphogenesis and oncogenesis of MCF-10A mammary epithelial acini grown in three-dimensional basement membrane cultures." Methods **30**: 256-268.

DeForest, C. A. and K. S. Anseth (2011). "Cytocompatible click-based hydrogels with dynamically tunable properties through orthogonal photoconjugation and photocleavage reactions." Nat Chem **3**(12): 925-931.

DeForest, C. A. and K. S. Anseth (2012). "Advances in bioactive hydrogels to probe and direct cell fate." Annu Rev Chem Biomol Eng **3**: 421-444.

DeForest, C. A. and K. S. Anseth (2012). "Photoreversible patterning of biomolecules within click-based hydrogels." Angew Chem Int Ed Engl **51**(8): 1816-1819.

DeForest, C. A., B. D. Polizzotti and K. S. Anseth (2009). "Sequential click reactions for synthesizing and patterning three-dimensional cell microenvironments." Nat Mater **8**(8): 659-664.

del Rio, A., R. Perez-Jimenez, R. Liu, P. Roca-Cusachs, J. M. Fernandez and M. P. Sheetz (2009). "Stretching single talin rod molecules activates vinculin binding." Science **323**: 638-641.

Dhoot, N. O., C. A. Tobias, I. Fischer and M. A. Wheatley (2004). "Peptide-modified alginate surfaces as a growth permissive substrate for neurite outgrowth." J Biomed Mater Res A **71**(2): 191-200.

Discher, D. E., P. Janmey and Y. L. Wang (2005). "Tissue cells feel and respond to the stiffness of their substrate." Science **310**(5751): 1139-1143.

Egeblad, M., M. G. Rasch and V. M. Weaver (2010). "Dynamic interplay between the collagen scaffold and tumor evolution." Curr Opin Cell Biol **22**(5): 697-706.

Elisseeff, J. H., K. S. Anseth, D. Sims, W. McIntosh, M. Randolph and R. Langer (1999). "Transdermal photopolymerization for minimally invasive implantation." Proc Natl Acad Sci U S A **96**: 3104-3107.

Emerman, J. T., J. Enami, D. R. Pitelka and S. Nandi (1977). "Hormonal effects on intracellular and secreted casein in cultures of mouse mammary epithelial cells on floating collagen membranes." Proc Natl Acad Sci U S A **74**(10): 4466-4470.

Emerman, J. T. and D. R. Pitelka (1977). "Maintenance and induction of morphological differentiation in dissociated mammary epithelium on floating collagen membranes." In Vitro **13**(5): 316-328.

Engler, A. J., L. Bacakova, C. Newman, A. Hategan, M. Griffin and D. Discher (2004). "Substrate compliance versus Ligand Density in Cell on Gel Responses." Biophys J **86**: 617-628.

Engler, A. J., S. Sen, H. L. Sweeney and D. E. Discher (2006). "Matrix elasticity directs stem cell lineage specification." Cell **126**(4): 677-689.

Fletcher, D. A. and R. D. Mullins (2010). "Cell mechanics and the cytoskeleton." Nature **463**(7280): 485-492.

Frantz, C., K. M. Stewart and V. M. Weaver (2010). "The extracellular matrix at a glance." J Cell Sci **123**(Pt 24): 4195-4200.

Friedl, P. and D. Gilmour (2009). "Collective cell migration in morphogenesis, regeneration and cancer." Nat Rev Mol Cell Biol **10**(7): 445-457.

Geiger, B., A. D. Bershadsky, R. Pankov and K. M. Yamada (2001). "Transmembrane Extracellular Matrix-Cytoskeleton Crosstalk." Nat Rev Mol Cell Biol **2**: 793-805.

Gilbert, P. M., K. L. Havenstrite, K. E. Magnusson, A. Sacco, N. A. Leonardi, P. Kraft, N. K. Nguyen, S. Thrun, M. P. Lutolf and H. M. Blau (2010). "Substrate elasticity regulates skeletal muscle stem cell self-renewal in culture." Science **329**(5995): 1078-1081.

Gillette, B. M., J. A. Jensen, M. Wang, J. Tchao and S. K. Sia (2010). "Dynamic hydrogels: switching of 3D microenvironments using two-component naturally derived extracellular matrices." Adv Mater **22**(6): 686-691.

Gilmore, A. P., C. Wood, V. Ohanian, P. Jackson, B. Patel, D. J. G. Rees, R. O. Hynes and D. R. Critchley (1993). "The cytoskeletal protein talin contains at least two distinct vinculin binding domains." J Cell Biol **122**(337-347).

Gombotz, W. R. and S. F. Wee (1998). "Protein release from alginate matrices." Adv Drug Deliv Rev **31**: 267-285.

Gramlich, W. M., J. L. Holloway, R. Rai and J. A. Burdick (2014). "Transdermal gelation of methacrylated macromers with near-infrared light and gold nanorods." Nanotechnology **25**(1): 014004.

Gregoriadis, G. (1995). "Engineering liposomes for drug delivery: progress and problems." Trends Biotechnol **13**: 527-537.

Gronthos, S., M. Mankani, J. Brahim, P. G. Robey and S. Shi (2000). "Postnatal human dental pulp stem cells (DPSCs) in vitro and in vivo." Proc Natl Acad Sci U S A **97**(25): 13625-13630.

Grove, J. E., E. Bruscia and D. S. Krause (2004). "Plasticity of Bone Marrow-Derived Stem Cells." Stem Cells **22**: 487-500.

Guo, C. L., M. Ouyang, J. Y. Yu, J. Maslov, A. Price and C. Y. Shen (2012). "Long-range mechanical force enables self-assembly of epithelial tubular patterns." Proc Natl Acad Sci U S A **109**(15): 5576-5582.

Guvendiren, M. and J. A. Burdick (2012). "Stiffening hydrogels to probe short- and long-term cellular responses to dynamic mechanics." Nat Commun **3**: 792.

Hahn, M. S., J. S. Miller and J. L. West (2006). "Three-Dimensional Biochemical and Biomechanical Patterning of Hydrogels for Guiding Cell Behavior." Adv Mater **18**: 2679-2684.

Harris, J. M. and R. B. Chess (2003). "Effect of pegylation on pharmaceuticals." Nat Rev Drug Discov **2**(3): 214-221.

Hern, D. L. and J. A. Hubbell (1998). "Incorporation of adhesion peptides into nonadhesive hydrogels for tissue resurfacing." J Biomed Mater Res **39**: 266-276.

Hoare, T. R. and D. S. Kohane (2008). "Hydrogels in drug delivery: Progress and challenges." Polymer **49**: 1993-2007.

Holle, A. W. and A. J. Engler (2011). "More than a feeling: discovering, understanding, and influencing mechanosensing pathways." Curr Opin Biotechnol **22**: 1-7.

Holy, T. E. and S. Leiber (1994). "Dynamic instability of microtubules as an efficient way to search in space." Proc Natl Acad Sci U S A **91**: 5682-5685.

Huang, X., I. H. El-Sayed, W. Qian and M. A. El-Sayed (2006). "Cancer cell imaging and photothermal therapy in the near-infrared region by using gold nanorods." J Am Chem Soc **128**(6): 2115-2120.

Huebsch, N., P. R. Arany, A. S. Mao, D. Shvartsman, O. A. Ali, S. A. Bencherif, J. Rivera-Feliciano and D. J. Mooney (2010). "Harnessing traction-mediated manipulation of the cell/matrix interface to control stem-cell fate." Nat Mater **9**(6): 518-526.

Huebsch, N., C. J. Kearney, X. Zhao, J. Kim, C. A. Cezar, Z. Suo and D. J. Mooney (2014). "Ultrasound-triggered disruption and self-healing of reversibly cross-linked hydrogels for drug delivery and enhanced chemotherapy." Proc Natl Acad Sci U S A **111**(27): 9762-9767.

Huxley, H. E. (1969). "The mechanism of muscular contraction." Science **164**: 1356-1366.

Hynes, R. O. (2009). "The extracellular matrix: not just pretty fibrils." Science **326**(5957): 1216-1219.

Ingber, D. E. (1997). "Tensegrity: The architectural basis of cellular mechanotransduction." annu Rev Physiol **59**: 575-599.

Ingber, D. E. (2006). "Cellular mechanotransduction: putting all the pieces together again." FASEB J **20**(7): 811-827.

Javvaji, V., A. G. Baradwaj, G. F. Payne and S. R. Raghavan (2011). "Light-activated ionic gelation of common biopolymers." Langmuir **27**(20): 12591-12596.

Juliano, R. L. (2002). "Signal transduction by cell adhesion receptors and the cytoskeleton." Annu. Rev. Pharmacol. Toxicol. **42**: 283-323.

Kano, K., Y. Tanaka, T. Ogawa, M. Shimomura and T. Kunitake (1981). "Photoresponsive artificial membrane. Regulation of membrane permeability of liposomal membrane by photoreversible cis-trans isomerization of azobenzenes." Photochemistry and Photobiology **34**: 323-329.

Karki, S. and E. L. F. Holzbaur (1999). "Cytoplasmic dynein and dynactin in cell division and intracellular transport." Curr Opin Cell Biol **11**: 45-53.

Kearney, C. J. and D. J. Mooney (2013). "Macroscale delivery systems for molecular and cellular payloads." Nat Mater **12**: 1004-1017.

Khetan, S., M. Guvendiren, W. R. Legant, D. M. Cohen, C. S. Chen and J. A. Burdick (2013). "Degradation-mediated cellular traction directs stem cell fate in covalently crosslinked three-dimensional hydrogels." Nat Mater **12**(5): 458-465.

Kim, J. H. and A. R. Asthagiri (2011). "Matrix stiffening sensitizes epithelial cells to EGF and enables the loss of contact inhibition of proliferation." J Cell Sci **124**(Pt 8): 1280-1287.

Kloxin, A. M., J. A. Benton and K. S. Anseth (2010). "In situ elasticity modulation with dynamic substrates to direct cell phenotype." Biomaterials **31**(1): 1-8.

Kloxin, A. M., A. M. Kasko, C. N. Salinas and K. S. Anseth (2009). "Photodegradable hydrogels for dynamic tuning of physical and chemical properties." Science **324**(5923): 59-63.

Kloxin, A. M., C. J. Kloxin, C. N. Bowman and K. S. Anseth (2010). "Mechanical properties of cellularly responsive hydrogels and their experimental determination." Adv Mater **22**(31): 3484-3494.

Korn, E. D., M. F. Carlier and D. Pantaloni (1987). "Actin polymerization and ATP hydrolysis." Science **238**: 638-644.

Kuo, C. K. and P. X. Ma (2008). "Maintaining dimensions and mechanical properties of ionically crosslinked alginate hydrogel scaffolds in vitro." J Biomed Mater Res A **84**(4): 899-907.

Lahlou, H., V. Sanguin-Gendreau, D. Zuo, R. D. Cardiff, G. W. McLean, M. C. Frame and W. J. Muller (2007). "Mammary epithelial-specific disruption of the focal adhesion kinase blocks mammary tumor progression." Proc Natl Acad Sci U S A **104**(51): 20302-20307.

Lee, E. Y., W. H. Lee, C. S. Kaetzel, G. Parry and M. J. Bissell (1985). "Interaction of mouse mammary epithelial cells with collagen substrata: regulation of casein gene expression and secretion." Proc Natl Acad Sci U S A **82**(5): 1419-1423.

Lee, E. Y., G. Parry and M. J. Bissell (1984). "Modulation of secreted proteins of mouse mammary epithelial cells by the collagenous substrata." J Cell Biol **98**(1): 146-155.

Lee, K. Y. and D. J. Mooney (2012). "Alginate: properties and biomedical applications." Prog Polym Sci **37**(1): 106-126.

Leight, J. L., M. A. Wozniak, S. Chen, M. L. Lynch and C. S. Chen (2012). "Matrix rigidity regulates a switch between TGF-beta1-induced apoptosis and epithelial-mesenchymal transition." Mol Biol Cell **23**(5): 781-791.

Lelievre, S., V. M. Weaver, J. A. Nickerson, C. A. Larabell, A. Bhaumik, O. W. Petersen and M. J. Bissell (1998). "Tissue phenotype depends on reciprocal interactions between the extracellular matrix and the structural organization of the nucleus." Proc Natl Acad Sci U S A **95**: 14711-14716.

Leung, S. J. and M. Romanowski (2012). "Light-activated content release from liposomes." Theranostics **2**(10): 1020-1036.

Levental, K. R., H. Yu, L. Kass, J. N. Lakins, M. Egeblad, J. T. Erler, S. F. Fong, K. Csiszar, A. Giaccia, W. Weninger, M. Yamauchi, D. L. Gasser and V. M. Weaver (2009). "Matrix crosslinking forces tumor progression by enhancing integrin signaling." Cell **139**(5): 891-906.

Lim, F. and R. D. Moss (1981). "Microencapsulation of living cells and tissues." J Pharm Sci **70**: 351-354.

Lim, Y., S. T. Lim, A. Tomar, M. Gardel, J. A. Bernard-Trifilo, X. L. Chen, S. A. Uryu, R. Canete-Soler, J. Zhai, H. Lin, W. W. Schlaepfer, P. Nalbant, G. Bokoch, D.

Ilic, C. Waterman-Storer and D. D. Schlaepfer (2008). "PyK2 and FAK connections to p190Rho guanine nucleotide exchange factor regulate RhoA activity, focal adhesion formation, and cell motility." J Cell Biol **180**(1): 187-203.

Lin, R. Z., Y. C. Chen, R. Moreno-Luna, A. Khademhosseini and J. M. Melero-Martin (2013). "Transdermal regulation of vascular network bioengineering using a photopolymerizable methacrylated gelatin hydrogel." Biomaterials **34**(28): 6785-6796.

Link, S., M. B. Mohamed and M. A. El-Sayed (1999). "Simulation of the optical absorption spectra of gold nanorods as a function of their aspect ratio and the effect of the medium dielectric constant." J Phys Chem B **103**: 3073-3077.

Lo, C.-M., H.-B. Wang, M. Dembo and Y.-L. Wang (2000). "Cell Movement is Guided by the Rigidity of the Substrate." Biophys J **79**: 144-152.

Lu, P., K. Takai, V. M. Weaver and Z. Werb (2011). "Extracellular matrix degradation and remodeling in development and disease." Cold Spring Harb Perspect Biol **3**(12).

Ludwig, B., A. Reichel, A. Steffen, B. Zimerman, A. V. Schally, N. L. Block, C. K. Colton, S. Ludwig, S. Kersting, E. Bonifacio, M. Solimena, Z. Gendler, A. Rotem, U. Barkai and S. R. Bornstein (2013). "Transplantation of human islets without immunosuppression." Proc Natl Acad Sci U S A **110**(47): 19054-19058.

Luo, Y. and M. S. Shoichet (2004). "A photolabile hydrogel for guided three-dimensional cell growth and migration." Nat Mater **3**(4): 249-253.

Lutolf, M. P. and J. A. Hubbell (2005). "Synthetic biomaterials as instructive extracellular microenvironments for morphogenesis in tissue engineering." Nat Biotechnol **23**(1): 47-55.

Mackanos, M. A., M. Larabi, R. Shinde, D. M. Simanovskii, S. Guccione and C. H. Contag (2009). "Laser-induced disruption of systemically administered liposomes for targeted drug delivery." J Biomed Opt **14**(4): 044009.

Maheshwari, G., G. Brown, D. A. Lauffenburger, A. Wells and L. G. Griffith (2000). "Cell adhesion and motility depend on nanoscale RGD clustering." J Cell Sci **113**: 1677-1686.

Malam, Y., M. Loizidou and A. M. Seifalian (2009). "Liposomes and nanoparticles: nanosized vehicles for drug delivery in cancer." Trends Pharmacol Sci **30**(11): 592-599.

Maniotis, A. J., C. S. Chen and D. E. Ingber (1997). "Demonstration of mechanical connections between integrins, cytoskeletal filaments, and nucleoplasm that stabilize nuclear structure." Proc Natl Acad Sci U S A **94**: 849-854.

Martens, P., A. Metters, K. S. Anseth and C. N. Bowman (2001). "A Generalized Bulk-Degradation Model for Hydrogel Networks Formed from Multivinyl

Cross-linking Molecules." J Phys Chem B **105**: 5131-5138.

Matson, J. B., R. H. Zha and S. I. Stupp (2011). "Peptide Self-Assembly for Crafting Functional Biological Materials." Curr Opin Solid State Mater Sci **15**(6): 225-235.

Messersmith, P. B. and S. Starke (1998). "Thermally triggered calcium phosphate formation from calcium-loaded liposomes." Chem Mater **10**: 117-124.

Messersmith, P. B., S. Vallabhaneni and V. Nguyen (1998). "Preparation of calcium-loaded liposomes and their use in calcium phosphate formation." Chem Mater **10**: 109-116.

Metters, A., C. N. Bowman and K. S. Anseth (2000). "A Statistical Kinetic Model for the Bulk Degradation of PLA-b-PEG-b-PLA Hydrogel

Networks." J Phys Chem B **104**: 7043-7049.

Metters, A. and J. Hubbell (2005). "Network formation and degradation behavior of hydrogels formed by Michael-type addition reactions." Biomacromolecules **6**(1): 290-301.

Mosahebi, A., M. Wiberg and G. Terenghi (2003). "Addition of Fibronectin to Alginate Matrix Improves Peripheral Nerve Regeneration in Tissue-Engineered Conduits." Tissue Eng **9**: 209-218.

Moscho, A., O. Orwar, D. T. Chiu, B. P. Modi and R. N. Zare (1996). "Rapid preparation of giant unilamellar vesicles." Proc Natl Acad Sci U S A **93**: 11443-11447.

Muranen, T., L. M. Selfors, D. T. Worster, M. P. Iwanicki, L. Song, F. C. Morales, S. Gao, G. B. Mills and J. S. Brugge (2012). "Inhibition of PI3K/mTOR leads to adaptive resistance in matrix-attached cancer cells." Cancer Cell **21**(2): 227-239.

Nelson, C. M. and M. J. Bissell (2005). "Modeling dynamic reciprocity: engineering three-dimensional culture models of breast architecture, function, and neoplastic transformation." Semin Cancer Biol **15**(5): 342-352.

Nguyen-Ngoc, K. V., K. J. Cheung, A. Brenot, E. R. Shamir, R. S. Gray, W. C. Hines, P. Yaswen, Z. Werb and A. J. Ewald (2012). "ECM microenvironment regulates collective migration and local dissemination in normal and malignant mammary epithelium." Proc Natl Acad Sci U S A **109**(39): E2595-2604.

Niessen, C. M., F. Hoegervorst, L. H. Jaspars, A. A. De Melker, G. O. Delwel, E. H. M. Hulsman, I. Kuikman and A. Sonnenberg (1994). "The alpha-6 beta-4 integrin is a receptor for both laminin and kalinin." Exp Cell Res **211**: 360-367.

Nunamaker, E. A., E. K. Purcell and D. R. Kipke (2007). "In vivo stability and biocompatibility of implanted calcium alginate disks." J Biomed Mater Res A **83**(4): 1128-1137.

Orive, G., S. Ponce, R. M. Hernandez, A. R. Gascon, M. Igartua and J. L. Pedraz (2002). "Biocompatibility of microcapsules for cell immobilization elaborated with different types of alginates." Biomaterials **23**: 3825-3831.

Paasonen, L., T. Laaksonen, C. Johans, M. Yliperttula, K. Kontturi and A. Urtti (2007). "Gold nanoparticles enable selective light-induced contents release from liposomes." J Control Release **122**(1): 86-93.

Paasonen, L., T. Sipila, A. Subrizi, P. Laurinmaki, S. J. Butcher, M. Rappolt, A. Yaghmur, A. Urtti and M. Yliperttula (2010). "Gold-embedded photosensitive liposomes for drug delivery: triggering mechanism and intracellular release." J Control Release **147**(1): 136-143.

Palazzo, A. F., T. A. Cook, A. S. Alberts and G. G. Gundersen (2001). "mDia mediates Rho-regulated formation and orientation of stable microtubules." Nat Cell Biol **3**: 723-729.

Pardi, R. (2010). "Signal Transduction by Adhesion Receptors." Nature Education **3**(9): 38-44.

Paszek, M. J., N. Zahir, K. R. Johnson, J. N. Lakins, G. I. Rozenberg, A. Gefen, C. A. Reinhart-King, S. S. Margulies, M. Dembo, D. Boettiger, D. A. Hammer and V. M. Weaver (2005). "Tensional homeostasis and the malignant phenotype." Cancer Cell **8**(3): 241-254.

Pathak, A. and S. Kumar (2011). "Biophysical regulation of tumor cell invasion: moving beyond matrix stiffness." Integr Biol (Camb) **3**(4): 267-278.

Peinado, H., D. Olmeda and A. Cano (2007). "Snail, Zeb and bHLH factors in tumour progression: an alliance against the epithelial phenotype?" Nat Rev Cancer **7**(6): 415-428.

Pelham, R. J. and Y.-L. Wang (1997). "Cell locomotion and focal adhesions are regulated by substrate flexibility." Proc Natl Acad Sci U S A **94**: 13661-13665.

Peppas, N. A., J. Z. Hilt, A. Khademhosseini and R. Langer (2006). "Hydrogels in Biology and Medicine: From Molecular Principles to Bionanotechnology." Adv Mater **18**: 1345-1360.

Pollard, T. D. and J. A. Cooper (2009). "Actin, a central player in cell shape and movement." Science **326**(5957): 1208-1212.

Prall, F. (2007). "Tumour budding in colorectal carcinoma." Histopathology **50**(1): 151-162.

Reichelt, J. (2007). "Mechanotransduction of keratinocytes in culture and in the epidermis." Eur J Cell Biol **86**(11-12): 807-816.

Rowley, J. A., G. Madlambayan and D. J. Mooney (1999). "Alginate hydrogels as synthetic extracellular matrix materials." Biomaterials **20**: 45-53.

Rubashkin, M. G., L. Cassereau, R. Bainer, C. C. DuFort, Y. Yui, G. Ou, M. J. Paszek, M. W. Davidson, Y. Y. Chen and V. M. Weaver (2014). "Force Engages Vinculin and Promotes Tumor Progression by Enhancing PI3K Activation of Phosphatidylinositol (3,4,5)-Triphosphate." Cancer Res **74**(17): 4597-4611.

Ruel-Gariepy, E. and J. C. Leroux (2004). "In situ-forming hydrogels--review of temperature-sensitive systems." Eur J Pharm Biopharm **58**(2): 409-426.

Saez, A., M. Ghibaudo, A. Buguin, P. Silberzan and B. Ladoux (2007). "Rigidity-driven growth and migration of epithelial cells on microstructured anisotropic substrates." Proc Natl Acad Sci U S A **104**(20): 8281-8286.

Saha, K., A. J. Keung, E. F. Irwin, Y. Li, L. Little, D. V. Schaffer and K. E. Healy (2008). "Substrate modulus directs neural stem cell behavior." Biophys J **95**(9): 4426-4438.

Sanborn, T. J., P. B. Messersmith and A. E. Barron (2002). "In situ crosslinking of a biomimetic peptide-PEG hydrogel via thermally activation of factor XIII." Biomaterials **23**: 2703-2710.

Sawhney, A. S., C. P. Pathak and J. A. Hubbell (1993). "Bioerodible Hydrogels Based on Photopolymerized Poly(ethylene glycol)-co-poly(a-hydroxyacid) Diacrylate Macromers." Macromolecules **26**: 581-587.

Schwartz, M. A. and C. S. Chen (2013). "Deconstructing dimensionality." Science **339**(6118): 402-404.

Sen, S., A. J. Engler and D. Discher (2009). "Matrix strains induced by cells: computing how far cells can feel." Cellular and Molecular Bioengineering **2**: 39-48.

Sivaramakrishnan, S., J. V. DeGiulio, L. Lorand, R. D. Goldman and K. M. Ridge (2008). "Micromechanical properties of keratin intermediate filament networks." Proc Natl Acad Sci U S A **105**(3): 889-894.

Skardal, A., D. Mack, A. Atala and S. Soker (2013). "Substrate elasticity controls cell proliferation, surface marker expression and motile phenotype in amniotic fluid-derived stem cells." J Mech Behav Biomed Mater **17**: 307-316.

Smith, A. M., J. J. Harris, R. M. Shelton and Y. Perrie (2007). "3D culture of bone-derived cells immobilised in alginate following light-triggered gelation." J Control Release **119**(1): 94-101.

Sobrado, V. R., G. Moreno-Bueno, E. Cubillo, L. J. Holt, M. A. Nieto, F. Portillo and A. Cano (2009). "The class I bHLH factors E2-2A and E2-2B regulate EMT." J Cell Sci **122**(Pt 7): 1014-1024.

Soon-Shiong, P., E. Feldman, R. Nelson, R. Heintz, Q. Yao, Z. Yao, T. Zheng, N. Merideth, G. Skjak-Braek, T. Espevik, O. Smidsrod and P. Sandford (1993).

"Long-term reversal of diabetes by the injection of immunoprotected islets." Proc Natl Acad Sci U S A **90**: 5843-5847.

Soon-Shiong, P., R. Heintz, N. Merideth, Q. Yao, Z. Yao, T. Zheng, M. Murphy, M. K. Moloney, M. Schmehl, M. Harris, R. Mendez and P. Sandford (1994). "Insulin independence in a type 1 diabetic patient after encapsulated islet transplantation." Lancet **343**: 950-951.

Stanley, S. A., J. E. Gagner, S. Damanpour, M. Yoshida, J. S. Dordick and J. M. Friedman (2012). "Radio-wave heating of iron oxide nanoparticles can regulate plasma glucose in mice." Science **336**(6081): 604-608.

Thiery, J. P., H. Acloque, R. Y. Huang and M. A. Nieto (2009). "Epithelial-mesenchymal transitions in development and disease." Cell **139**(5): 871-890.

Tibbitt, M. W. and K. S. Anseth (2009). "Hydrogels as extracellular matrix mimics for 3D cell culture." Biotechnol Bioeng **103**(4): 655-663.

Tikshdeep, C., A. Sonia, P. Bharat and C. Abhishek (2012). "Liposomes Drug Delivery: A Review." International Journal of Pharmaceutical and Chemical Sciences **1**: 1103-1113.

Trappmann, B. and C. S. Chen (2013). "How cells sense extracellular matrix stiffness: a material's perspective." Curr Opin Biotechnol **24**(5): 948-953.

Turner, C. E., J. R. Glenney Jr. and K. Burridge (1990). "Paxillin: A new vinculin-binding protein present in focal adhesions." J Cell Biol **111**: 1059-1068.

Ulrich, T. A., E. M. de Juan Pardo and S. Kumar (2009). "The mechanical rigidity of the extracellular matrix regulates the structure, motility, and proliferation of glioma cells." Cancer Res **69**(10): 4167-4174.

Vats, K. and D. S. Benoit (2013). "Dynamic manipulation of hydrogels to control cell behavior: a review." Tissue Eng Part B Rev **19**(6): 455-469.

Venkatesan, R., A. Pichaimani, K. Hari, P. K. Balasubramanian, J. Kulandaivel and K. Premkumar (2013). "Doxorubicin conjugated gold nanorods: a sustained drug delivery carrier for improved anticancer therapy." J Mater Chem B **1**: 1010-1018.

von Maltzahn, G., J. H. Park, A. Agrawal, N. K. Bandaru, S. K. Das, M. J. Sailor and S. N. Bhatia (2009). "Computationally guided photothermal tumor therapy using long-circulating gold nanorod antennas." Cancer Res **69**(9): 3892-3900.

von Maltzahn, G., J. H. Park, K. Y. Lin, N. Singh, C. Schwoppe, R. Mesters, W. E. Berdel, E. Ruoslahti, M. J. Sailor and S. N. Bhatia (2011). "Nanoparticles that communicate in vivo to amplify tumour targeting." Nat Mater **10**(7): 545-552.

Wang, H., S. M. Haeger, A. M. Kloxin, L. A. Leinwand and K. S. Anseth (2012). "Redirecting valvular myofibroblasts into dormant fibroblasts through light-mediated reduction in substrate modulus." PLoS One **7**(7): e39969.

Wang, H., M. W. Tibbitt, S. J. Langer, L. A. Leinwand and K. S. Anseth (2013). "Hydrogels preserve native phenotypes of valvular fibroblasts through an elasticity-regulated

PI3K/AKT pathway." Proc Natl Acad Sci U S A **110**: 19336-19341.

Wang, N. and Z. Suo (2005). "Long-distance propagation of forces in a cell." Biochem Biophys Res Commun **328**(4): 1133-1138.

Wang, X., M. Zheng, G. Liu, W. Xia, P. J. McKeown-Longo, M. C. Hung and J. Zhao (2007). "Kruppel-like factor 8 induces epithelial to mesenchymal transition and epithelial cell invasion." Cancer Res **67**(15): 7184-7193.

Weaver, V. M., O. W. Petersen, F. Wang, C. A. Larabell, P. Briand, C. Damsky and M. J. Bissell (1997). "Reversion of the Malignant Phenotype of Human Breast Cells in Three-Dimensional Culture and In Vivo by Integrin Blocking Antibodies." J Cell Biol **137**: 231-245.

Weissleder, R. (2001). "A clearer vision for in vivo imaging." Nat Biotechnol **19**: 316-317.

West, J. L. and J. Hubbell (1999). "Polymeric Biomaterials with Degradation Sites for Proteases Involved in Cell Migration." Macromolecules **32**: 241-244.

Westhaus, E. and P. B. Messersmith (2001). "Triggered release of calcium from lipid vesicles: a bioinspired strategy for rapid gelation of polysaccharide and protein hydrogels." Biomaterials **22**: 453-462.

Wirtz, D., K. Konstantopoulos and P. C. Searson (2011). "The physics of cancer: the role of physical interactions and mechanical forces in metastasis." Nat Rev Cancer **11**(7): 512-522.

Wu, G., A. Mikhailovsky, H. A. Khant, C. Fu, W. Chiu and J. A. Zasadzinski (2008). "Remotely triggered liposome release by near-infrared light absorption via hollow gold nanoshells." J Am Chem Soc **130**: 8175-8177.

Yang, C., M. W. Tibbitt, L. Basta and K. S. Anseth (2014). "Mechanical memory and dosing influence stem cell fate." Nat Mater **13**(6): 645-652.

Yang, J. and R. A. Weinberg (2008). "Epithelial-mesenchymal transition: at the crossroads of development and tumor metastasis." Dev Cell **14**(6): 818-829.

Young, J. L. and A. J. Engler (2011). "Hydrogels with time-dependent material properties enhance cardiomyocyte differentiation in vitro." Biomaterials **32**(4): 1002-1009.

Yu, H., J. K. Mouw and V. M. Weaver (2011). "Forcing form and function: biomechanical regulation of tumor evolution." Trends Cell Biol **21**(1): 47-56.

Zhang, J. and N. A. Peppas (2000). "Synthesis and characterization of pH- and temperature-sensitive poly(methacrylic acid)/poly(N-isopropylacrylamide) interpenetrating polymeric networks." Macromolecules **33**: 102-107.

Zhang, Z. Y., P. Shum, M. Yates, P. B. Messersmith and D. H. Thompson (2002). "Formation of fibrinogen-based hydrogels using phototriggerable diplasmalogen liposomes." Bioconjugate Chem **13**: 640-646.

Zhao, X., J. Kim, C. A. Cezar, N. Huebsch, K. Lee, K. Bouhadir and D. J. Mooney (2011). "Active scaffolds for on-demand drug and cell delivery." Proc Natl Acad Sci U S A **108**(1): 67-72.

Zhu, J. (2010). "Bioactive modification of poly(ethylene glycol) hydrogels for tissue engineering." Biomaterials **31**(17): 4639-4656.

Vita

Ryan Scott Stowers was born in Greenville, SC. He graduated from Wren High School in Piedmont, SC in 2005. He graduated from Clemson University in 2009 with a B.S. in Bioengineering magna cum laude and with General Honors. Ryan entered the Ph.D. program at the University of Texas at Austin in the fall of 2009. He joined Dr. Laura Suggs's laboratory, where his research focused on development of dynamically phototunable 3D hydrogel systems.

Permanent email address: ryan.s.stowers@gmail.com

This dissertation was typed by the author.